Noise sources in photometry and radial velocities

Mahmoud Oshagh

Institute for Astrophysics, University of Göttingen, Germany
Institute of Astrophysics and Space Science, Portugal

Outline

- Stellar oscillation
- Stellar granulation
- Stellar active regions
- Stellar magnetic cycle

Short time scale

Long time scale

Stellar oscillation

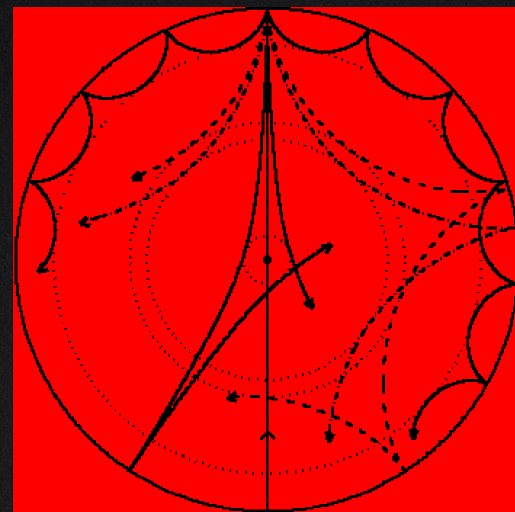

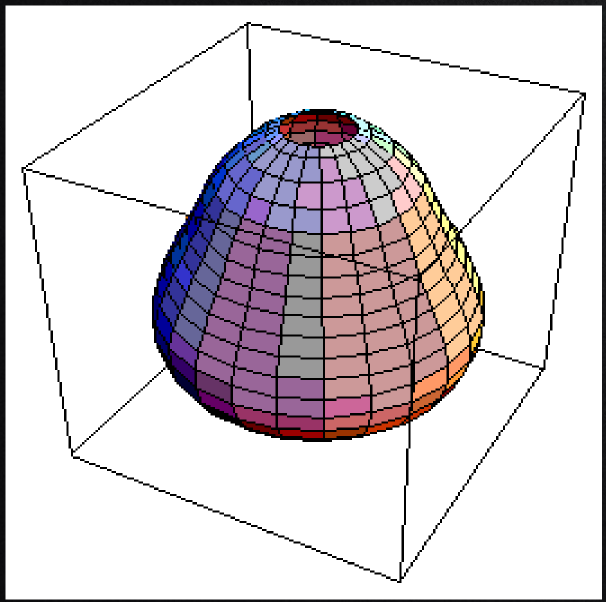

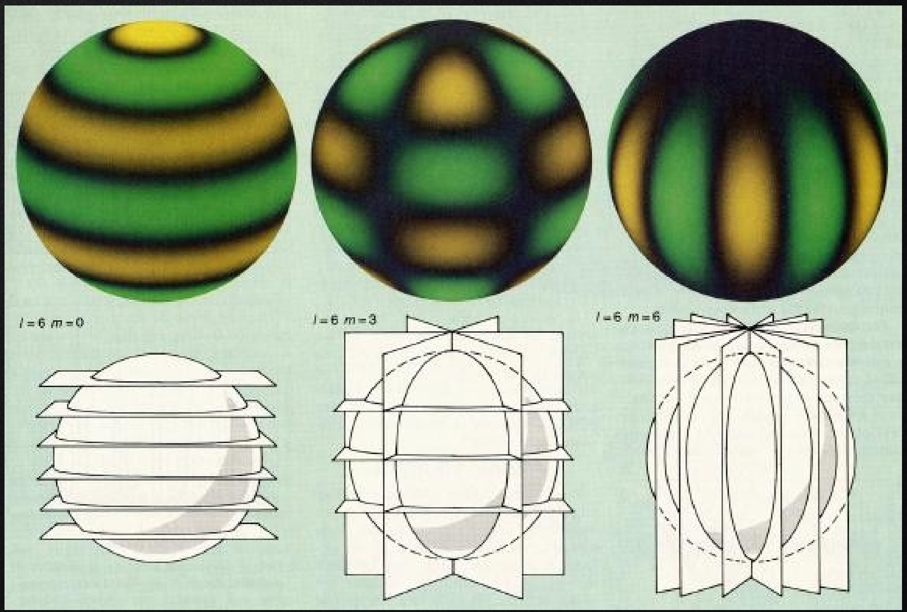

Stellar oscillation in RV

Time scale: 4-10 min
RV amplitude: 0.2-3 m/s

α Centauri A

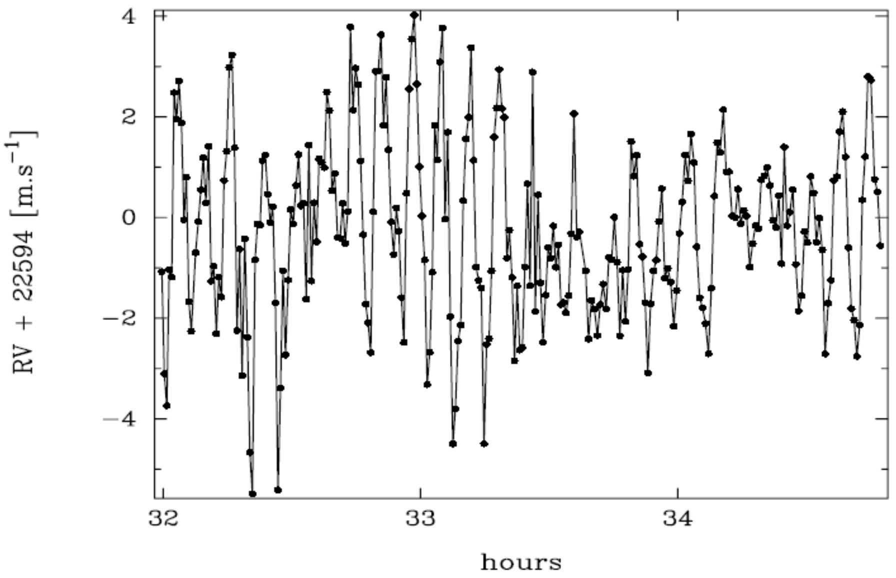

Fig. 2. Zoom of radial velocity measurements in a three-hour sequence, taken during the third night, showing the presence of p-modes in the time series with periods of around 7 min. The semi-amplitude of about 3 m s^{-1} does not represent the individual amplitude of p-modes but comes from the interference of several modes.

Bazot + 2007

Sun

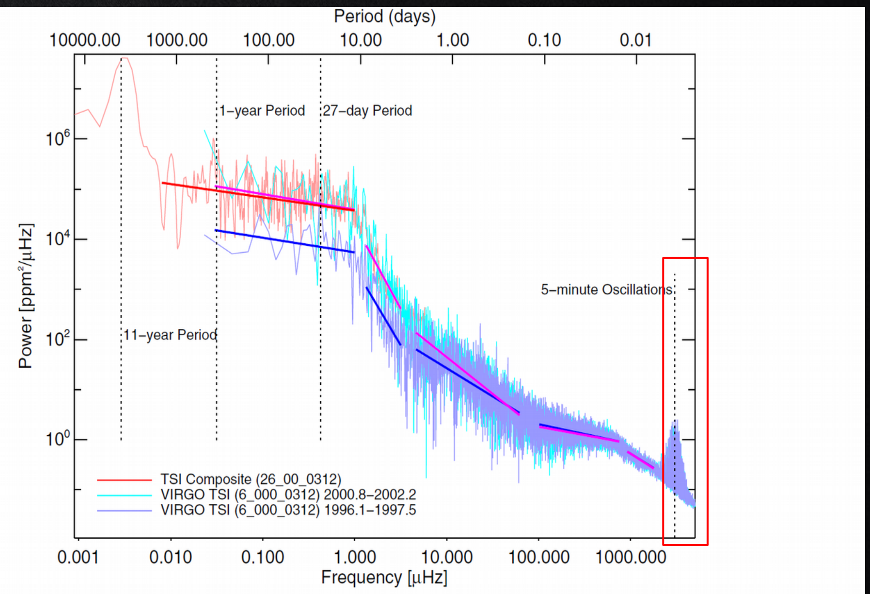

Fig. 12. Shown is the power spectrum of the composite record of daily total solar irradiance for the period from 1978 until 2002 (red). To illustrate the solar cycle variability in the frequency domain, the power spectra of data from VIRGO during solar minimum (Feb. 1996–Aug. 1997) are compared to that of solar maximum (Oct. 2000–Feb. 2002). The solar cycle influence is evident in the differences in power at low frequencies

Frohlich & Lean (2004)

Stellar oscillation in RV

Minimum exposures of **15 min (900 seconds)** to average out stellar oscillations.

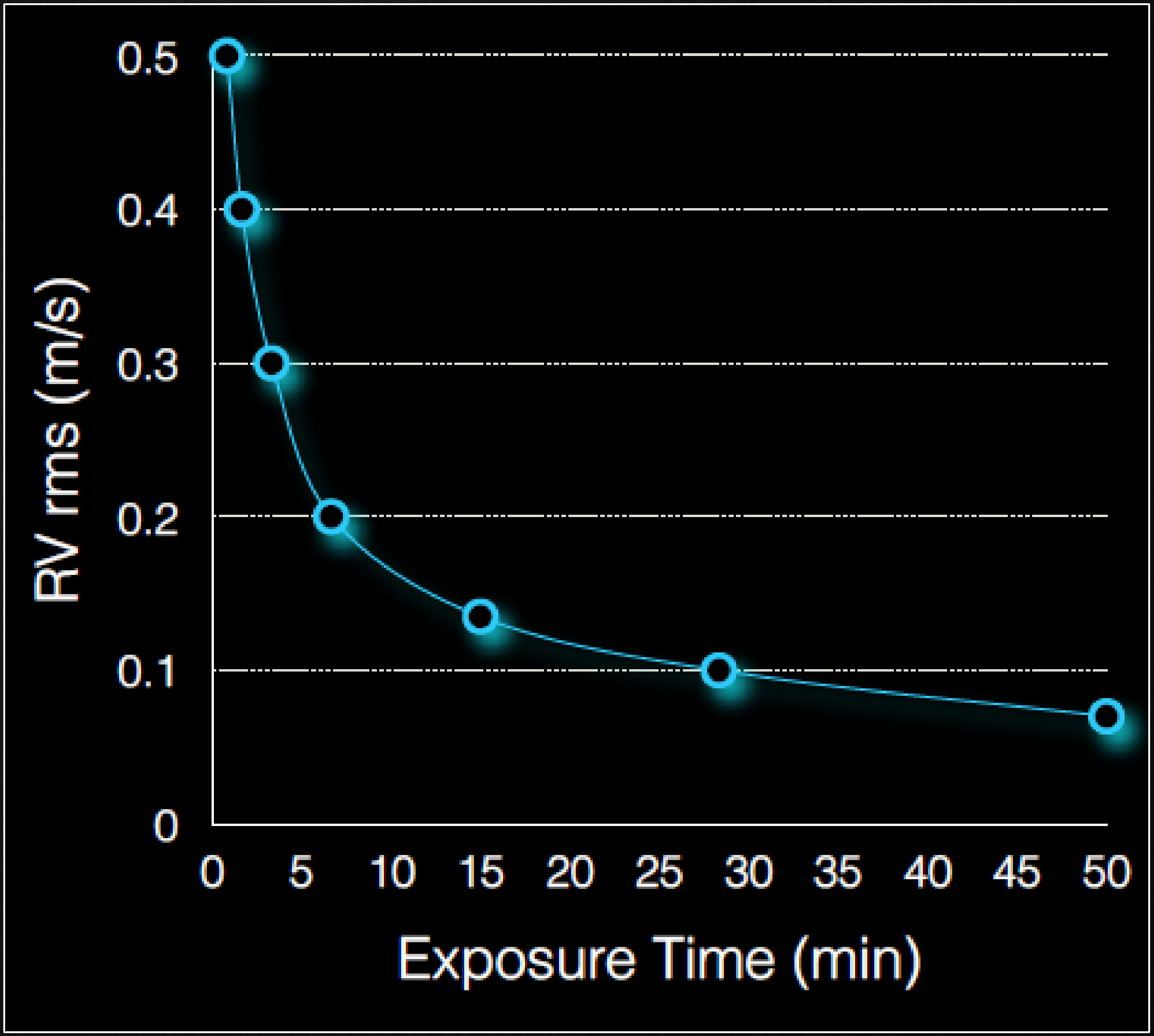

Dumusque+2011

Stellar oscillation in photometry

Time scale: 4-10 min
Flux amplitude: 100-300 ppm

Kepler-36c

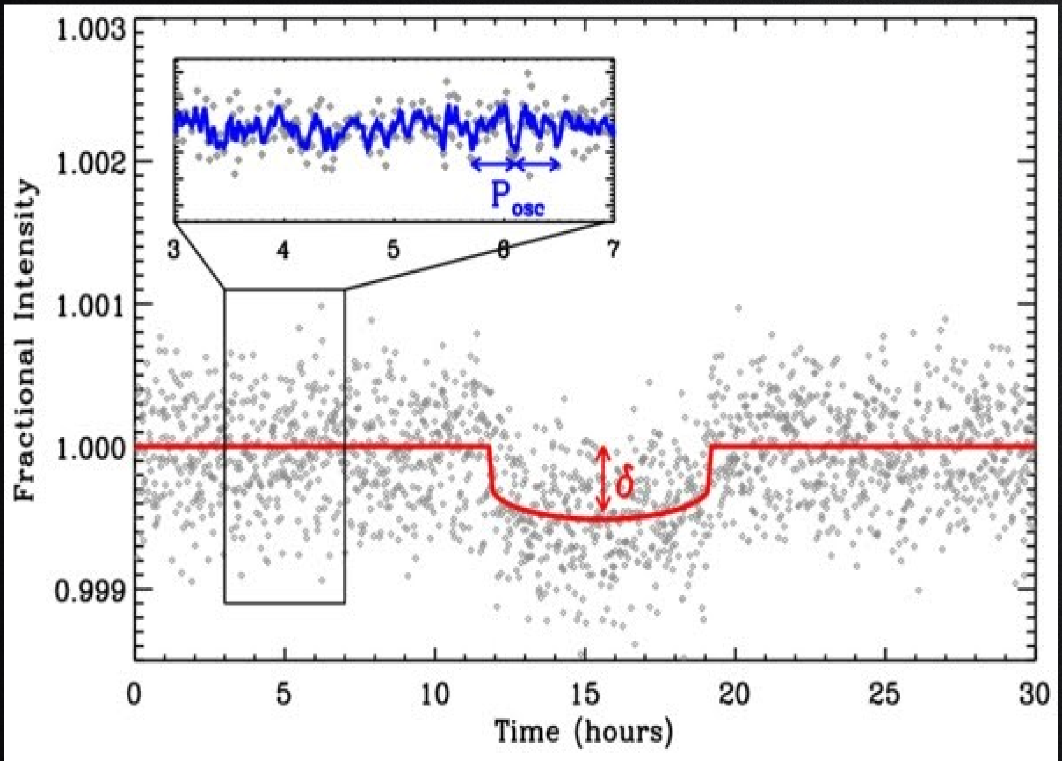

Carter+2012

Sun

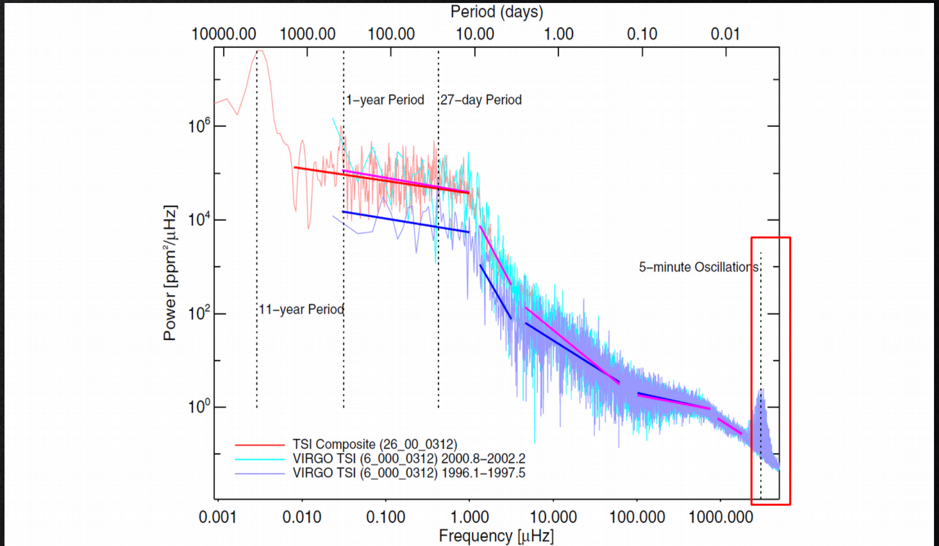

Fig. 12. Shown is the power spectrum of the composite record of daily total solar irradiance for the period from 1978 until 2002 (red). To illustrate the solar cycle variability in the frequency domain, the power spectra of data from VIRGO during solar minimum (Feb. 1996–Aug. 1997) are compared to that of solar maximum (Oct. 2000–Feb. 2002). The solar cycle influence is evident in the differences in power at low frequencies

Frohlich & Lean (2004)

Stellar oscillation in photometry

The Kepler space telescope data were obtained on short cadence (1 minute) and long cadence (30 minutes) integration time.

Kepler-37 b, c , d

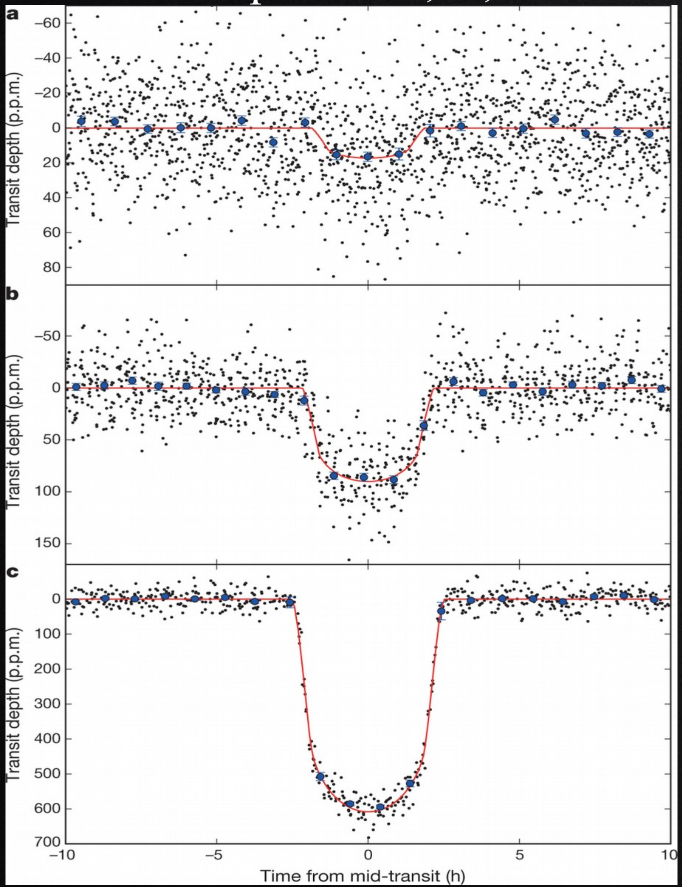

Barclay+2013

Kepler-432b

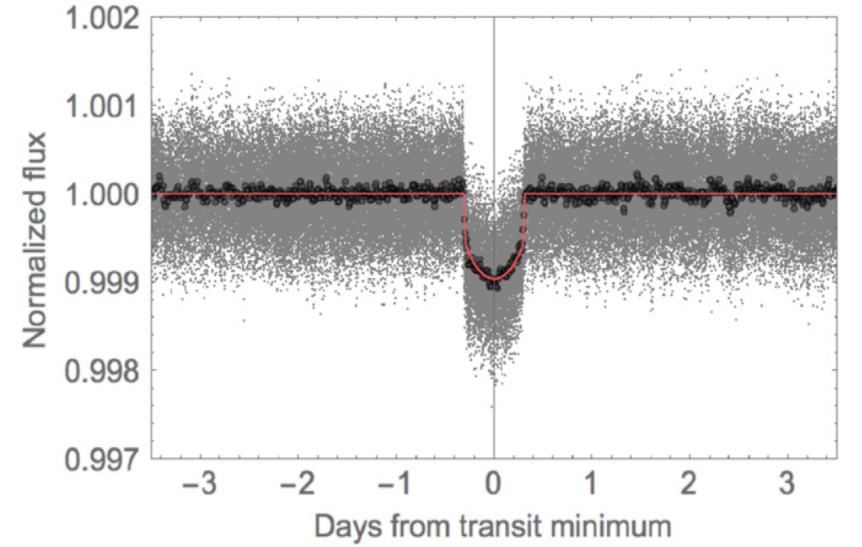

Figure 2. Folded short-cadence *Kepler* light-curve, shown as gray points. For clarity, the binned data (every 100 points) are overplotted as large dark circles, and the best fit, with parameters reported in Table 1, is indicated by the solid red line.

Quinn+2015

Convective zone

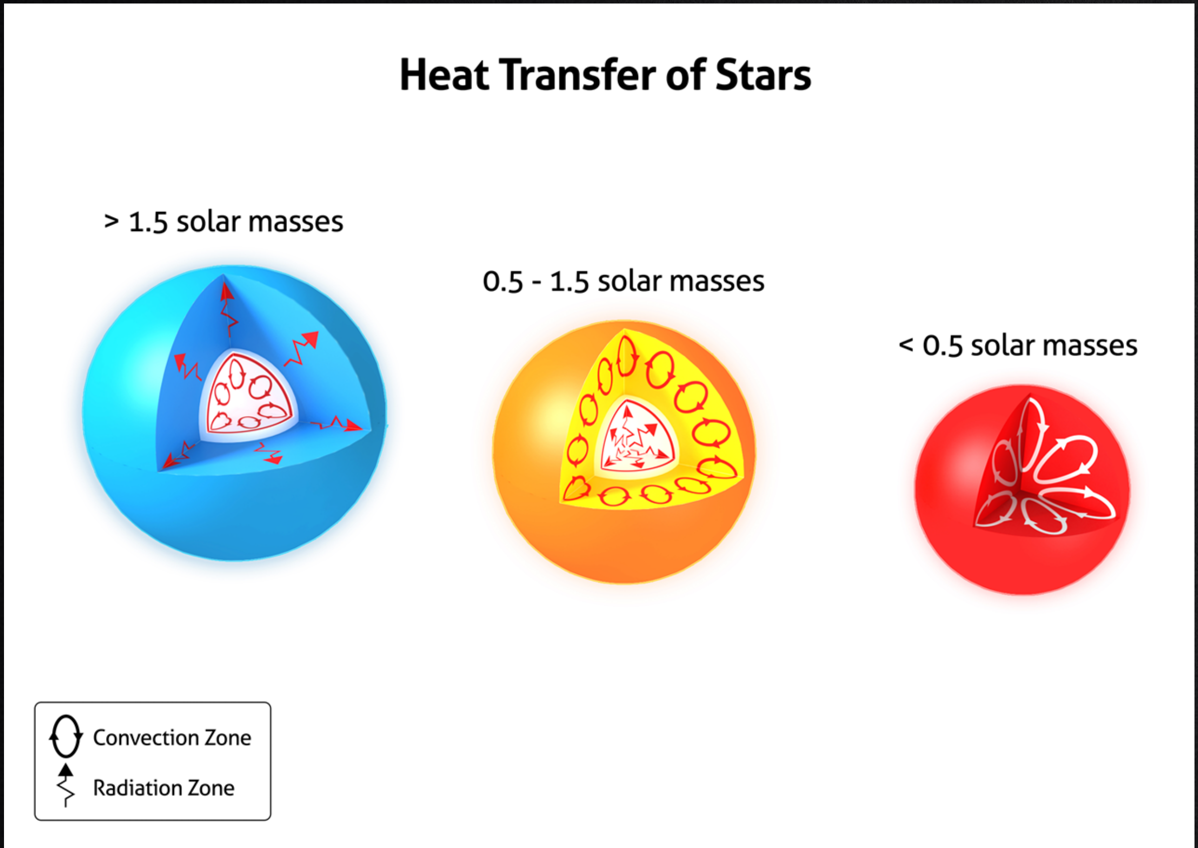

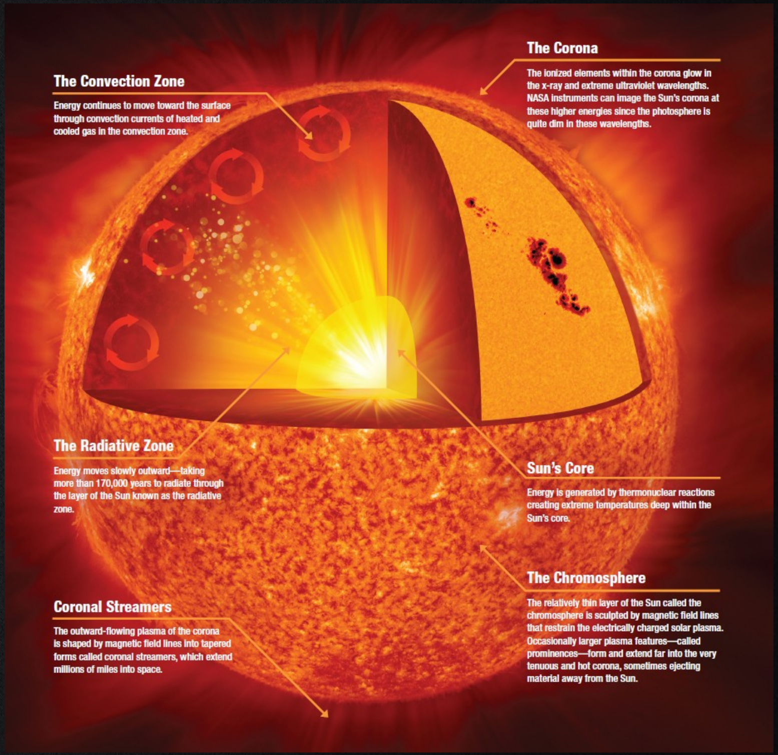

Granulation

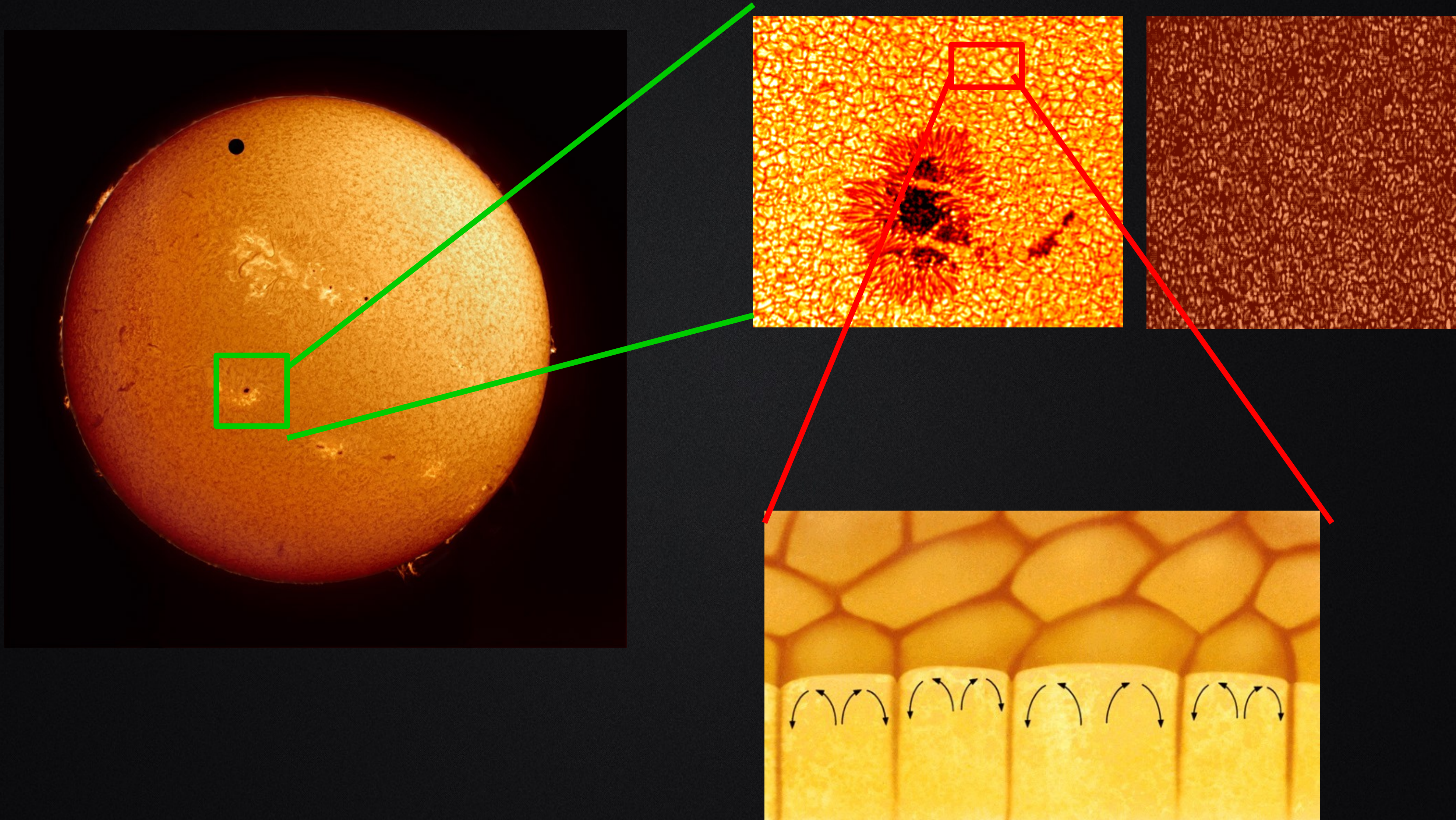

Granulation in RV

$$P(\nu) = \sum_{i=1}^{3} \frac{A_i}{1 + (B_i \nu)^{C_i}}$$

SG = supergranulation, MG = mesogranulation, G = granulation

Star	A_{SG}	B_{SG} [h]	C_{SG}	A_{MG}	B_{MG} [h]	C_{MG}	A_G	B_G[min]	C_G
β Hyi	0.055	24.3	4.3	0.021	3.4	4.0	11.6×10^{-3}	72.8	5.0
μ Ara	0.029	13.0	6.0	0.027	3.4	5.0	1.1×10^{-3}	43.8	4.5
α Cen A	0.027	7.4	3.1	0.003	1.2	3.9	0.3×10^{-3}	17.9	8.9
τ Ceti	0.027	6.7	2.6	0.002	1.2	8.9	0.3×10^{-3}	18.5	19.8
α Cen B	0.002	12.0	4.8	0.001	0.7	4.4	0.1×10^{-3}	8.9	7.5

Time scale: 10min -24 hours
RV amplitude: 1-30 m/s

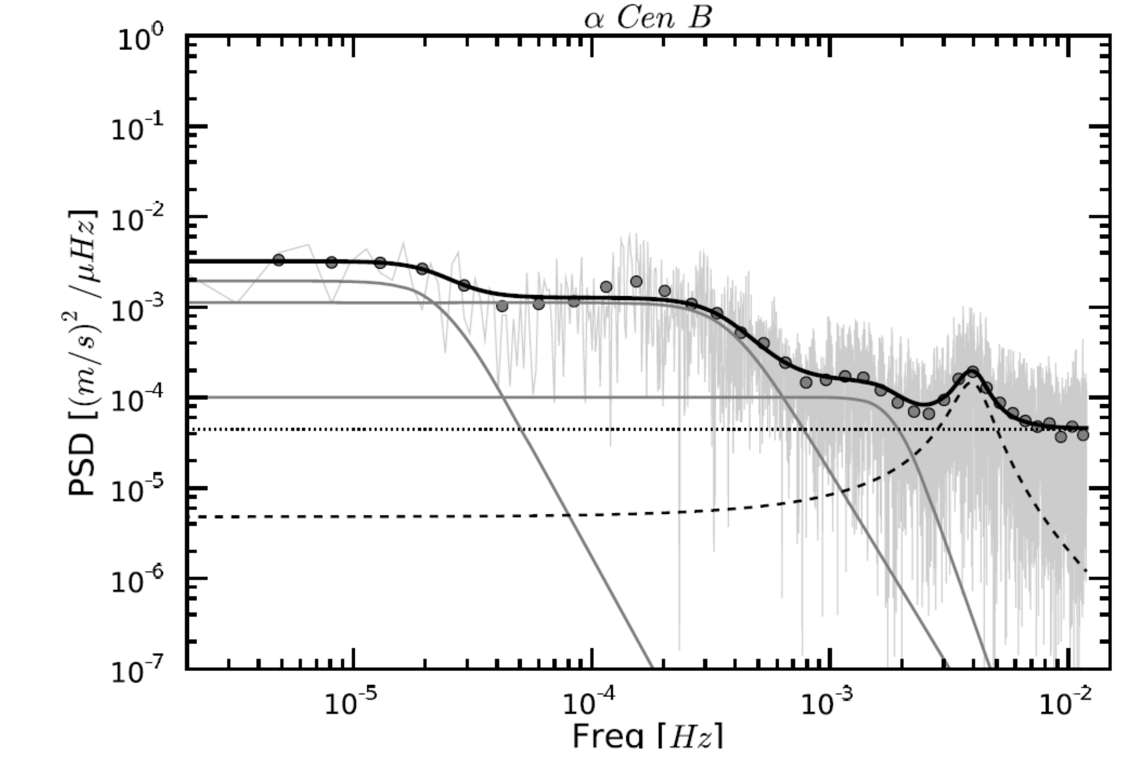

Dumusque+2011

Granulation in RV

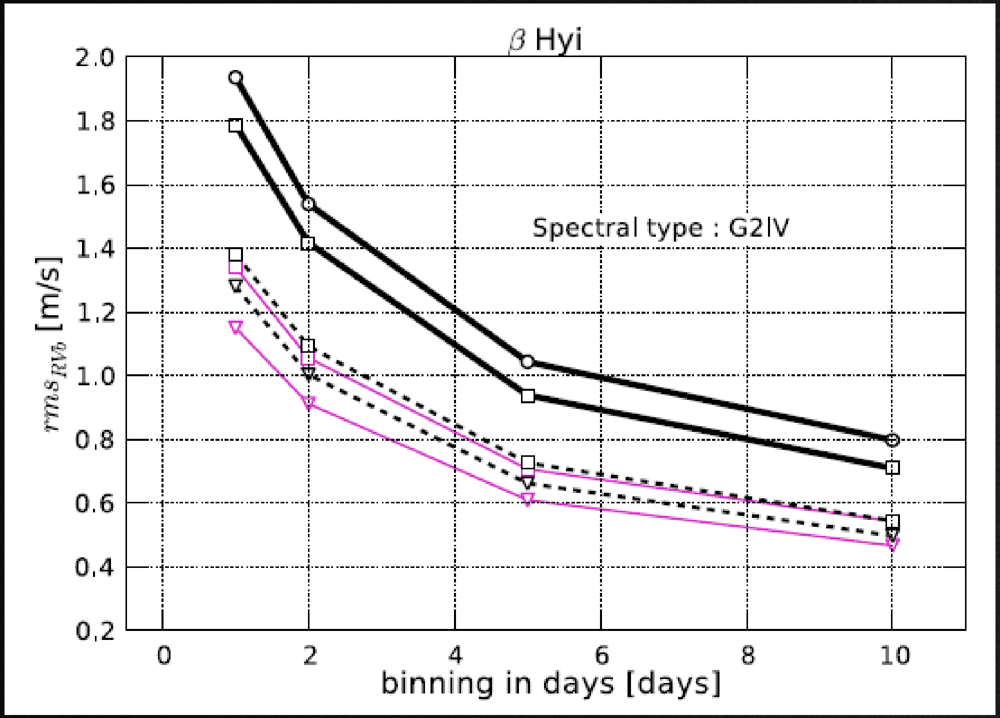

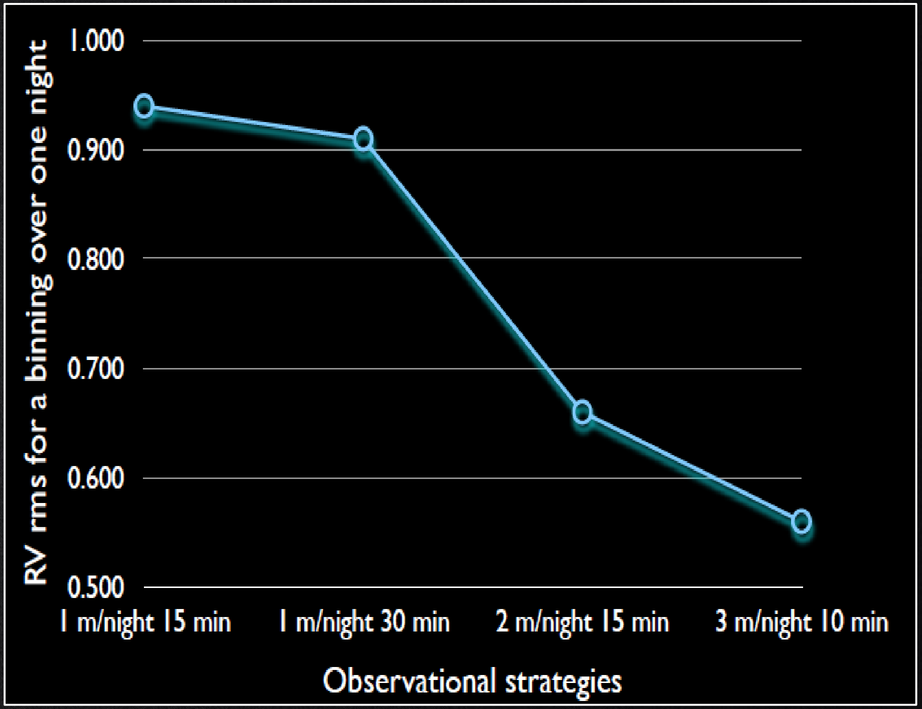

Dumusque+2011

$$RV(t_i) = \sum_{\nu} \sqrt{\mathrm{VPSD}(\nu)}(\sin(2\pi\nu t_i + phase(\nu))),$$

Granulation in photometry

$$\tau_{\rm gran} \propto \frac{1}{\nu_{\rm ac}} \propto \frac{1}{\nu_{\rm max}},$$

$$\sigma_{\rm gran} \propto \nu_{\rm max}^{-0.5}$$

$$\nu_{\rm max} \propto M R^{-2} T_{\rm eff}^{-0.5}$$

$$\tau_{\rm gran} = 220 \left(\frac{M}{M_\odot}\right)^{-1} \left(\frac{R}{R_\odot}\right)^{2} \left(\frac{T_{\rm eff}}{T_{\rm eff,\odot}}\right)^{0.5} \ {\rm s},$$

$$\sigma_{\rm gran} = 75 \left(\frac{M}{M_\odot}\right)^{-0.5} \left(\frac{R}{R_\odot}\right) \left(\frac{T_{\rm eff}}{T_{\rm eff,\odot}}\right)^{0.25} \ {\rm ppm},$$

Kjeldsen & Bedding-11
Chaplin+11

Gilliland+11

Granulation in photometry

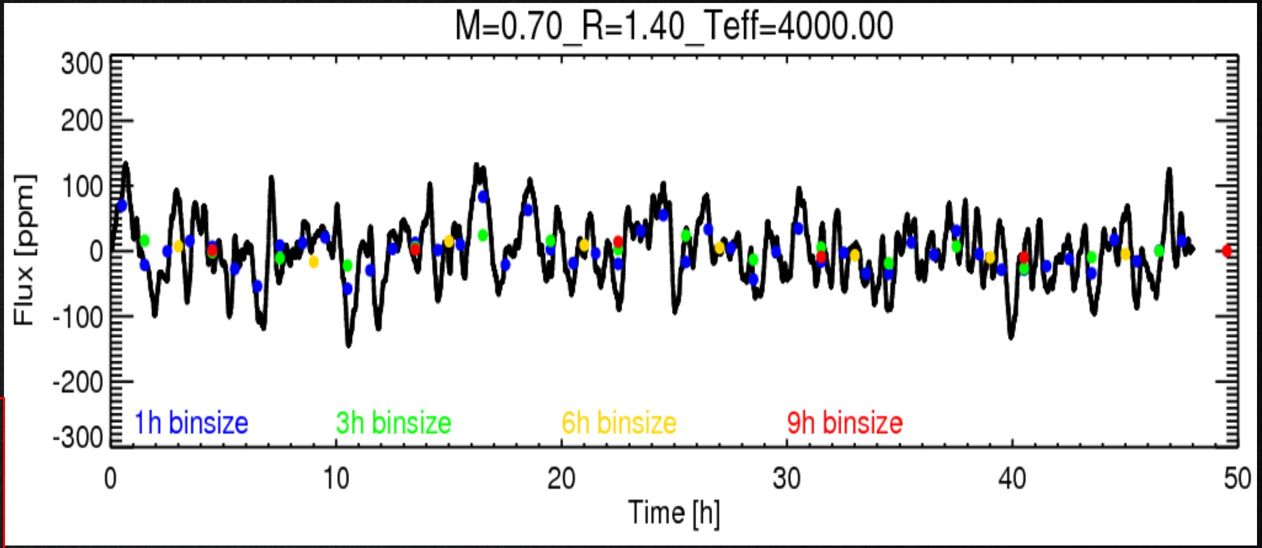

Time scale: 10min -24 hours
Flux amplitude:50-500 ppm

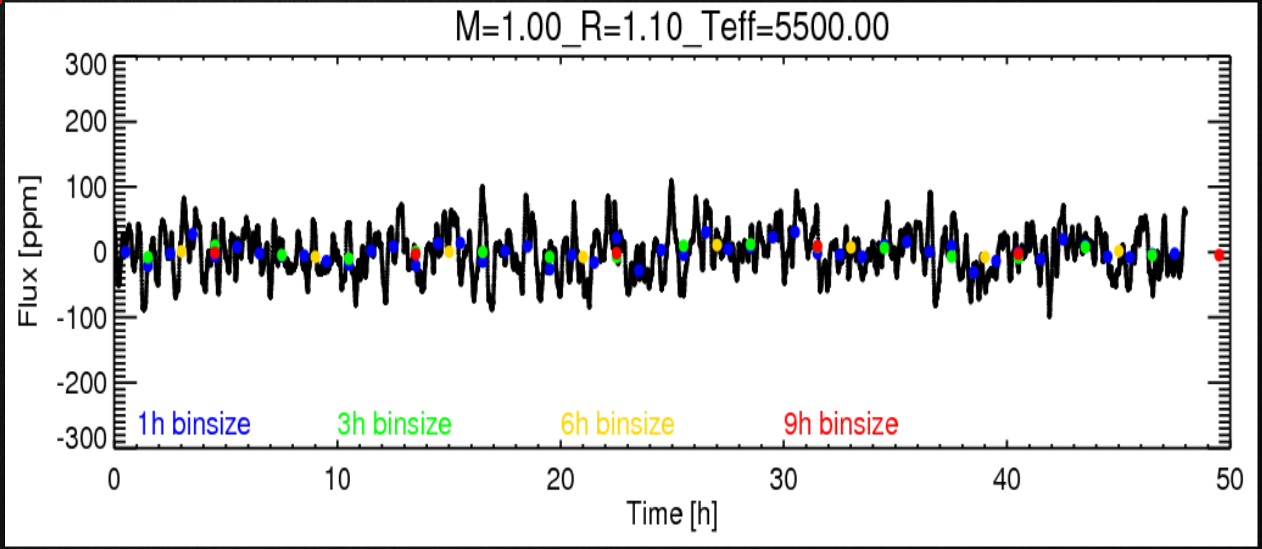

Stellar activity

“Stellar Activity” is a collective name used to describe a group phenomena which generate the variability observed in the outer atmospheres of late type-stars mainly due to the presence of highly structured magnetic fields emerging from the convective envelope, namely **spots**, **plage**, facula, flares.

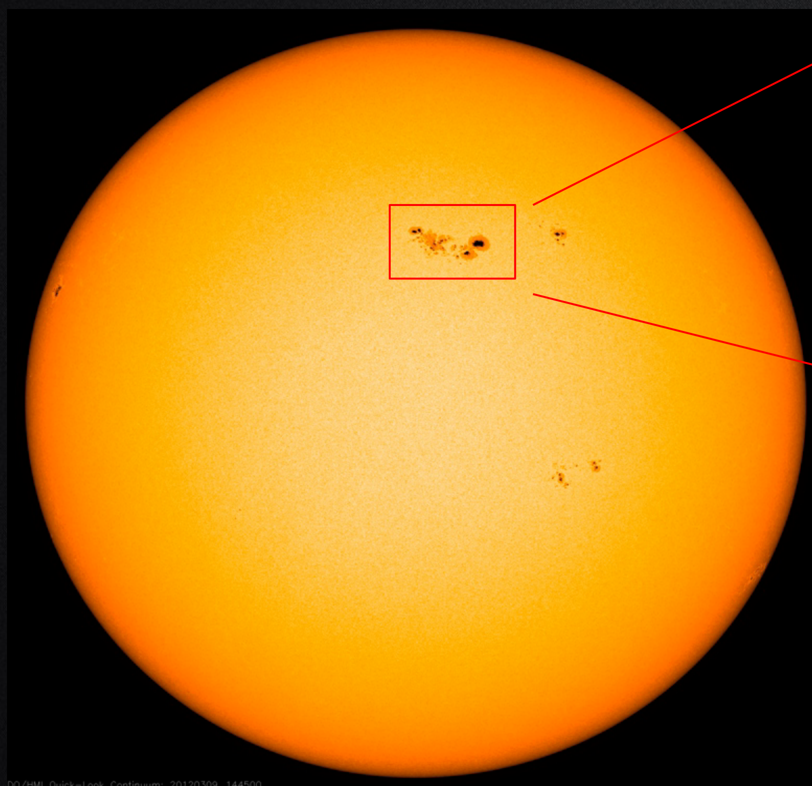

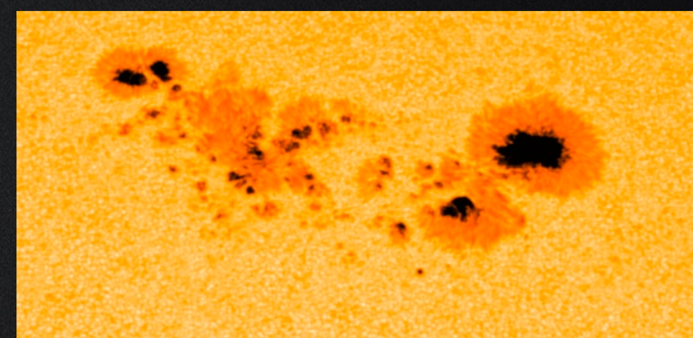

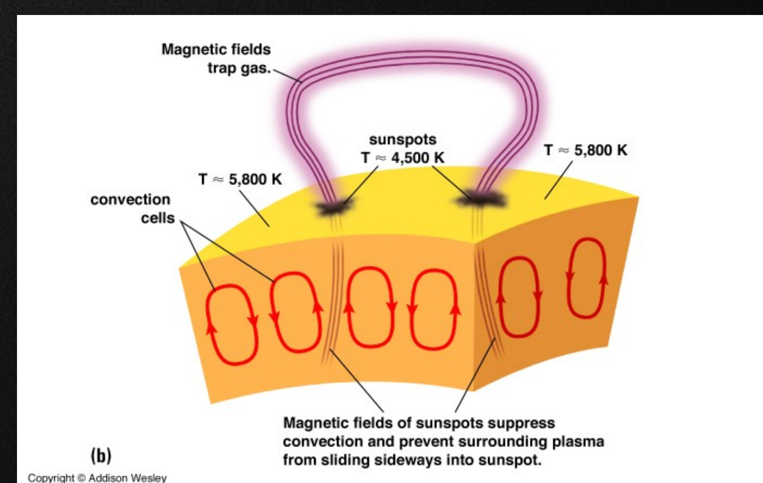

Stellar activity

About 33% of stars in Kepler field of view are more active than the Sun at its maximum activity cycle.

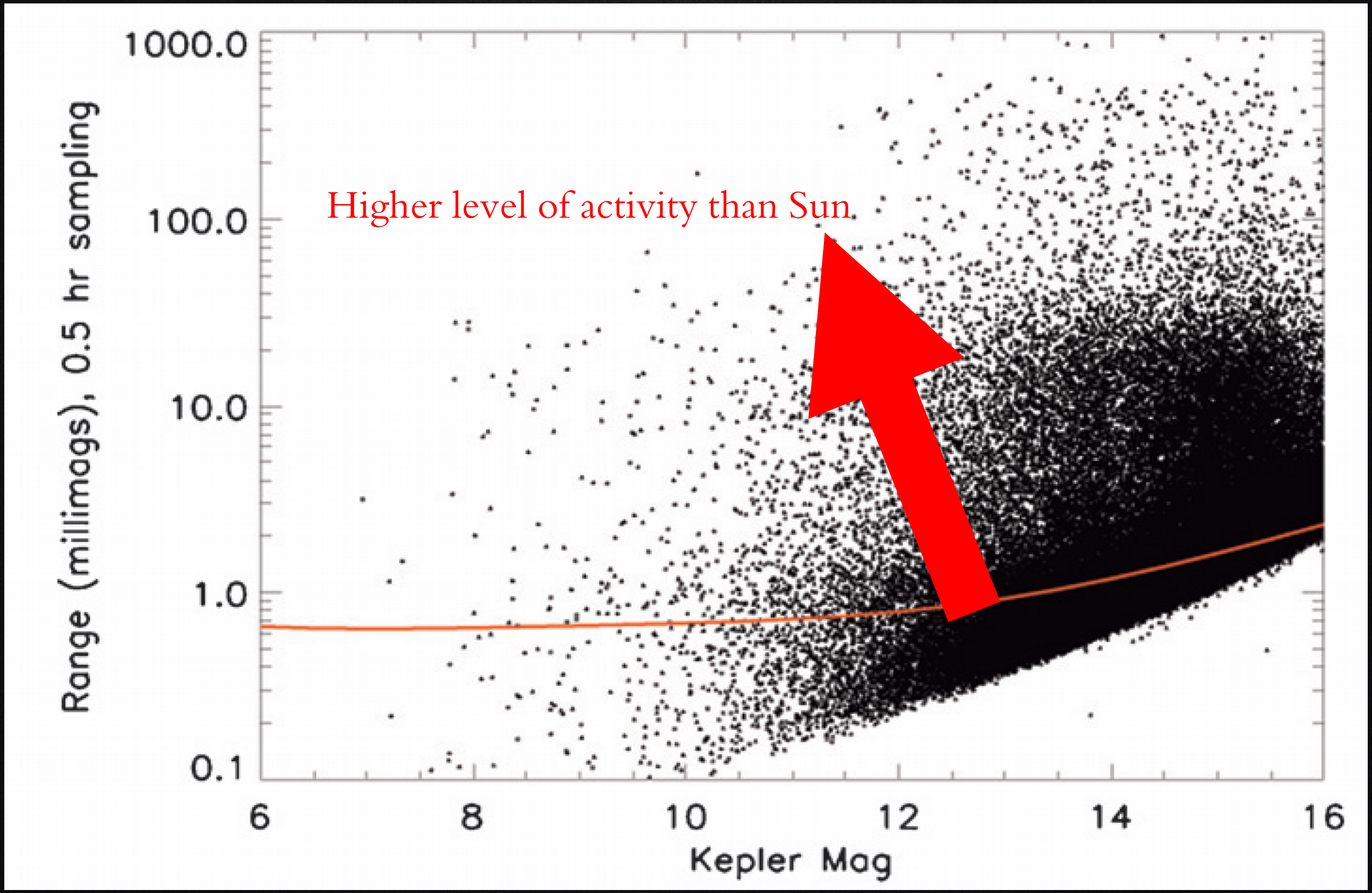

Basri+13

Stellar active regions properties

Stellar spot's temperature contrast

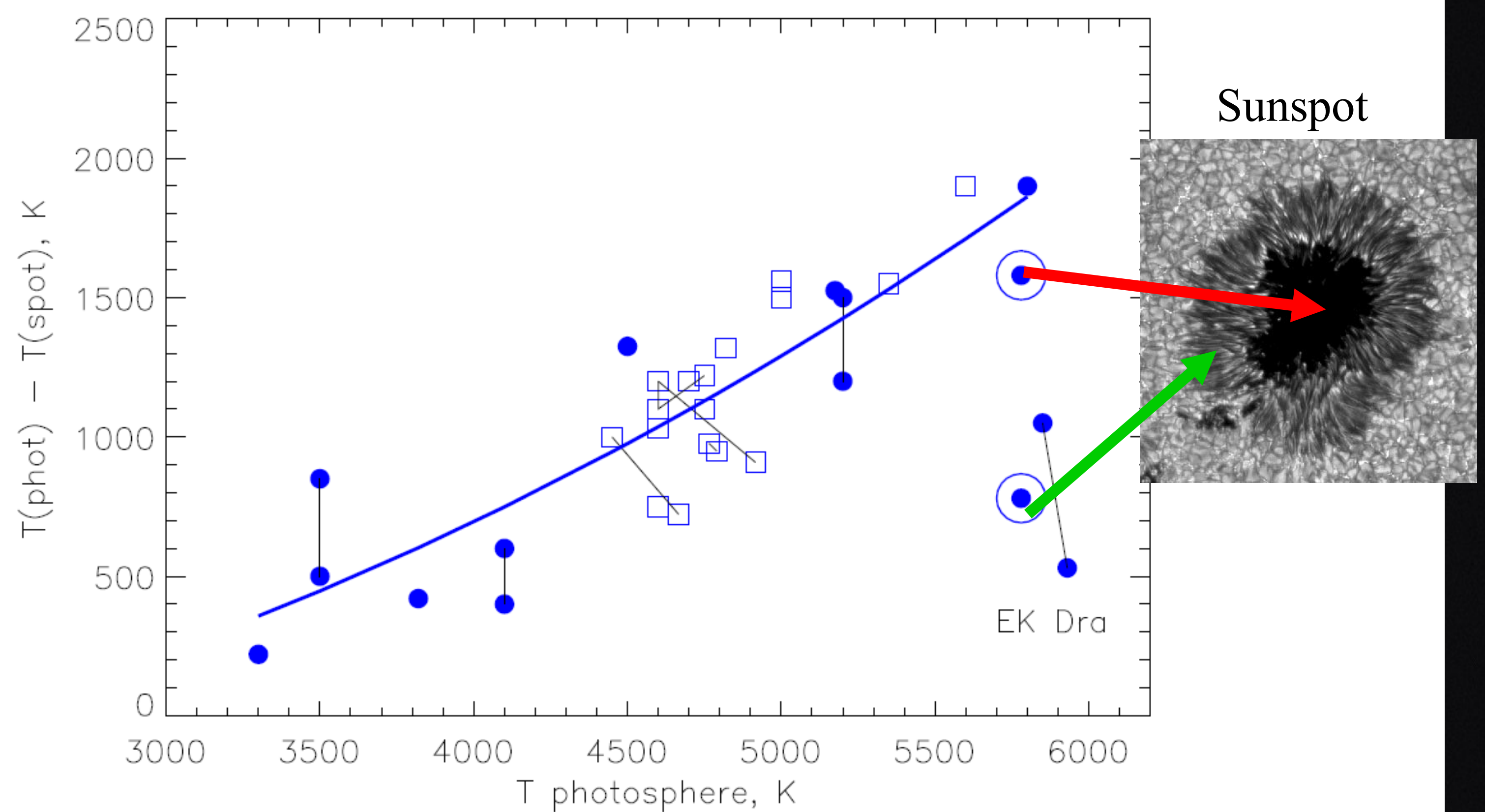

Figure 7: Spot temperature contrast with respect to the photospheric temperature in active giants (squares) and dwarfs (circles). Thin lines connect symbols referring to the same star. The thick solid line is a second order polynomial fit to the data excluding EK Dra. Dots in circles indicate solar umbra ($\Delta T = 1700$ K) and penumbra ($\Delta T = 750$ K) (based on data in Table 5).

Berdyugina, 2005

Center to limb temperature contrast

Sunspot shows limb darkening behavior which mean Sunspot on the center of sun has maximum temperature contrast and on Sun's limb show minimum temperature contrast.

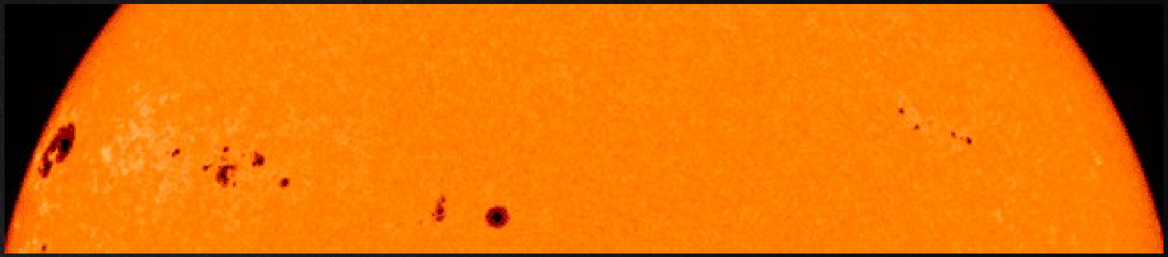

Sun'plage shows limb brightening behavior, which is opposite to the Sunspot behavior.

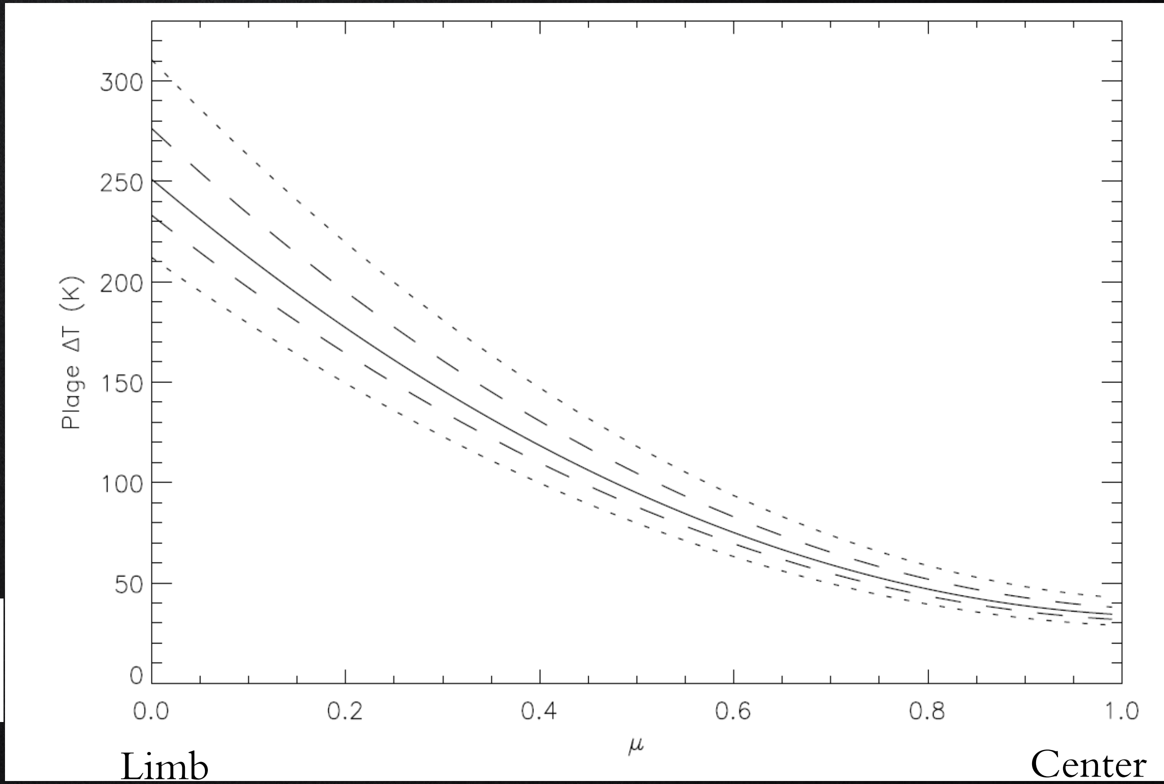

$$\Delta T_P = 250.9 - 407.7\cos\theta + 190.9\cos^2\theta,$$

$$\mu = \cos\theta$$

Meunier+2010

Size of Sunspots and plages

Sunspot' filling factor varies in the range of minimum of 0.01% and **maximum of 1%**.

$$f = \frac{A_{spot}}{A_{star}} = \left(\frac{R_{spot}}{R_*}\right)^2$$

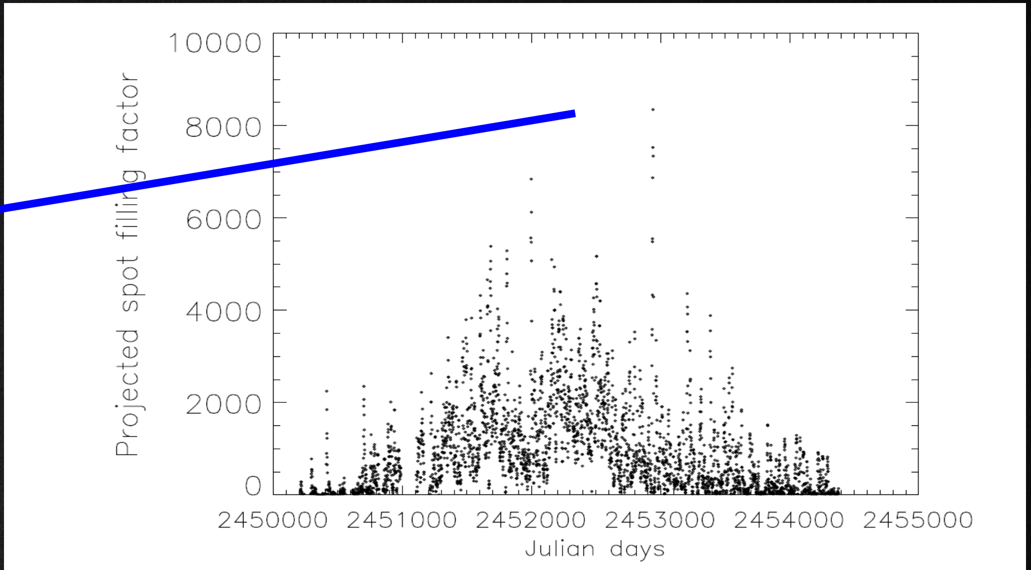

Sun's plage filling factor varies in the range of minimum of 0.25%, and **maximum of 6%.**

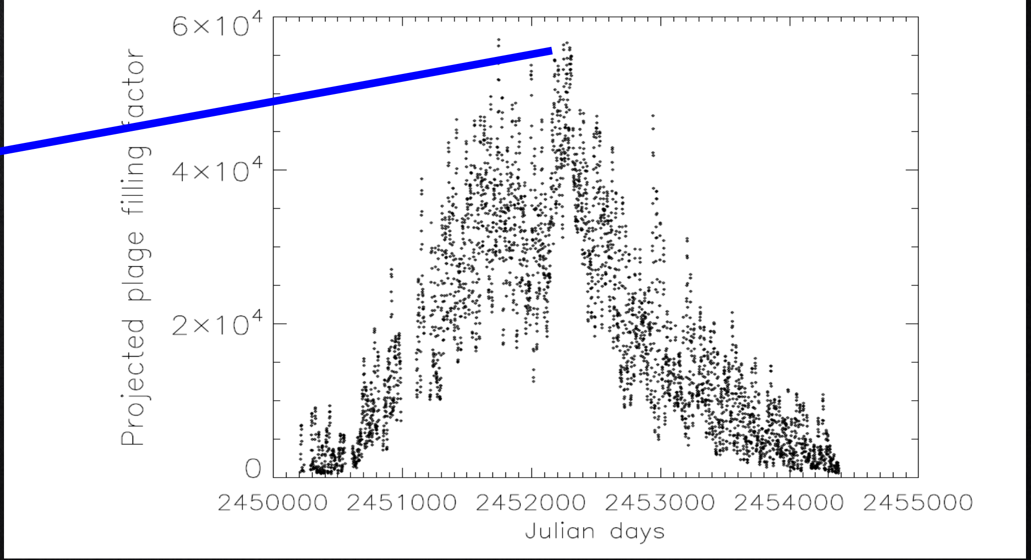

Meunier+2010

Sunspot size distribution

Smaller sunspots are more common than larger ones.

$$\frac{dN}{dA} = \left(\frac{dN}{dA}\right)_m \mathrm{Exp}\left[-\frac{(lnA - ln\langle A\rangle)}{2ln\sigma_A}\right],$$

where $\left(\frac{dN}{dA}\right)_m = 9.4$ is the maximum that the distribution will reach, $\sigma_A = 4$ is the width of the log-normal distribution, and $\langle A\rangle = 0.55$ is the mean sunspot area (in units of $10^{-6}A_{\frac{1}{2}\odot}$) (Bogdan et al., 1988). The log-normal fit to the data

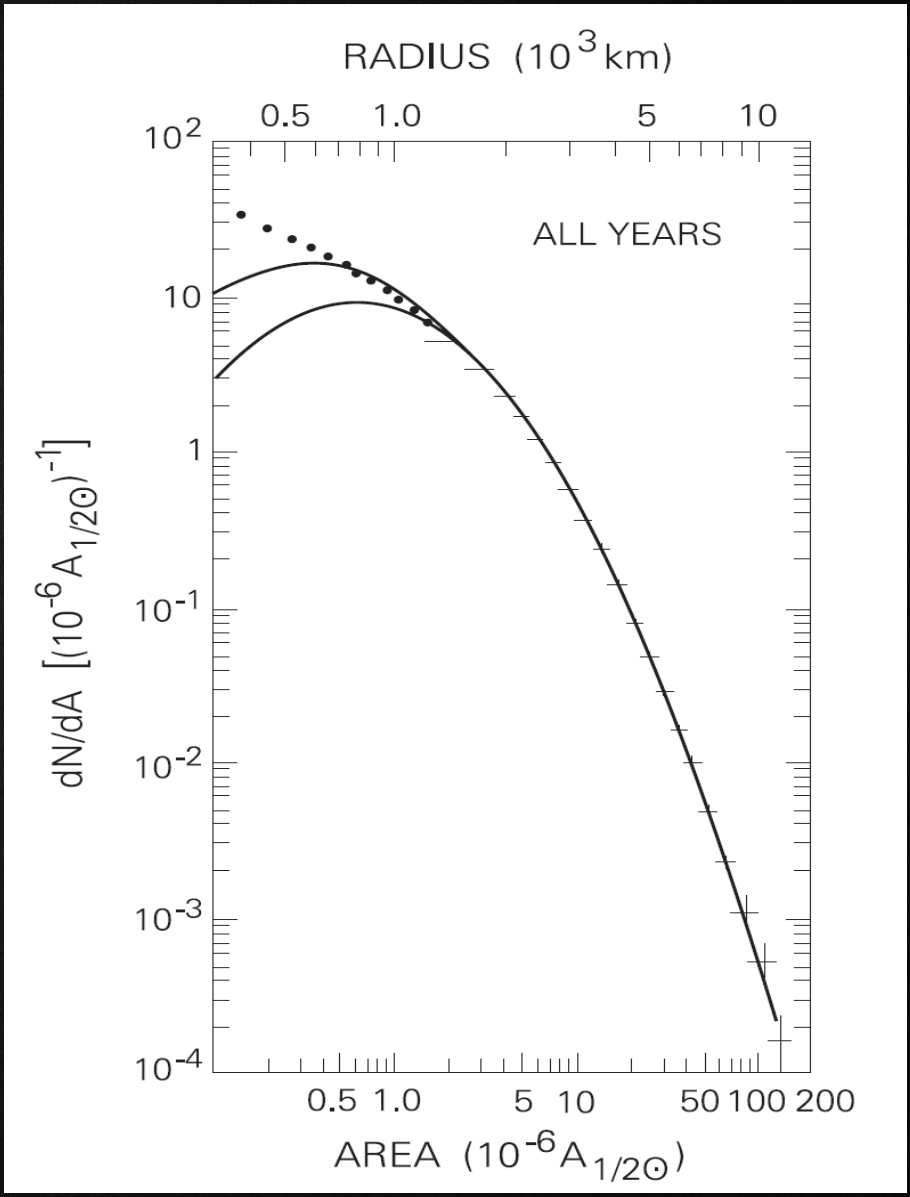

Bogdan + 1988, Solanki, 2003

Size and temperature contrast

Smaller sunspots or plages show higher temperature contrast.

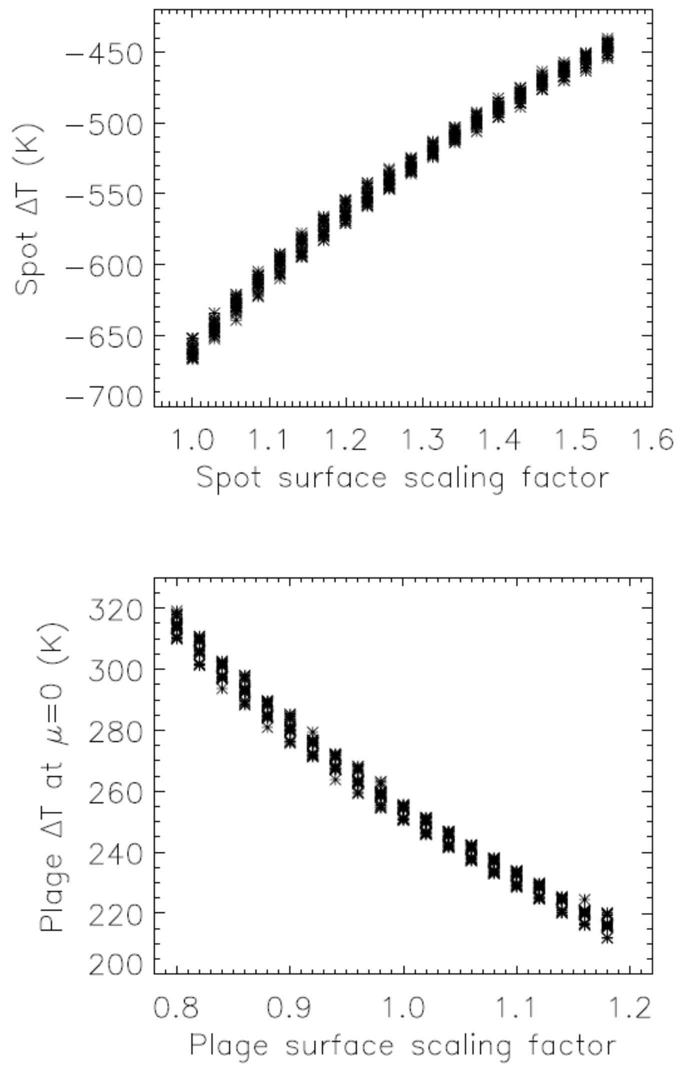

Fig. 4. *Upper panel*: spot temperature deficit versus the spot-surface scaling factor for the explored range of scaling factors (see text for details). For a given spot-surface scaling factor, the various points correspond to different plage-surface scaling factors. *Bottom panel*: same for plages at $\mu = 0$.

Meunier+2010

Stellar spot's size

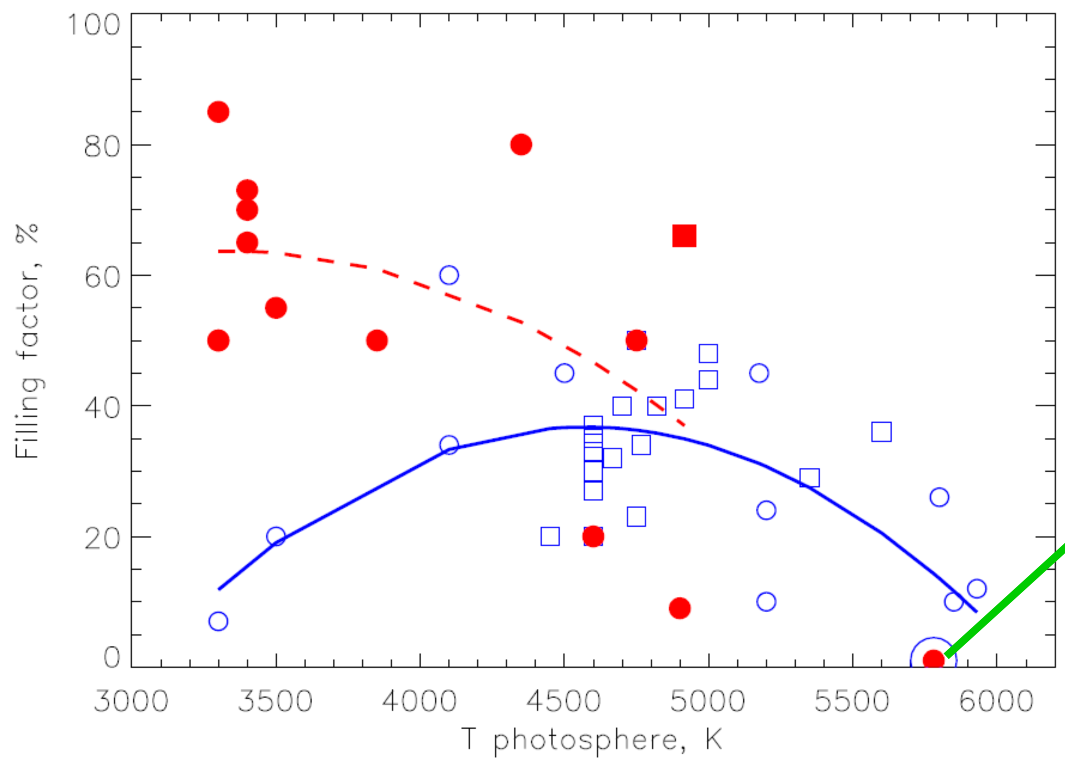

Sunspot

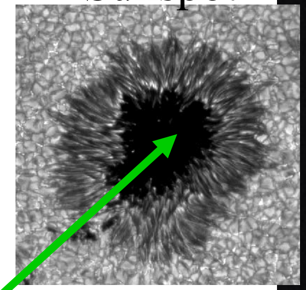

Figure 10: Filling factors of spots (open symbols) and magnetic fields (filled symbols) on the surfaces of active dwarfs (circles) and giants (squares) versus the photosphere temperature. The thick solid line is a polynomial fit to the spot filling factors. The dashed line is a fit to the magnetic field filling factor, excluding the Sun. A big circle emphasises the sunspot umbra ($f \sim 1\%$) (based on data in Tables 5 and 6).

Meunier+2010

Huge stellar spots

Huge stellar spots mostly appear on the stellar pole, which can suggest different mechanism for their formation than the normal spots.

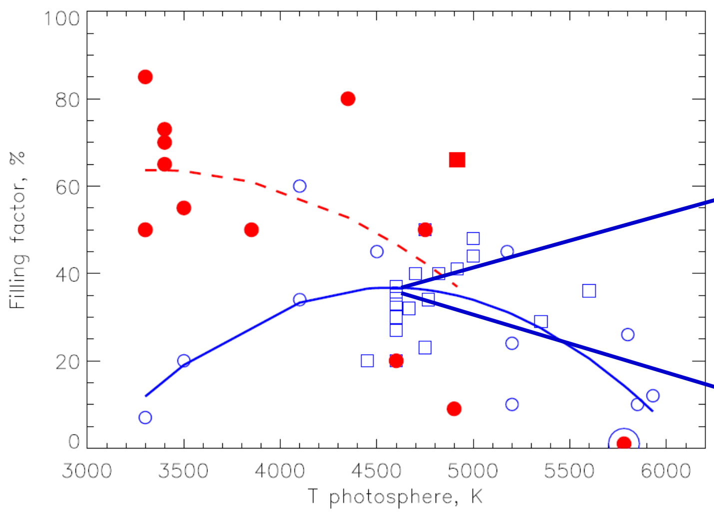

Figure 10: Filling factors of spots (open symbols) and magnetic fields (filled symbols) on the surfaces of active dwarfs (circles) and giants (squares) versus the photosphere temperature. The thick solid line is a polynomial fit to the spot filling factors. The dashed line is a fit to the magnetic field filling factor, excluding the Sun. A big circle emphasises the sunspot umbra ($f \sim 1\%$) (based on data in Tables 5 and 6).

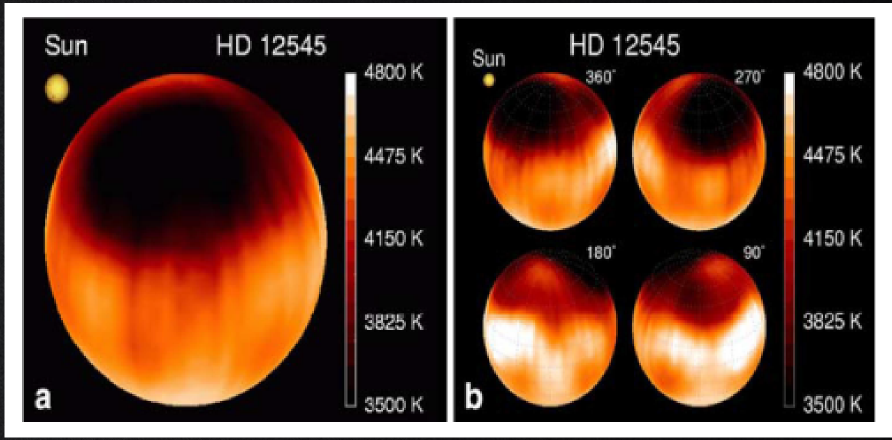

Strassmeier (1999).

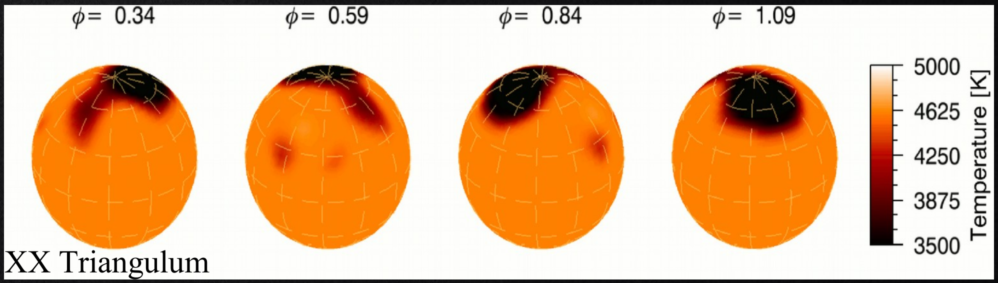

Künstler 2015

Sunspot’s lifetime

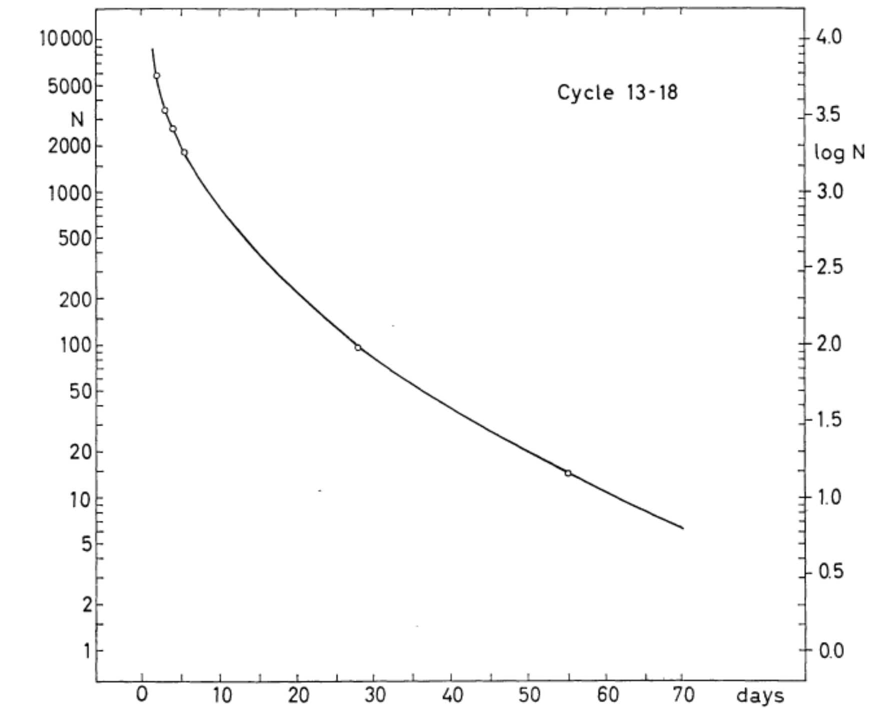

Fig. 1. The number of sunspot groups as a function of lifetime. Cycles 13–18.

Lifetimes of spots are proportional to their sizes:

$$T_{life} = \frac{A}{W},$$

Gnevyshev-Walldemeier law

$$W = 10.89 \pm 0.18 \text{ which is in units of } 10^{-6} A_{\frac{1}{2}\odot} day^{-}$$

Sunspot's latitude

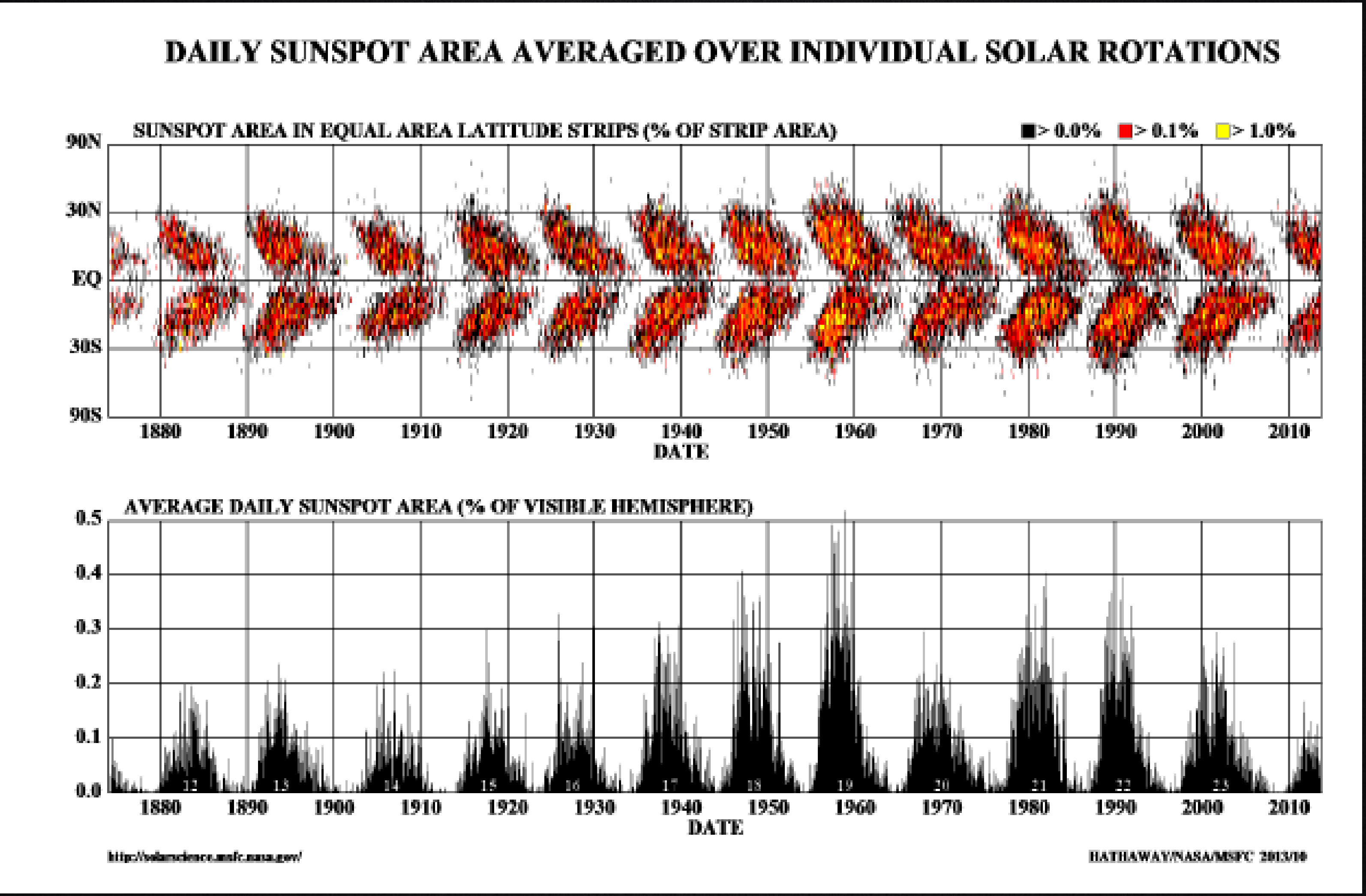

Active longitude

There is not a specific longitudinal distribution for Sun spots, Furthermore, it has been noticed that spots tend to appear more frequently at some longitudes, with respect to others, called "active longitudes" and they increase in number from zero at the solar minimum to maximum, with even four and more active longitudes (Malik & Bohm, 2009).

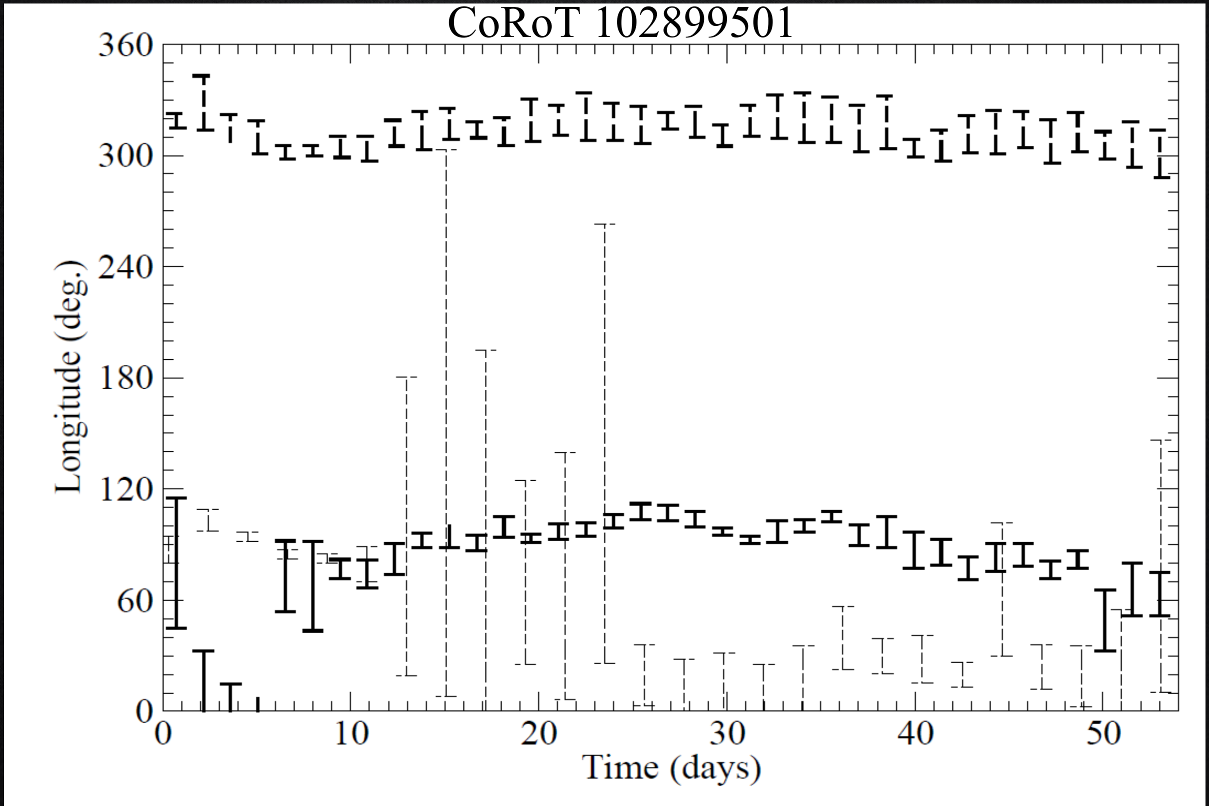

Gondoin+2012

Impact of stellar active region on RV

What happens to the CCF of a rotating star if a portion of its surface becomes dark?

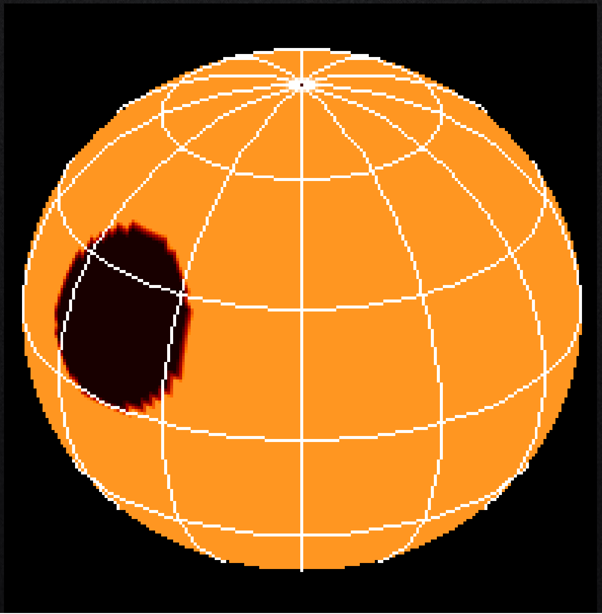

What happens to the CCF of a rotating star if a portion of its surface becomes dark?

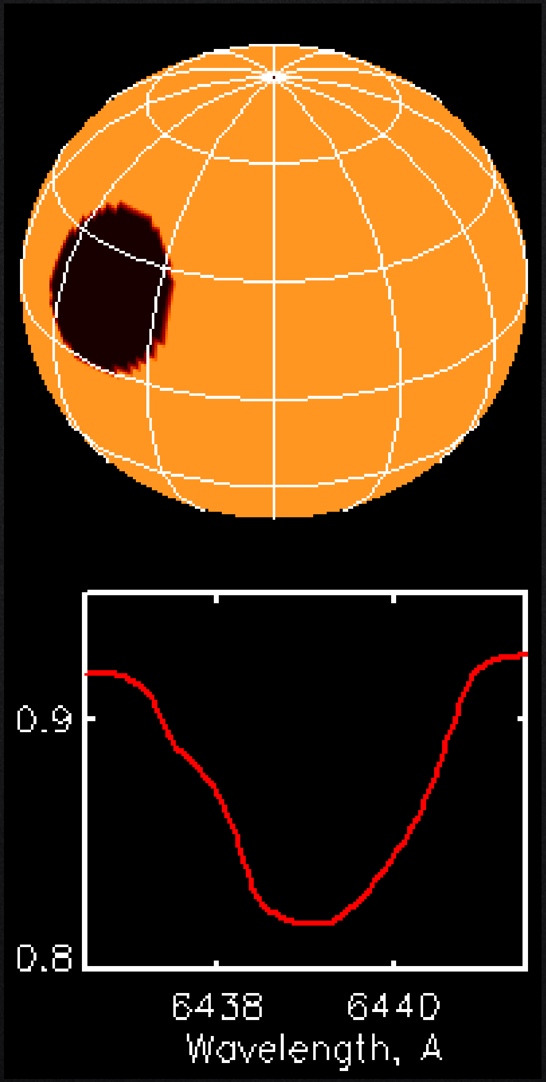

Stellar active region (contrast+rotation)

CCF (mean line of the spectra) fitted with a Gaussian to estimate the RV.

Active regions deform the CCF and thus induce variations on the RV periodically.

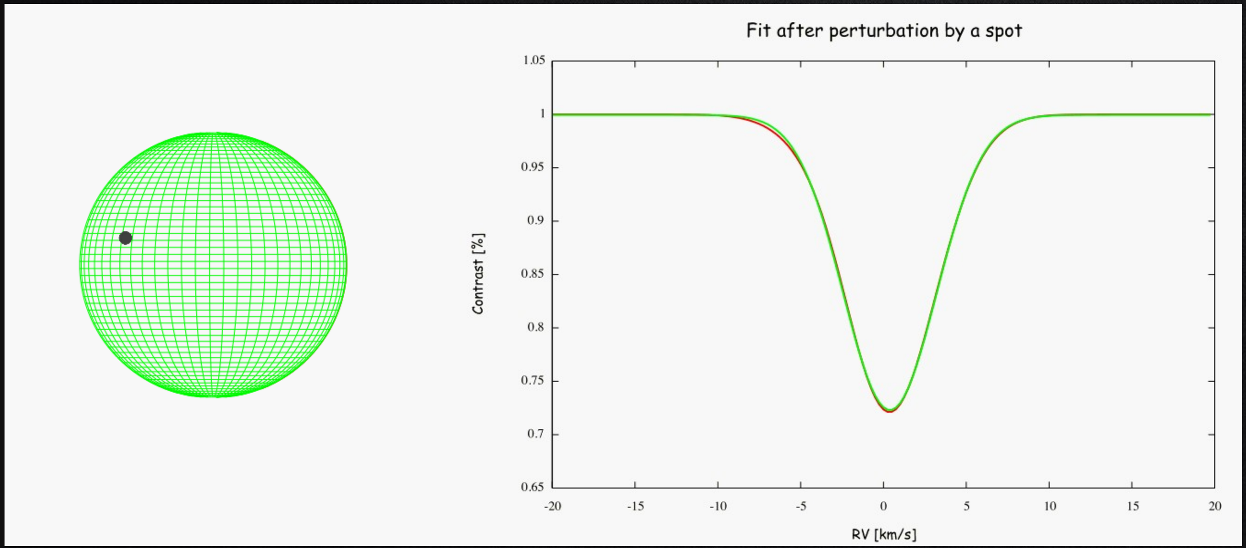

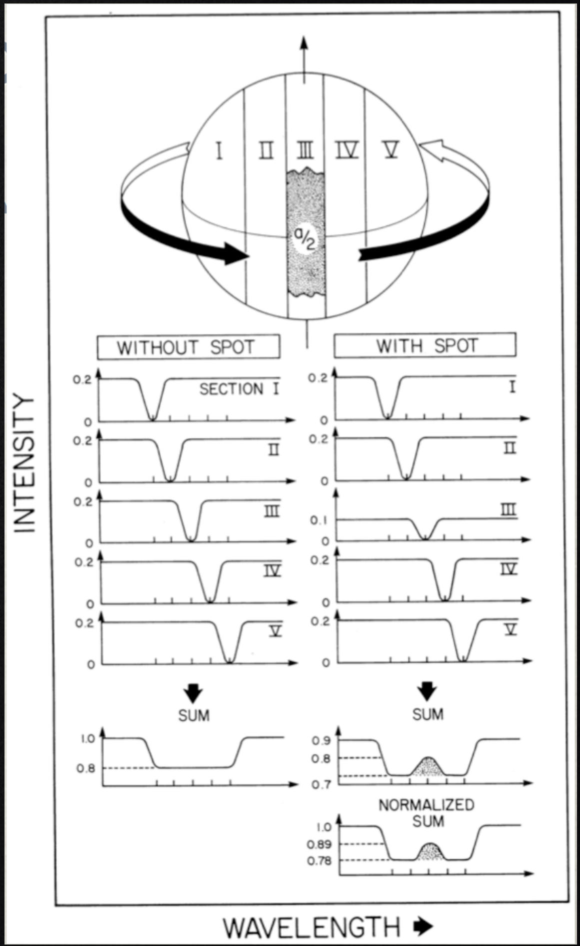

Vogt & Penrod 1983

Stellar active region (contrast+rotation)

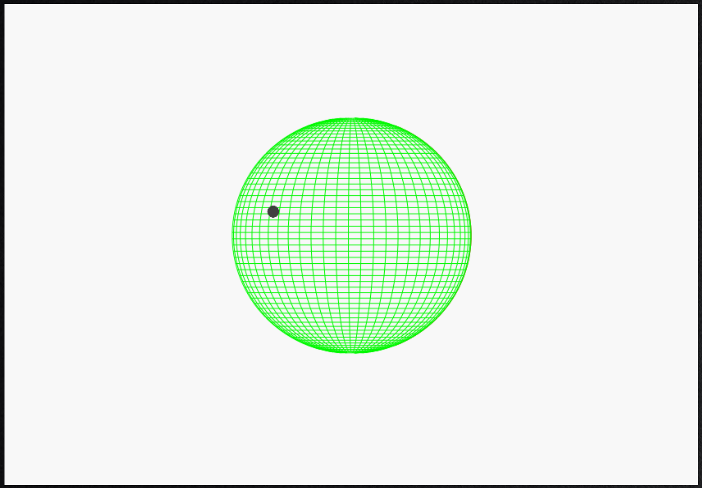

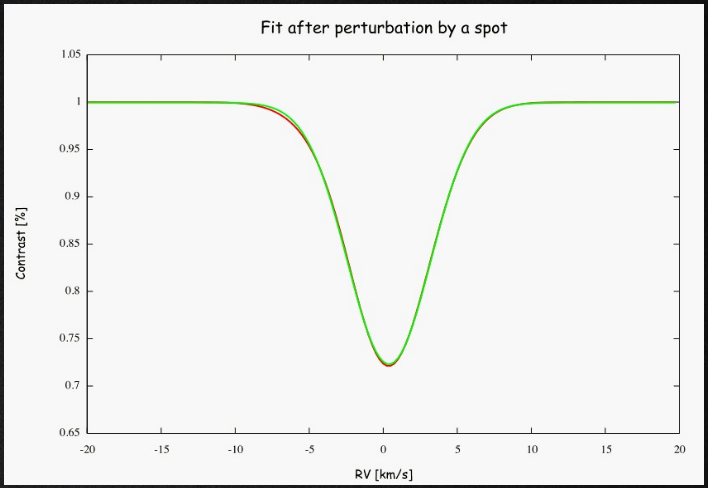

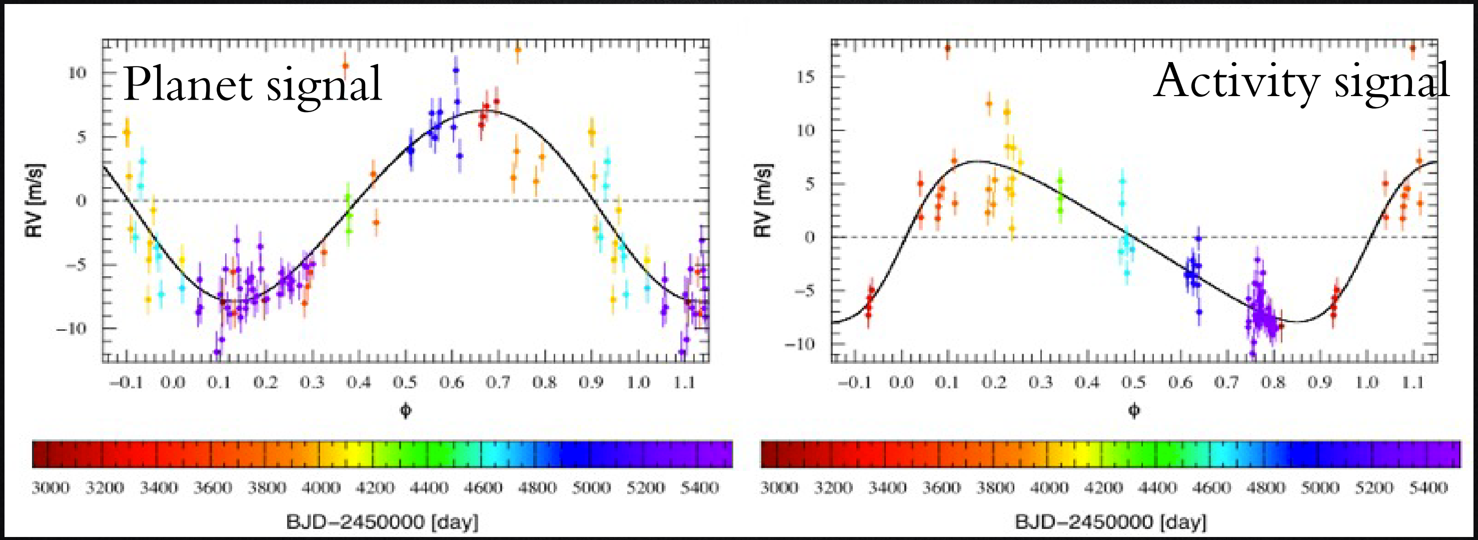

Dumusque+2011

Stellar active region (Inhibition of convective blueshift)

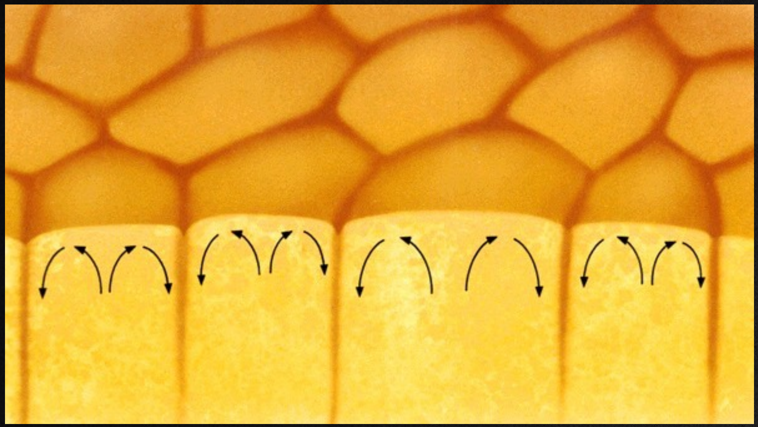

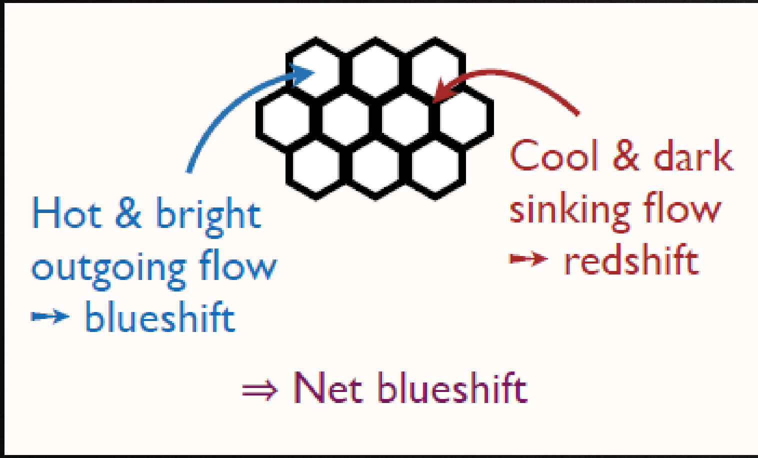

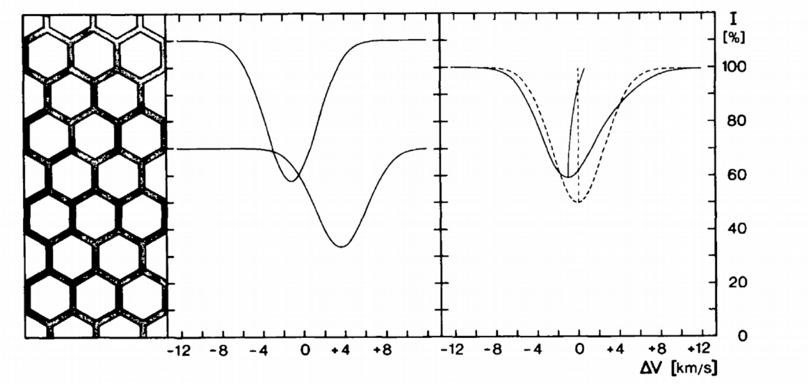

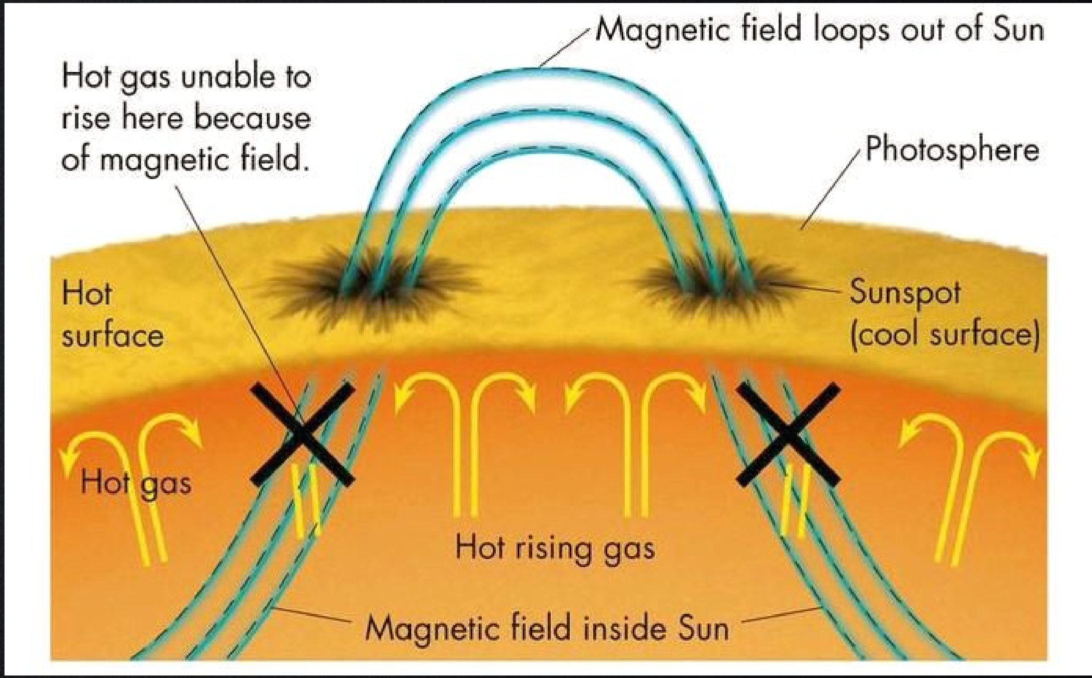

Dravins-1981

Stellar active region (total)

Contrast+Rotation

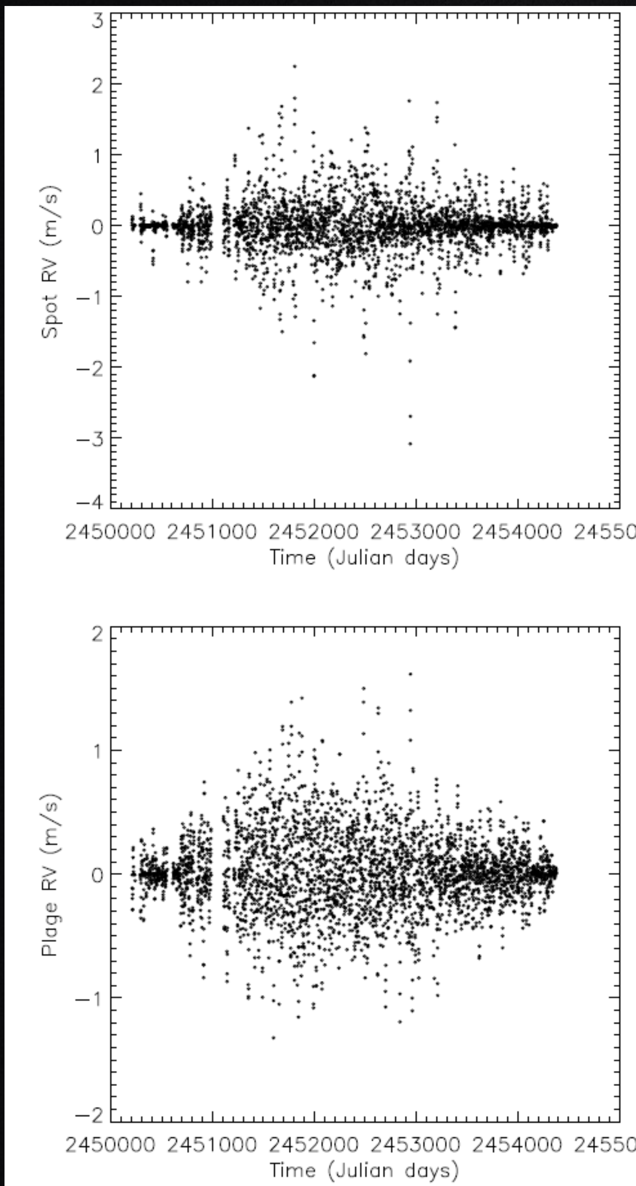

+

Inhibition of CB

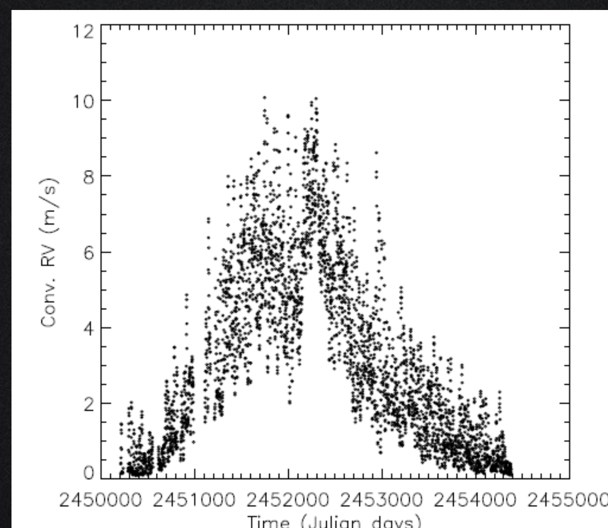

=

Total

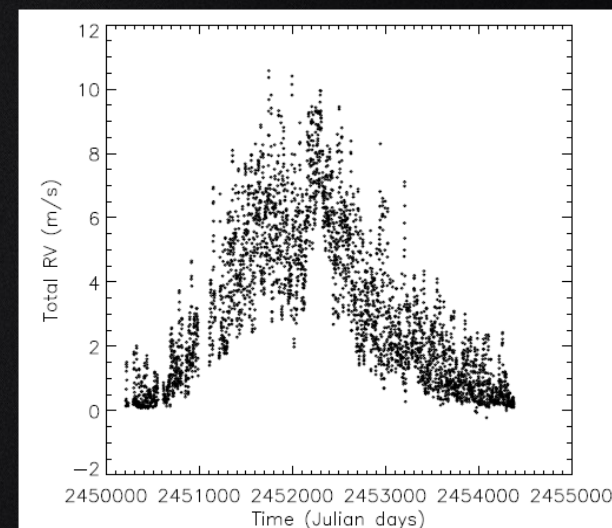

Meunier+2010

Case of CoRoT-7

Transiting planet CoRoT-7b, was discovered with CoRoT telescope, with an orbital period of 0.85 days and radius of 1.68 Re (Leger+09)

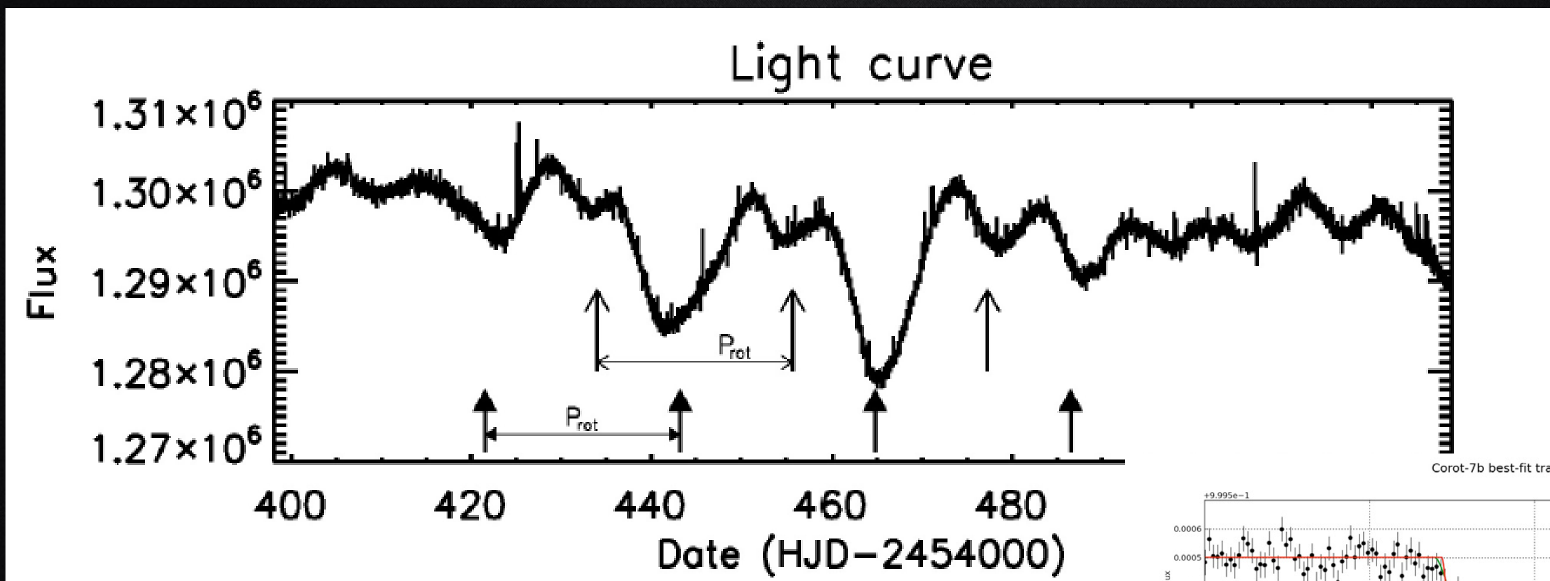

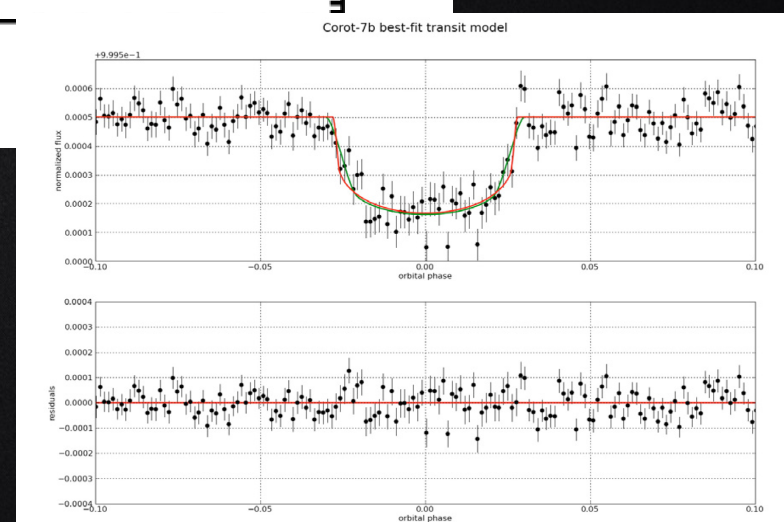

Case of CoRoT-7

Stellar activity causes difficulties in detecting low mass planet's signal and also determine the accurate mass of them.

CoRoT-7b	CoRoT-7c	Reference
$4.8 \pm 0.8 M_\oplus$	$\boxed{8.4 \pm 0.9 M_\oplus}$	Queloz et al. (2009)
$6.9 \pm 1.4 M_\oplus$	$12.4 \pm 0.42 M_\oplus$	Hatzes et al. (2010)
$\boxed{7.42 \pm 1.21 M_\oplus}$	-	Hatzes et al. (2011)
$\boxed{2.3 \pm 1.8 M_\oplus}$	-	Pont et al. (2011)
$5.7 \pm 2.5 M_\oplus$	$13.2 \pm 4.1 M_\oplus$	Boisse et al. (2011)
$8.0 \pm 1.2 M_\oplus$	$13.6 \pm 1.4 M_\oplus$	Ferraz-Mello et al. (2011)
$4.8 \pm 2.4 M_\oplus$	$11.8 \pm 3.4 M_\oplus$	Tuomi et al. (2014)
$4.73 \pm 0.95 M_\oplus$	$\boxed{13.56 \pm 1.08 M_\oplus}$	Haywood et al. (2014)
$5.52 \pm 0.78 M_\oplus$	-	Barros et al. (2014)
$5.53 \pm 0.86 M_\oplus$	$12.62 \pm 0.77 M_\oplus$	Faria et al. (2016)

Disentangling between stellar activity and planetary signals

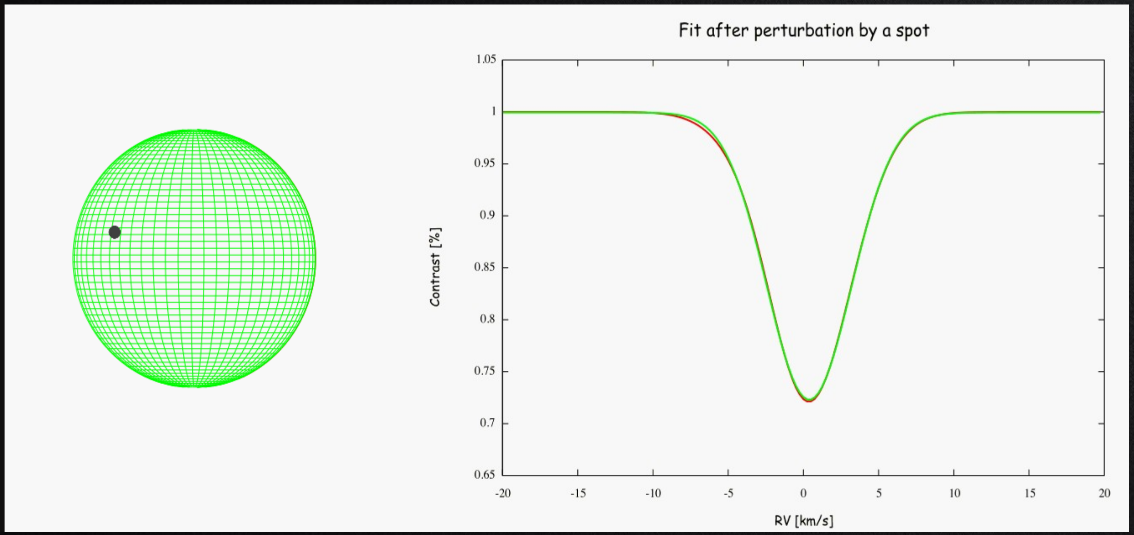

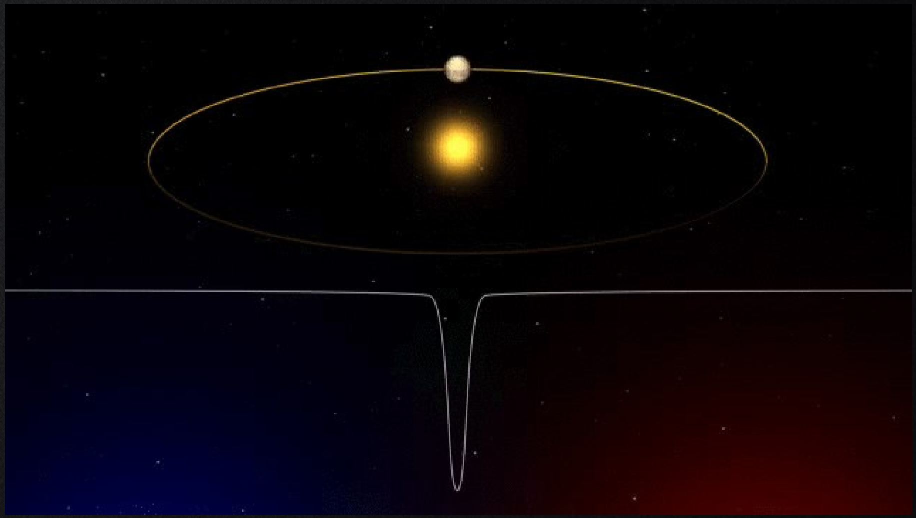

Line profile indicator (BIS)

BIS = Vhigh−Vlow

Vhigh/low are simply the average of the velocity of the points in top and bottom of the CCFs, respectively.

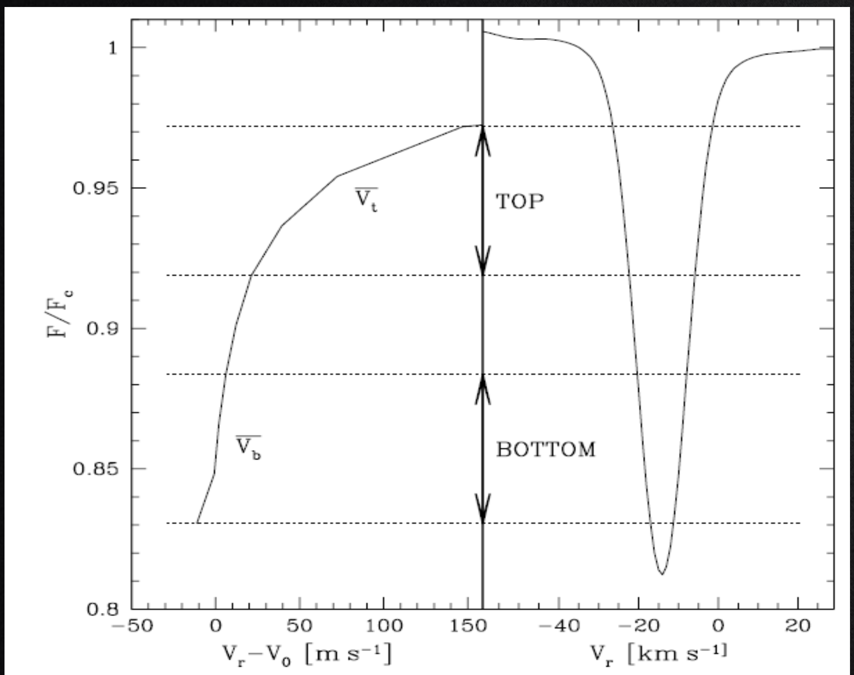

Fig. 5. Right: the mean CCF function of HD 166435's spectra constructed with a template selecting only the weak and non-saturated lines. This profile represents the mean spectral-line profile of the lines selected by the template. Left: the bisector of the CCF. V_0 is an arbitrary offset. Note the definition of the boundaries for the computation of ($\overline{V_t}$ and $\overline{V_b}$).

Queloz + 2001

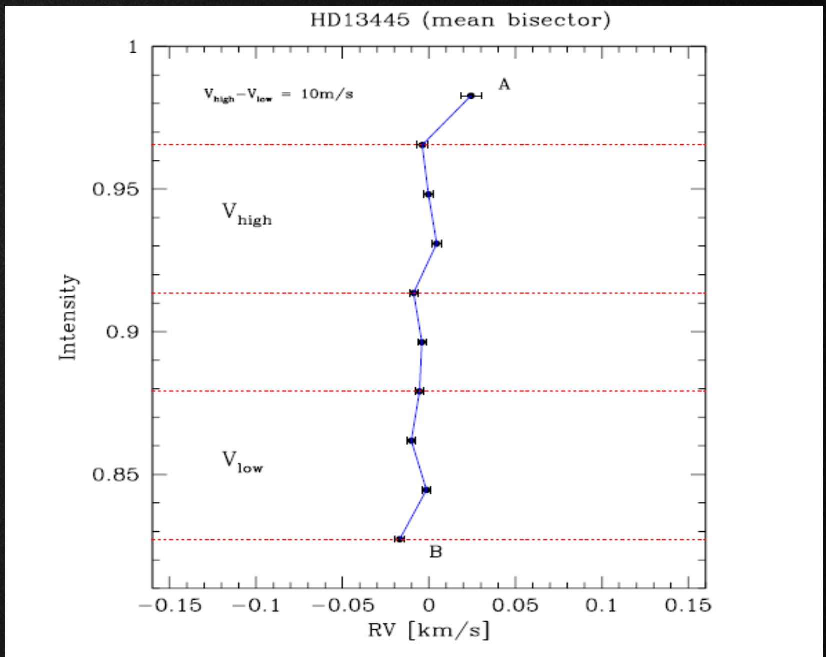

Fig. 7. Average bisector for the K0 dwarf HD 13445. This figure shows that the line bisector is almost vertical for a star of this spectral type. The two regions denoted by the dotted lines (V_{low} and V_{high}) represent the intervals used to compute the Bisector Inverse Slope (BIS), defined as BIS = $V_{high}-V_{low}$: $V_{high/low}$ are simply the average of the velocity of the 4 "points" in each of the intervals (for more details see Queloz et al. 2001b). The error bars

Santos + 2002

Line profile indicator (BIS)

CoRoT-7

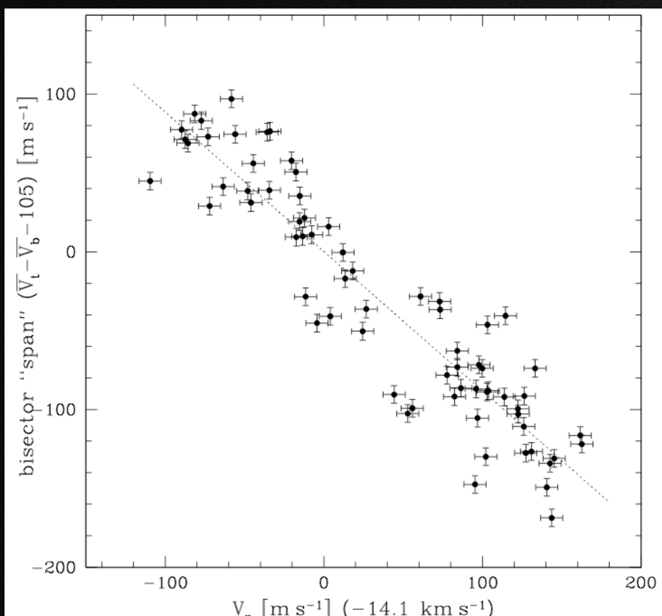

Queloz + 2001

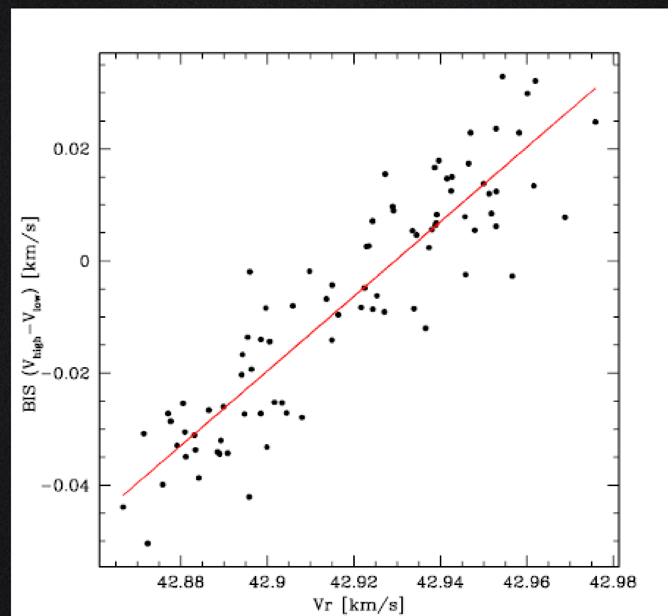

Santos+2002

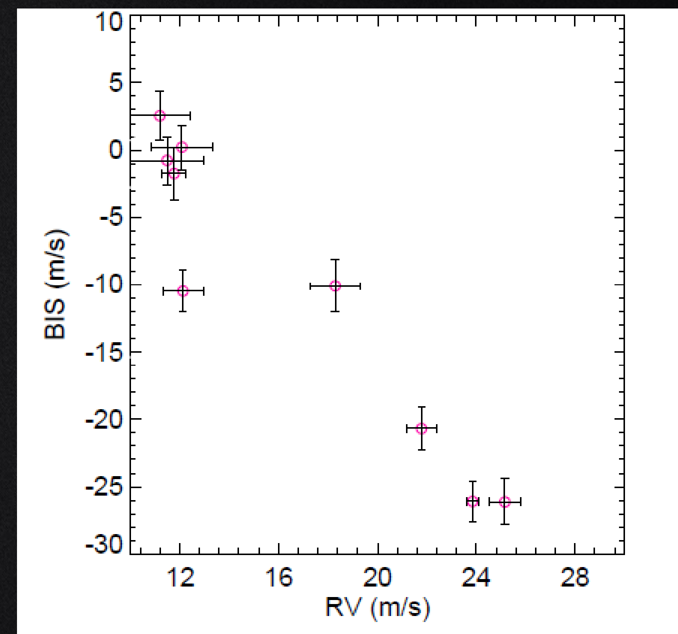

Cakırlı+2013

Line profile indicator (Vspan)

Vspan=RV_high - RV_low

RV high = Gaussian fit to upper part of the CCF
RV high = Gaussian fit to lower part of the CCF

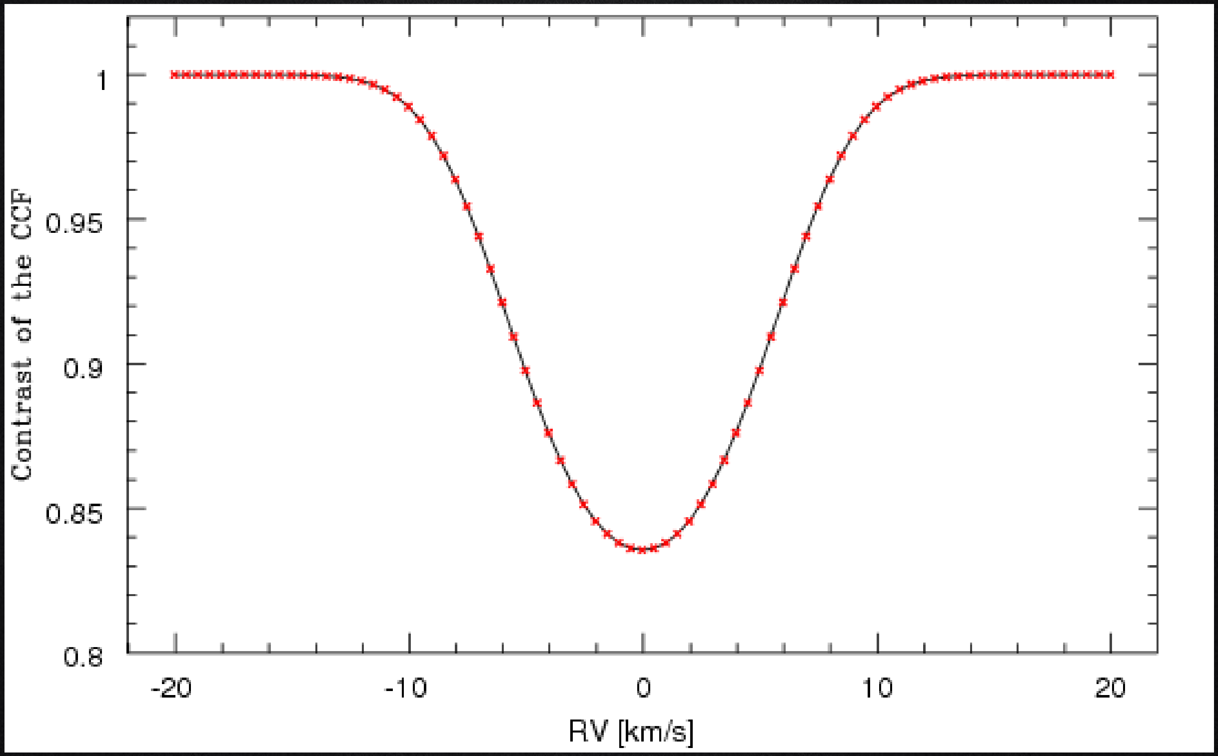

The construction of the Vspan indicator was motivated by the analysis of line-profile variations for cases of low S/N

Line profile indicator (Vspan)

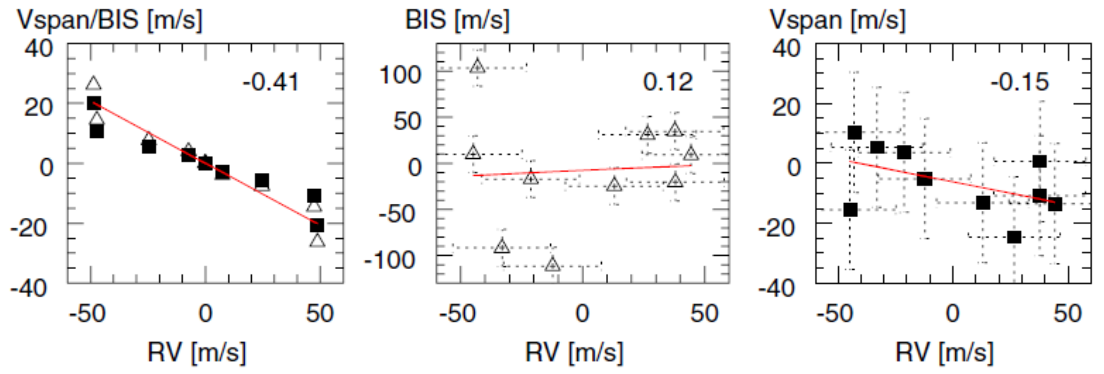

Fig. 5. *Left*: BIS (triangles) and V_{span} (squares) as a function of RV for a simulated spot rotating at latitude +50° on a star with an inclination $i = 40°$. *Middle and Right*: respectively, BIS (Queloz et al. 2001) and V_{span} (this paper) as a function of RV for the same simulated spot with 20 m s^{-1} additional photonic noise in the CCF. The lines are the least squares fit to the data. The numbers in the right-hand corner is the value of the slope of the fit.

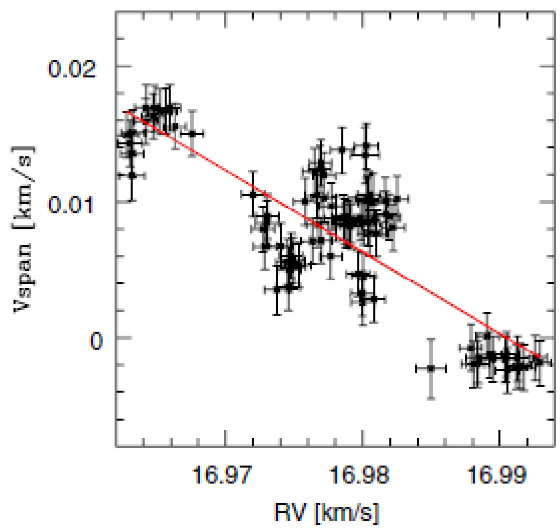

Fig. 20. $V_{span} = RV_{high} - RV_{low}$ as a function of RV of ι Hor derived from HARPS spectra. The line is the least squares fit. The ranges have the same extents along the *x*- and *y*-axes. The error bars are also plotted. One may compare this shape with that of the simulation of two spots separated by 120° in longitude in Fig. 13 (*bottom*).

Boisse+2011

Line profile indicator (FWHM)

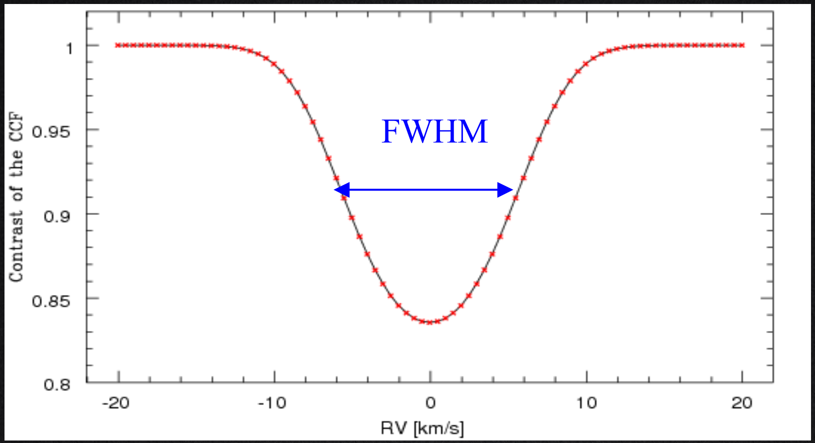

CoRoT-7

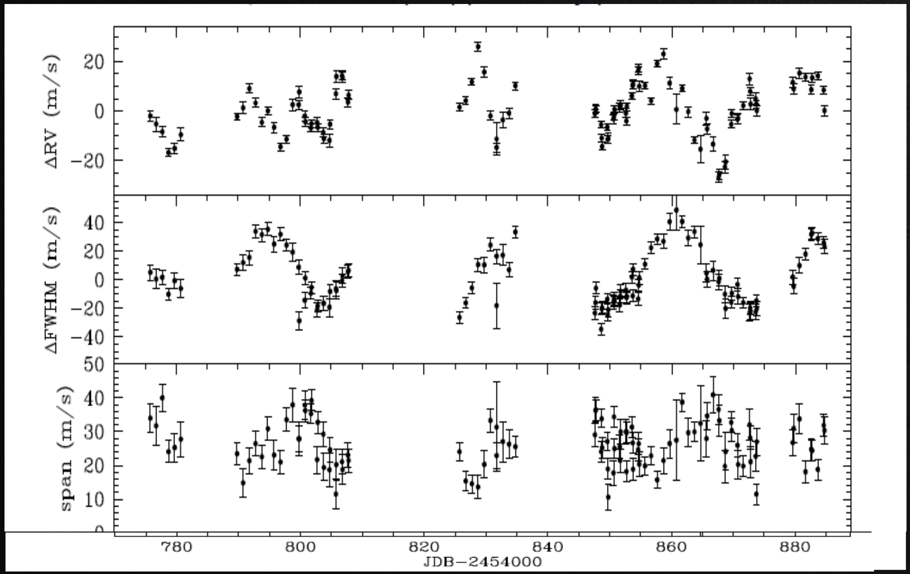

Queloz+2009

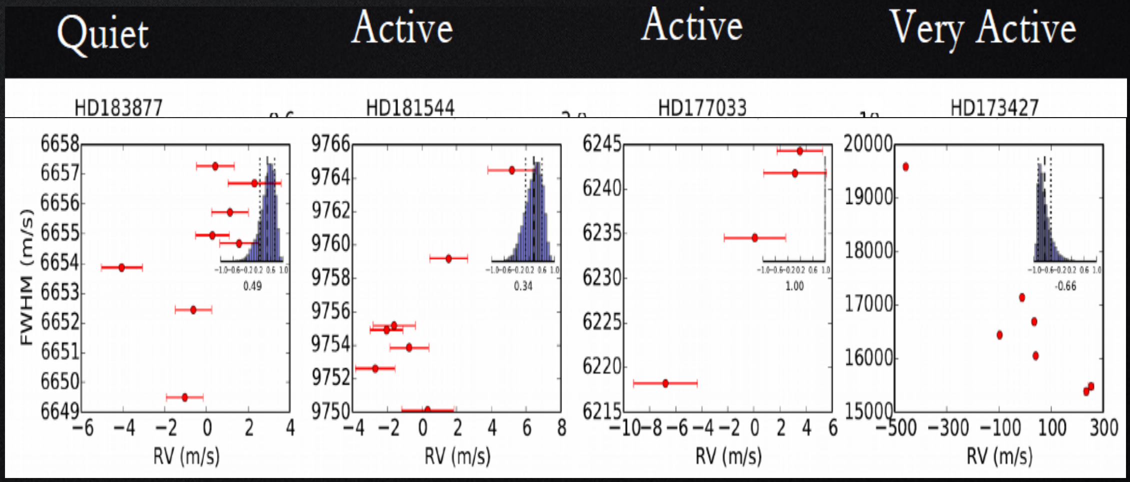

Oshagh+2016

Activity index (simultaneous photometry)

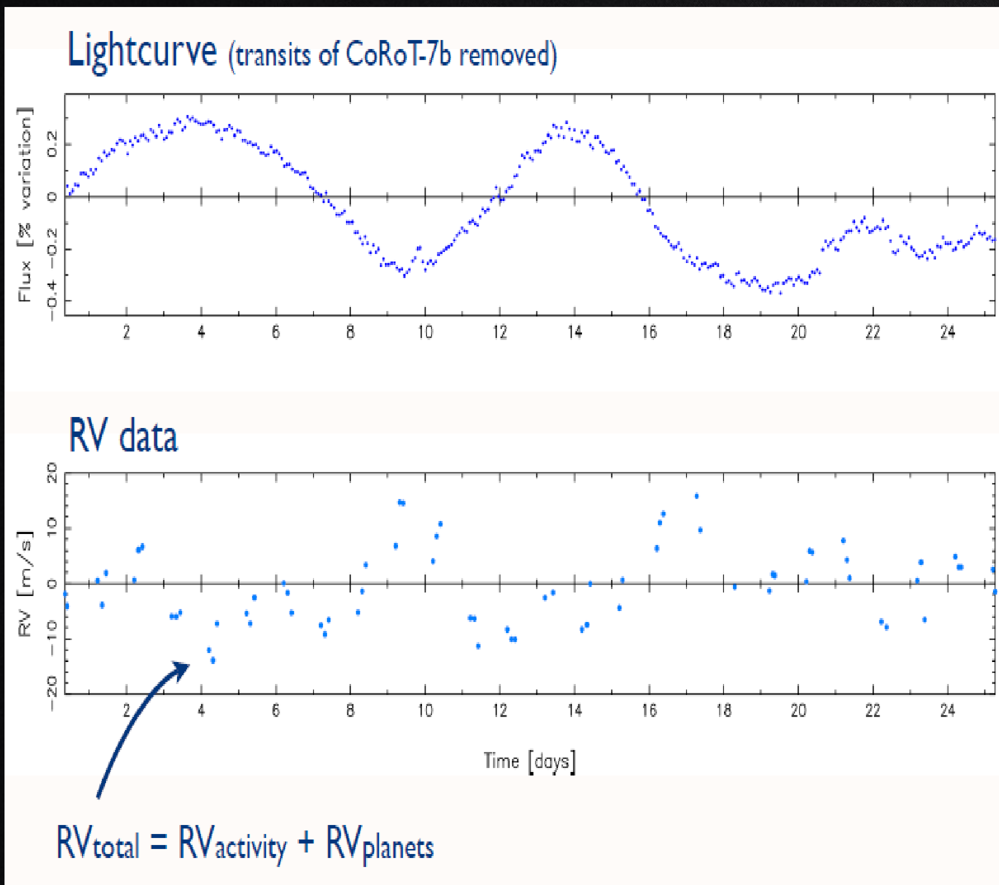

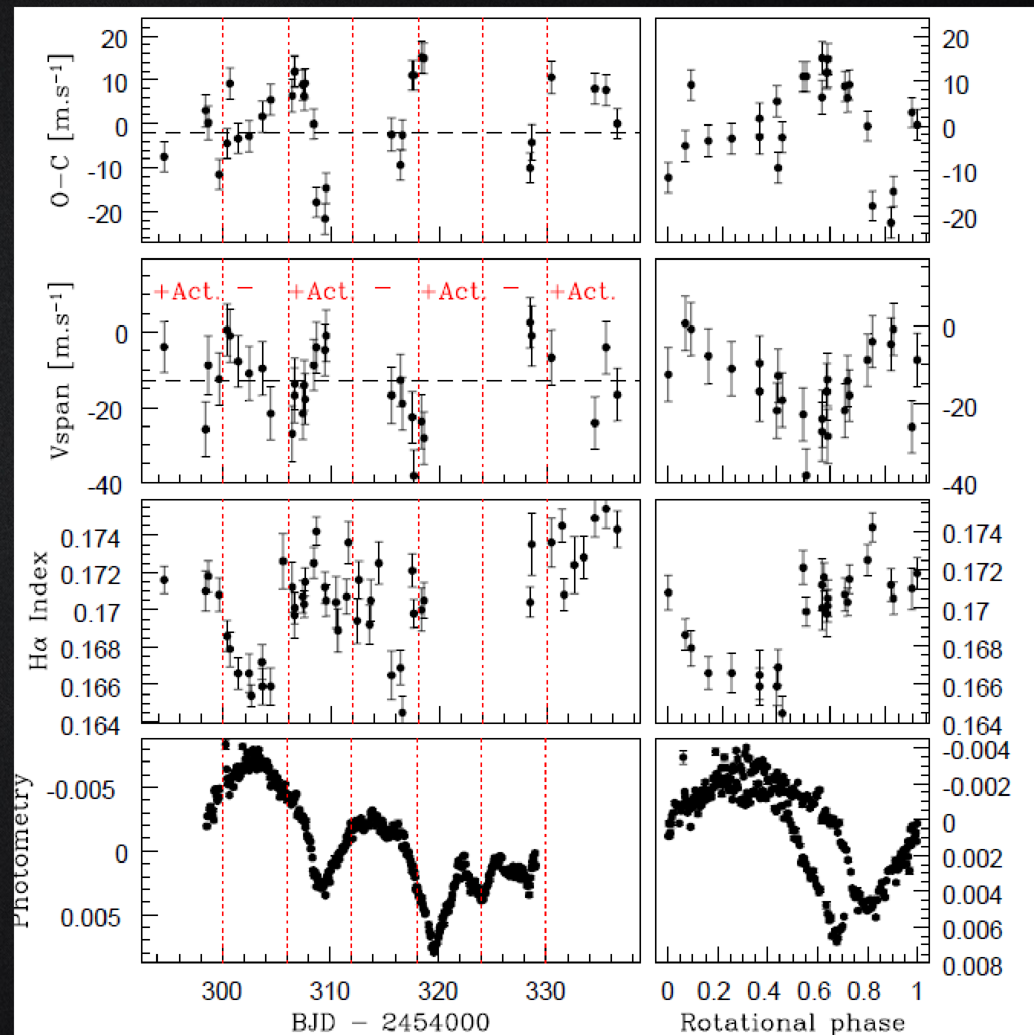

Haywood+2014

Boisse+2009

Activity index (simultaneous photometry)

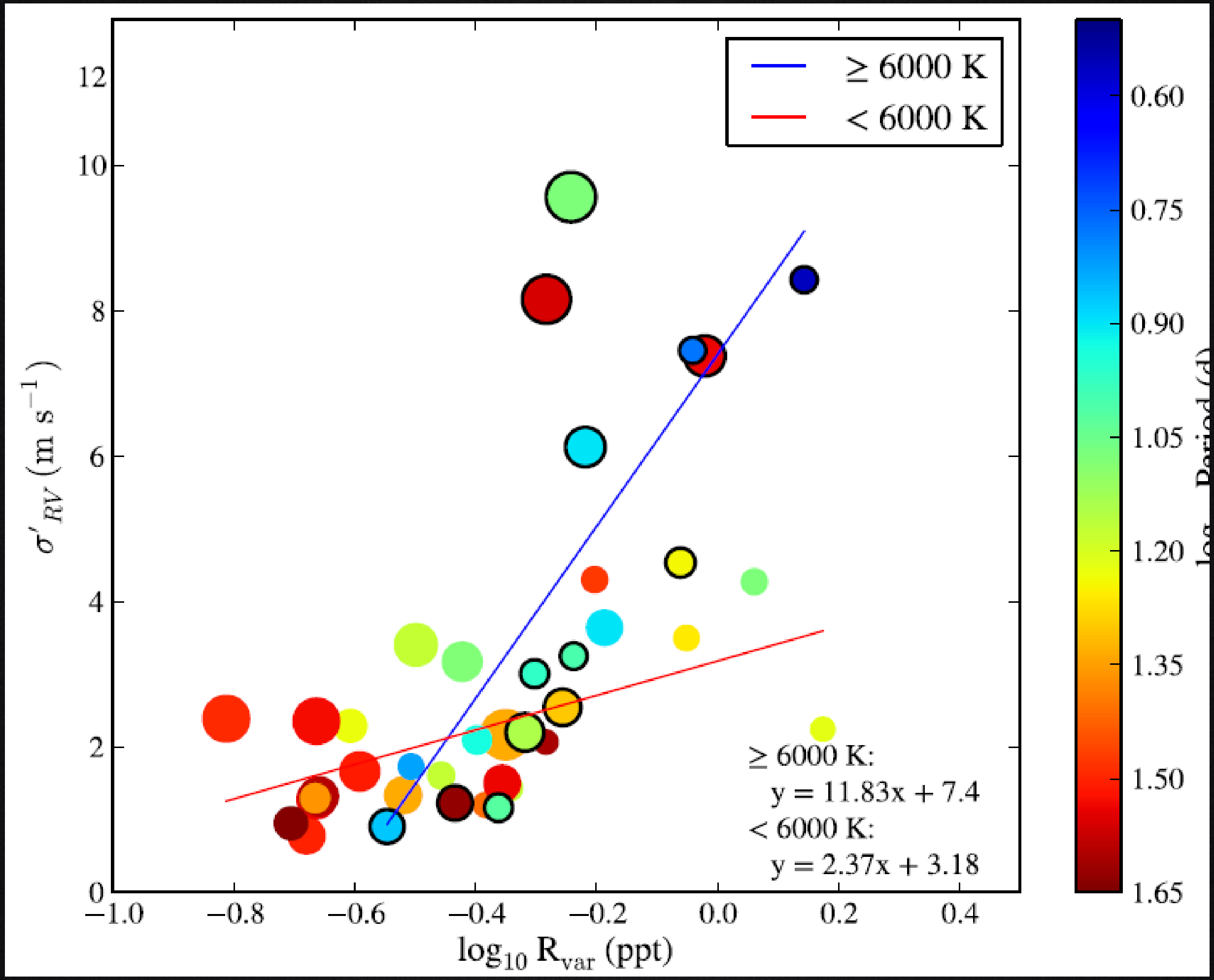

Cegla+2014

$$\sigma'_{\rm RV}\,({\rm ms}^{-1}) = 11.83 \times \log_{10} R_{\rm var}\,({\rm ppt}) + 7.4\;(\geqslant 6000\,{\rm K}),$$

$$\sigma'_{\rm RV}\,({\rm ms}^{-1}) = 2.37 \times \log_{10} R_{\rm var}\,({\rm ppt}) + 3.18\;(<6000\,{\rm K}).$$

Activity index (magnetic field)

Sunspots have typical magnetic flux densities of several 100–1000G (Solanki 2003).

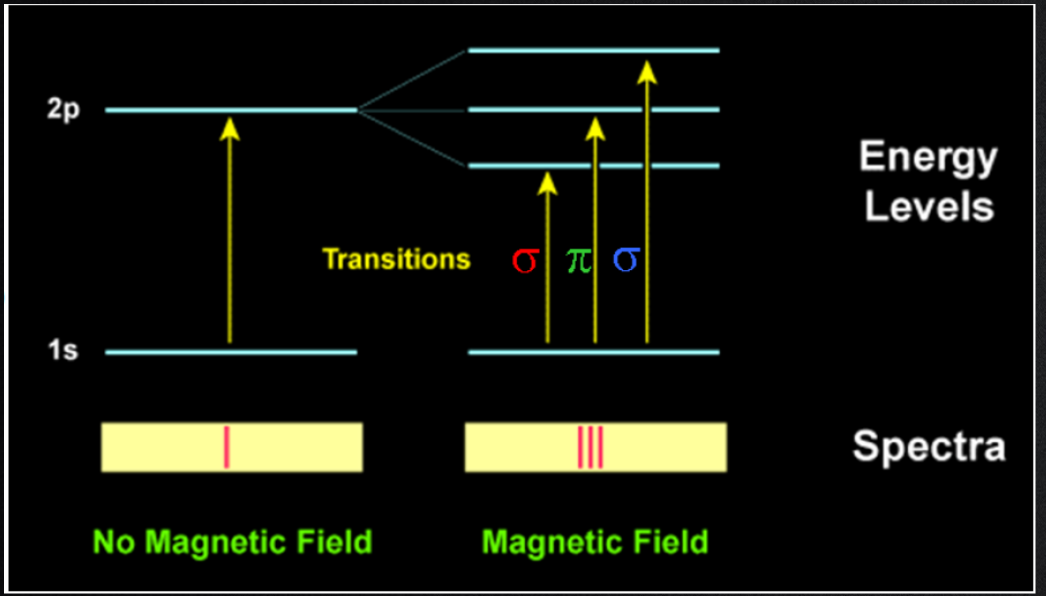

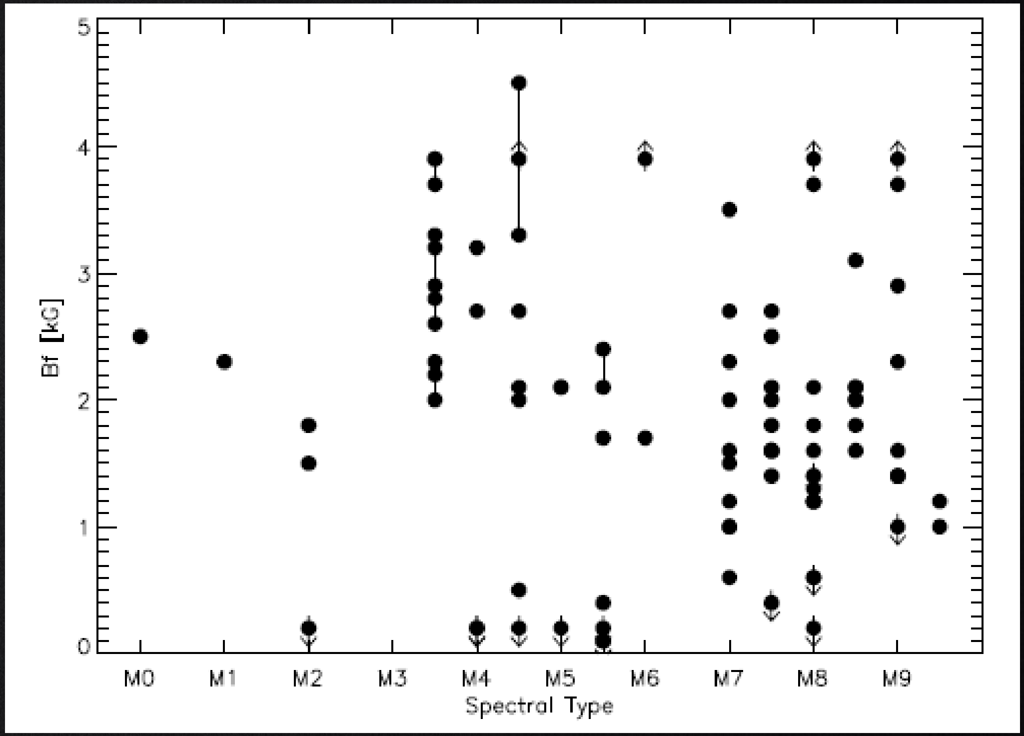

Reiners+12

$$\Delta\lambda = 46.67\, g\lambda_0^2 B,$$

Where $\Delta\lambda$ in m°A, $\lambda 0$ in µm, and B in kG.

Activity index (magnetic field)

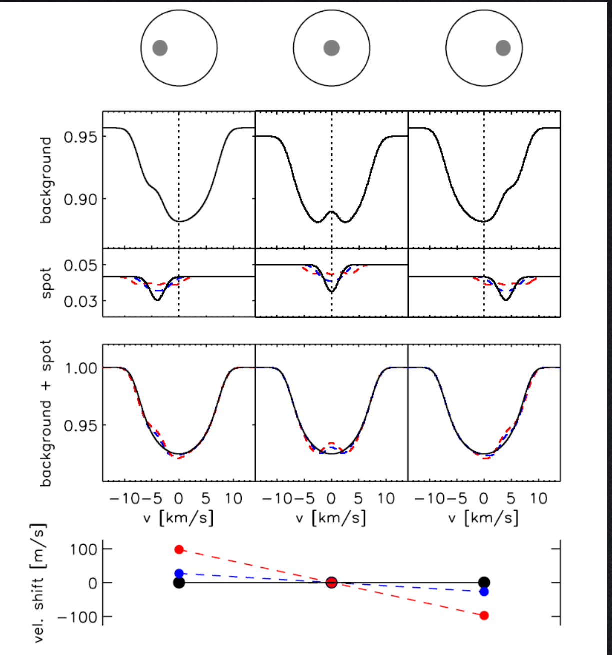

Fig. 1. Sketch of the effect of a magnetic spot on RV measurements. *Top*: rotating star with large spot, covering 5% of the visible surface if observed at disk center, seen at three phases. The star is rotating with the spot approaching in the *left column*, centered in the *middle column*, and rotating out of view in the *right column*. *Second row*: stellar line profile broadened by rotation but without spot flux, showing the impact of a dark star spot. *Third row*: flux emerging from spot only, assuming the same temperature as in the photosphere. *Row four*: sum of surrounding and the spot region. *Row five*: radial velocity determined from fitting a Gaussian profile to the spectral lines in row four. In rows three to five, black solid lines show the case without a magnetic field (and zero spot temperature contrast). Blue and red dashed lines show cases in which the spot area has B = 1 kG and 2 kG, respectively (λ = 1.2 μm and g = 1.0).

$$\Delta\lambda = 46.67\, g\lambda_0^2 B, \longrightarrow \Delta v_{\mathrm{Zeeman}} = 1.4\, g\, \lambda\, B$$

with v in ms−1, λ in μm, and *B* in Gauss. The Landé-factor g is on the order of unity.

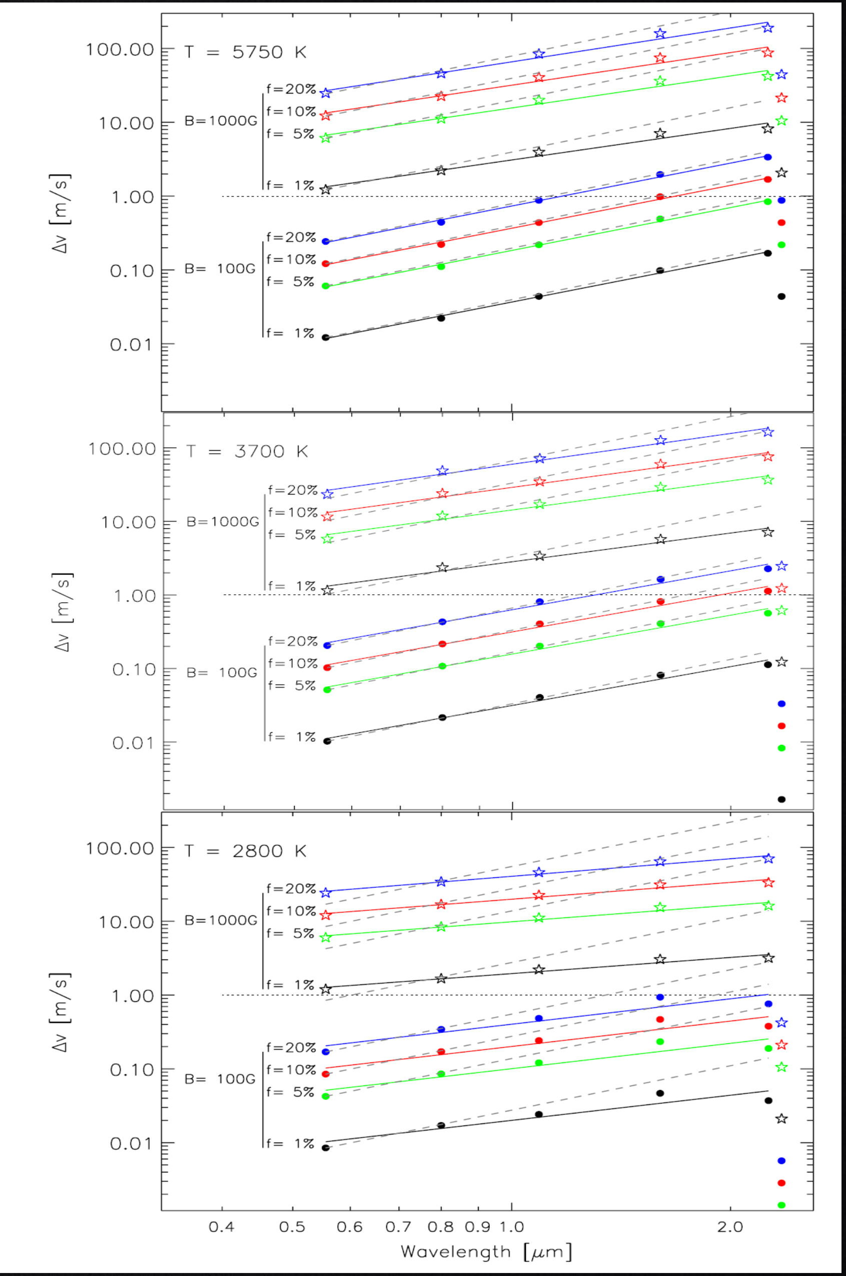

Reiners+13

Activity index (magnetic field)

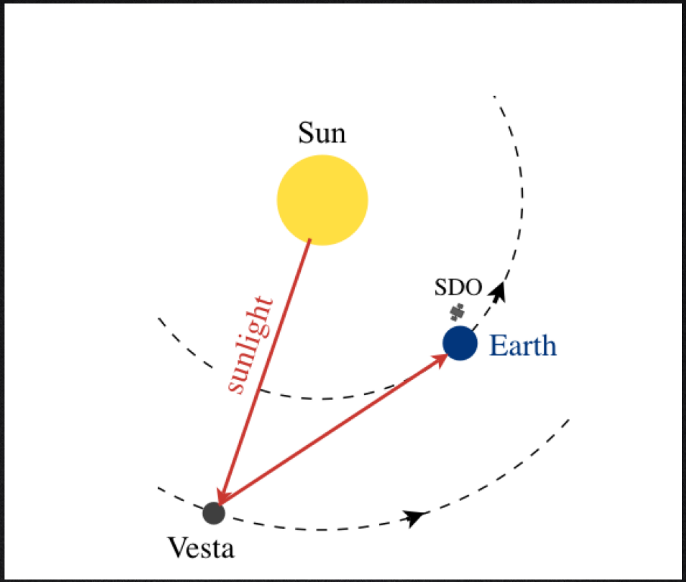

Sun

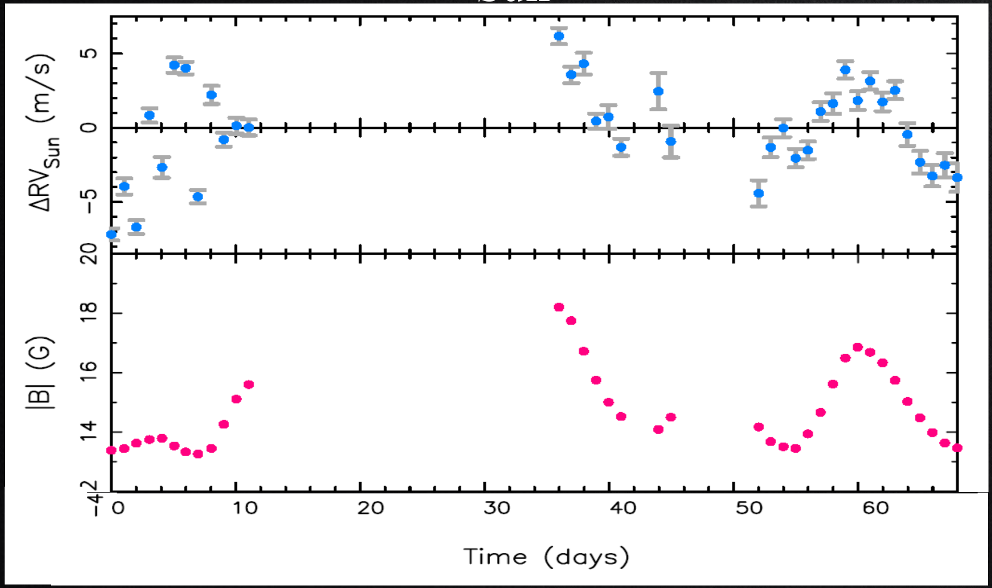

Sun

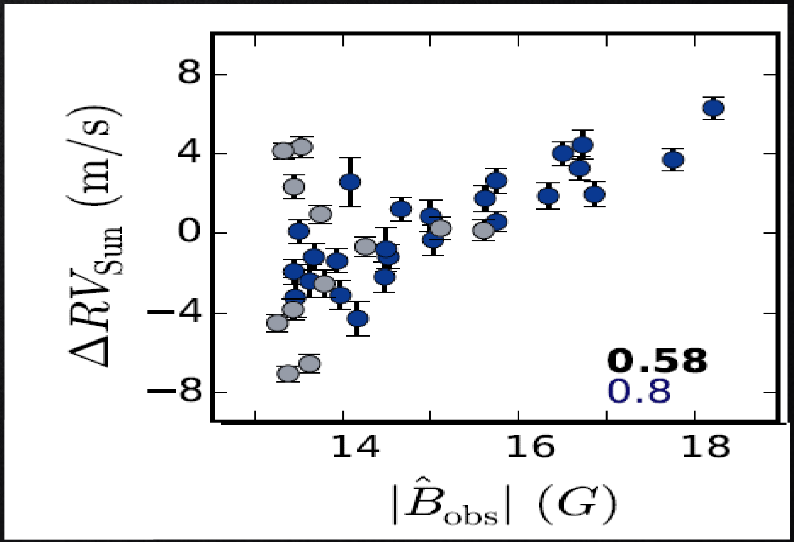

Haywood+16

Activity index (magnetic field)

Spectropolarimetry

$$B_l = \frac{-2.14 \times 10^{11}}{\lambda_0 g_{\rm eff} c} \frac{\int v V(v) dv}{\int [I_c - I(v)]\, dv},$$ with I and V denoting the Stokes parameters

GJ 410

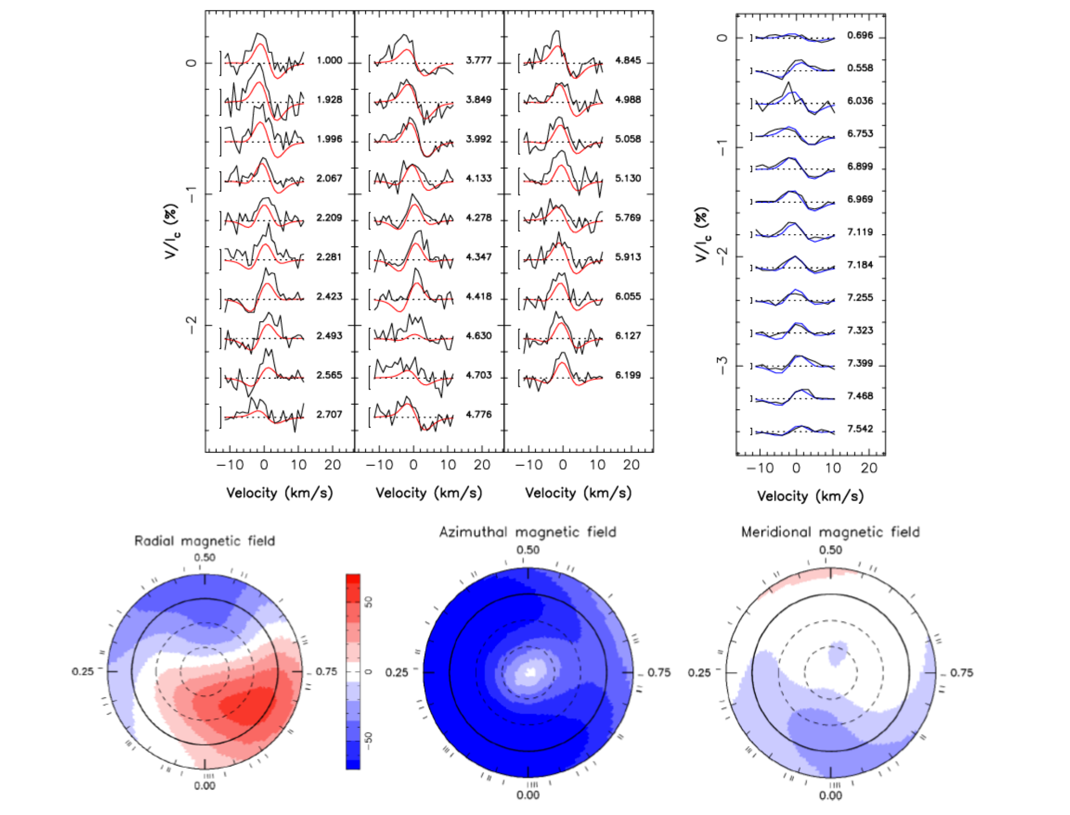

Figure 4. Same as Fig. 3 for GJ 410. LSD Stokes *V* profiles in the top left and top right panels correspond to HARPS-Pol and NARVAL observations respectively.

GJ 410

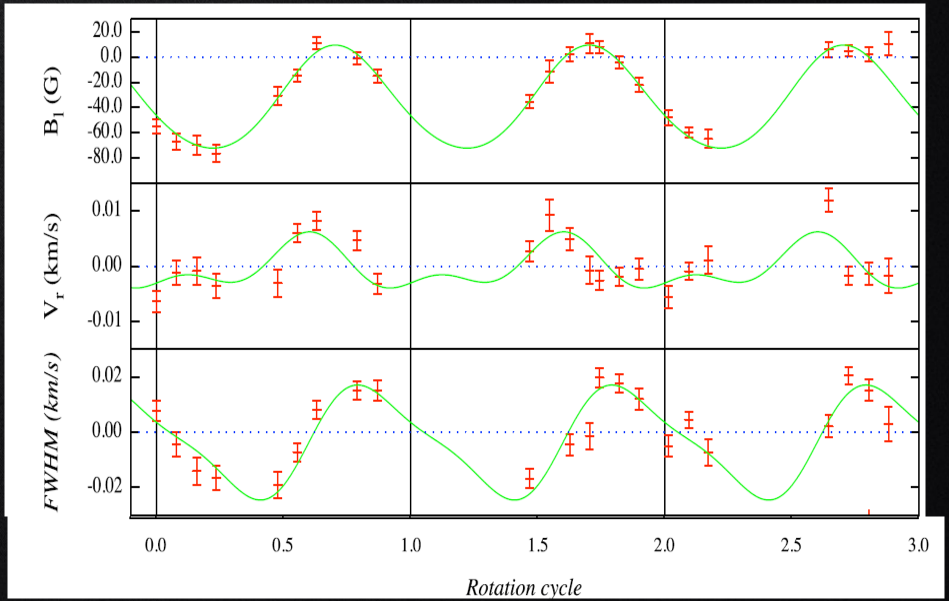

Hébrard+2016

Activity index (S-index)

Mount Wilson S-index is a measure of the emission line cores of the Ca II H and K lines

$$S = \alpha \frac{H + K}{R + V},$$

where *H*, *K*, *R*, and *V* are the values for the flux measured in the according bandpasses and α is an instrumental calibration factor.

S-index reflect the non-thermal chromospheric heating which is associated with magnetic field (Wilson, 1978, Noyes+1984).

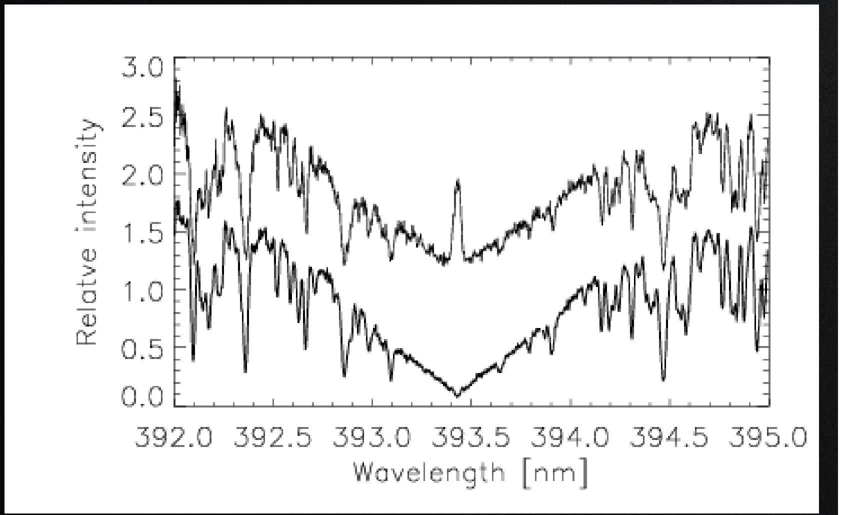

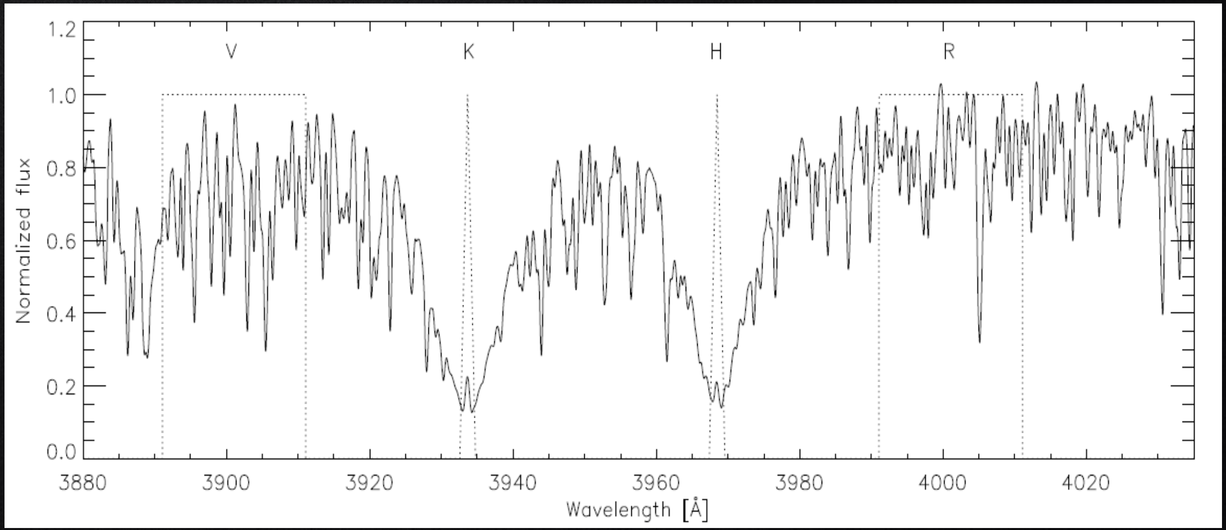

Karoff+2010

Activity index (S-index)

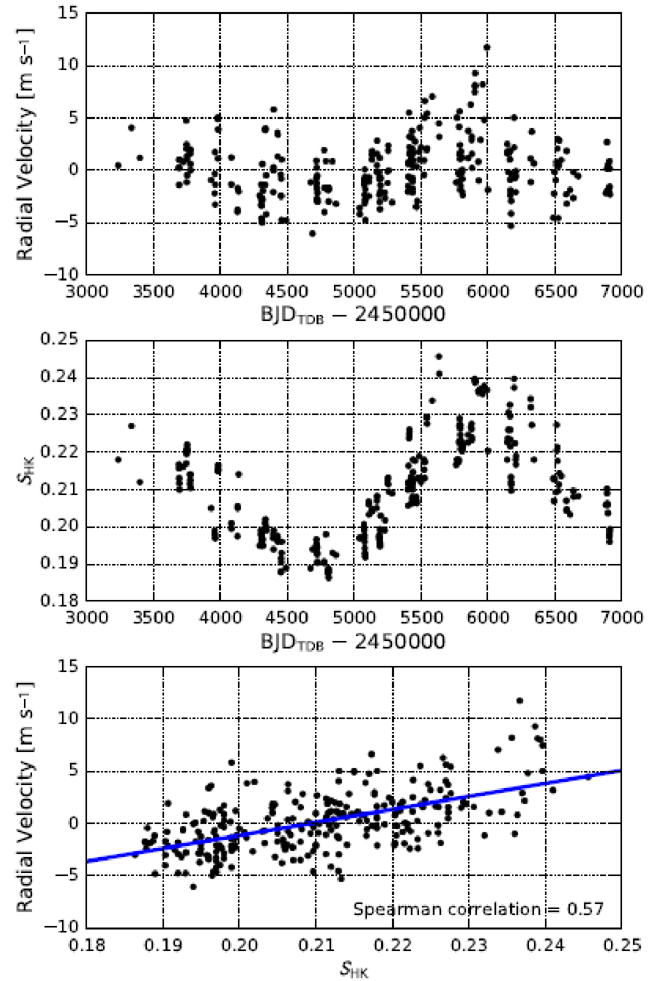

FIG. 2.— Velocity-activity correlation. *Top:* Binned RV time series of the post-upgrade Keck data with planets b, c, and d subtracted. *Middle:* Binned S_{HK} time series of the post-upgrade Keck data only. Note the similarities between the variability in the top and middle panels. *Bottom:* Spearman rank correlation test of the velocities with S_{HK} values (Spearman 1904).

Fulton+2015

Activity index (Log R'HK)

Log R'HK gives the emission in the narrow bands normalized by the bolometric brightness of the star.

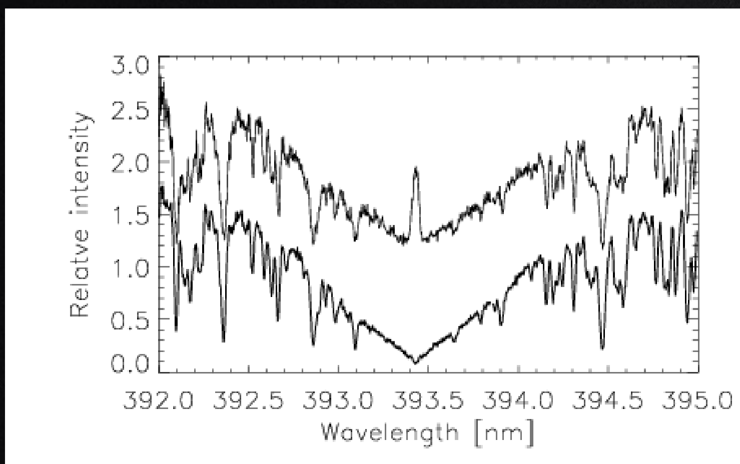

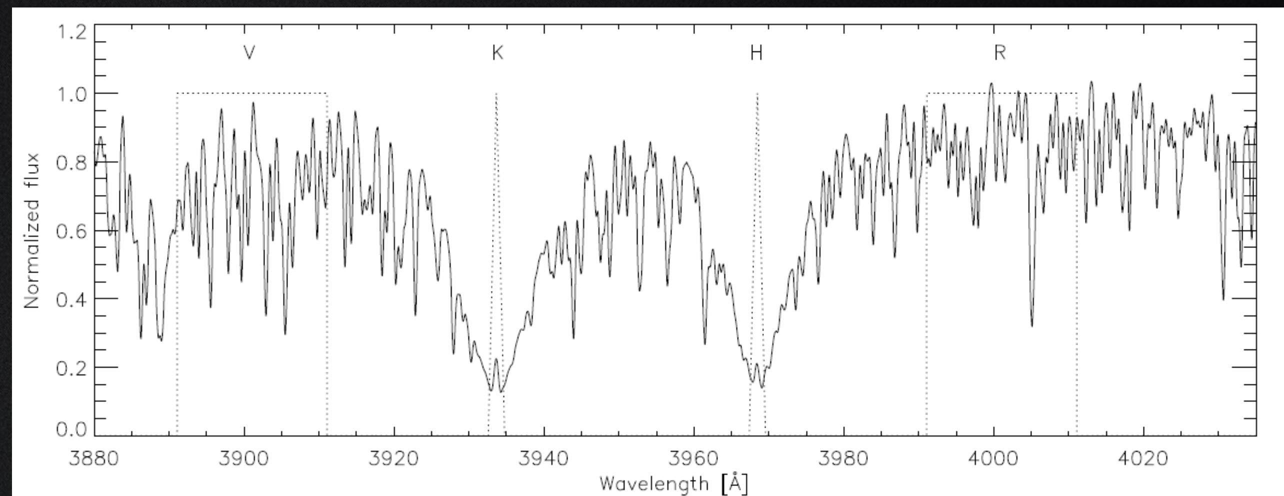

$$R_{HK} = \frac{4\pi R_s^2 (F_H + F_K)}{4\pi R_s^2 \sigma T_{eff}^4} = \frac{F_H + F_K}{\sigma T_{eff}^4}$$

$$\log R_{\mathrm{phot}} = -4.898 + 1.918(B-V)^2 - 2.893(B-V)^3$$

$$R'_{\mathrm{HK}} = R_{\mathrm{HK}} - R_{\mathrm{phot}}$$

Log R'HK is closely related to the S-index,

$$\begin{aligned} \mathrm{Log}(\mathrm{R'}_{HK}) &= \mathrm{Log}\left[1.34.10^{-4}\, C_{cf}\, S_{\mathrm{index}}\right], \\ C_{cf} &= 1.13(B-V)^3 - 3.91(B-V)^2 + 2.84(B-V) - 0.47, \end{aligned}$$

Activity index (Log R'HK)

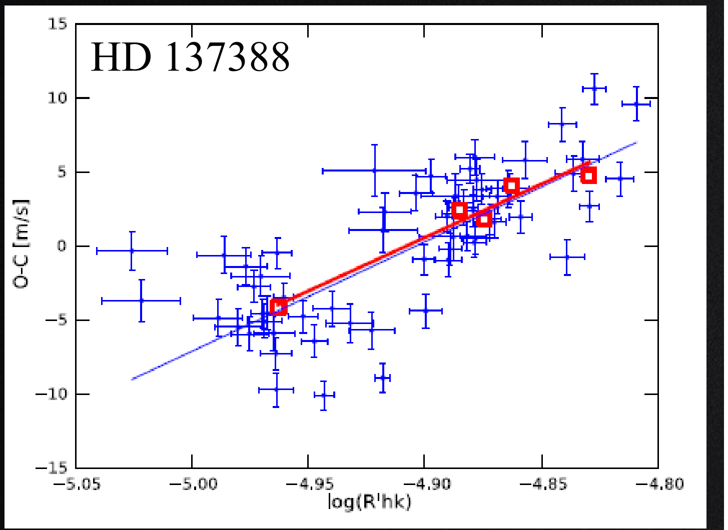

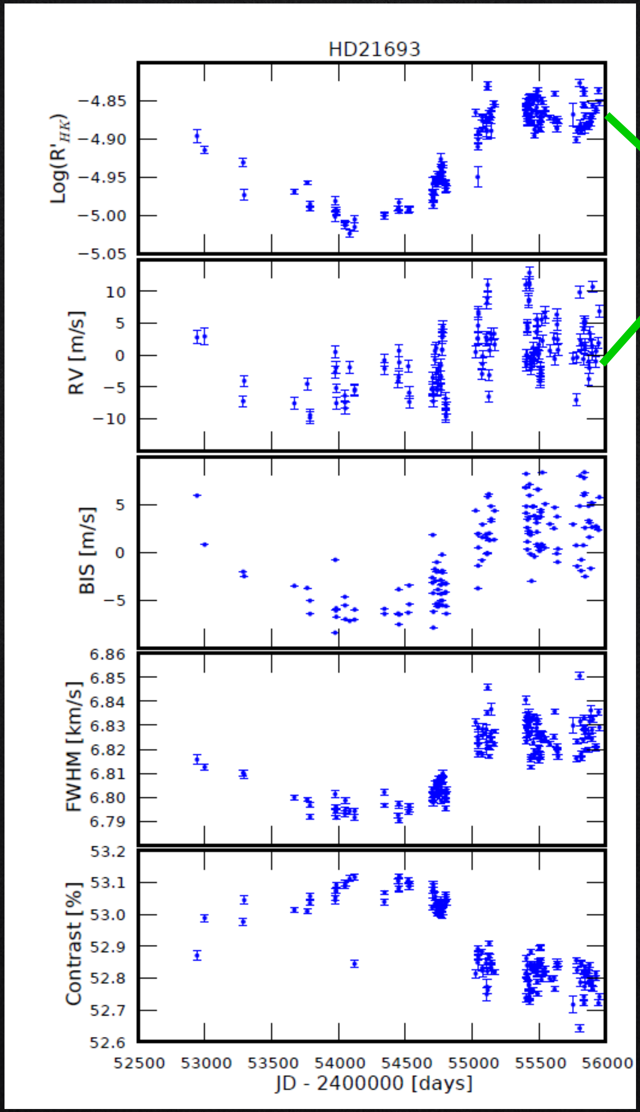

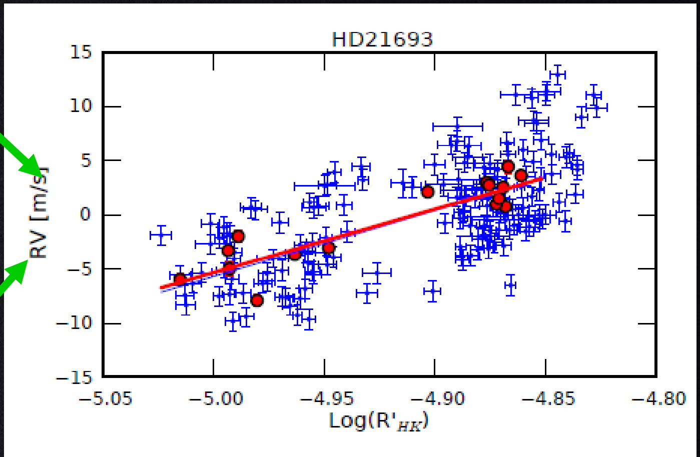

Dumusuqe+2011

Most of the methods which were presented (line profile indicator and activity indexes) have been used to identify present of stellar activity in RV signal.

Now we are going to learn methods which are able to model RV induced and then remove it from the RV observations.

Stellar activity modeling (FF' method)

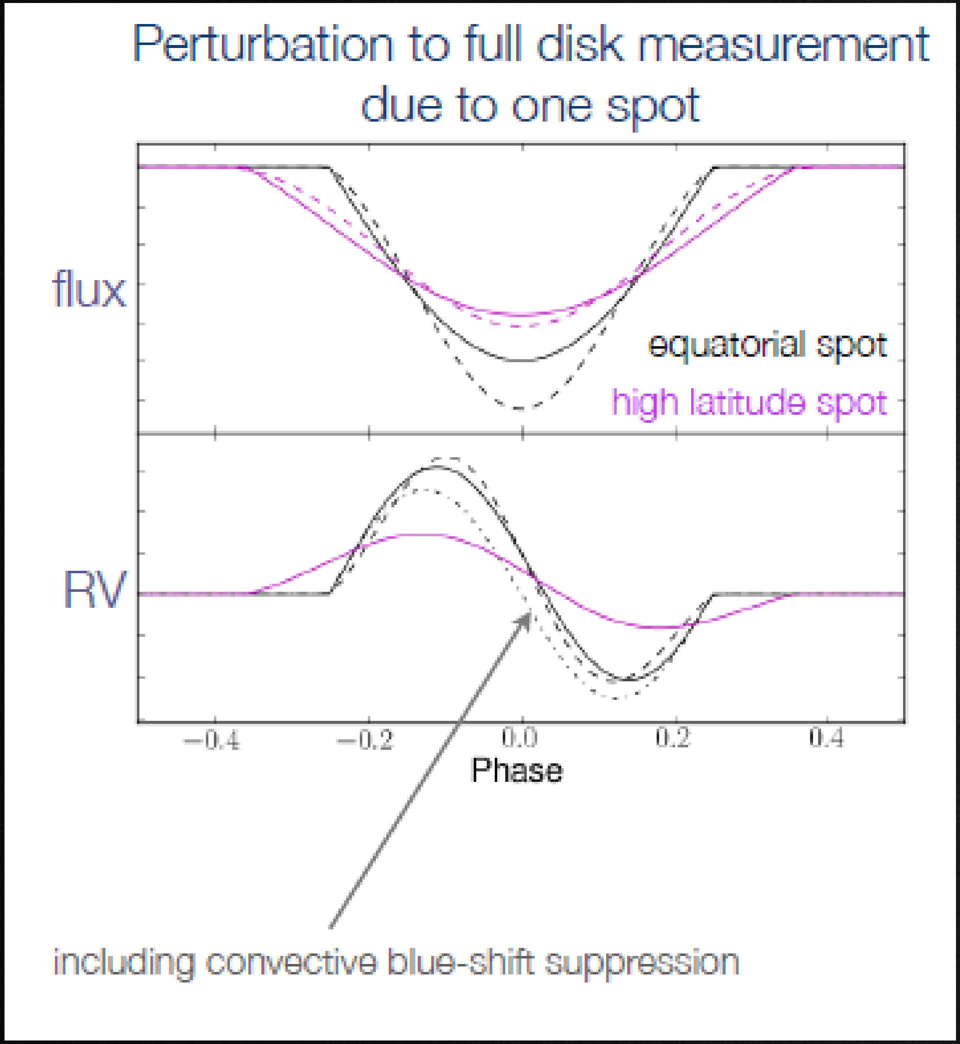

Aigrain+2012

$$\Delta RV_{\rm rot}(t) = -\frac{\dot{\Psi}(t)}{\Psi_0}\left[1 - \frac{\Psi(t)}{\Psi_0}\right]\frac{R_\star}{f}$$

$$f \approx \frac{\Psi_0 - \Phi_{\rm min}}{\Psi_0}$$

$$\Delta RV_{\rm conv}(t) = \left[1 - \frac{\Psi(t)}{\Psi_0}\right]^2 \frac{\delta V_c\, \kappa}{f}$$

Delta Vc is the difference between the convective blueshift in the unspotted and spotted area, and k is the ratio of these two area.

$$\Delta RV_{\rm activity} = A \Delta RV_{\rm rot} + B \Delta RV_{\rm conv}$$

Stellar activity modeling (FF' method)

Limitations:

1. It is assumed that the spots are small

2. Limb-darkening is ignored.

3. Some spot configuration can give no signal in photometry, but some important signals in RV

HD189733

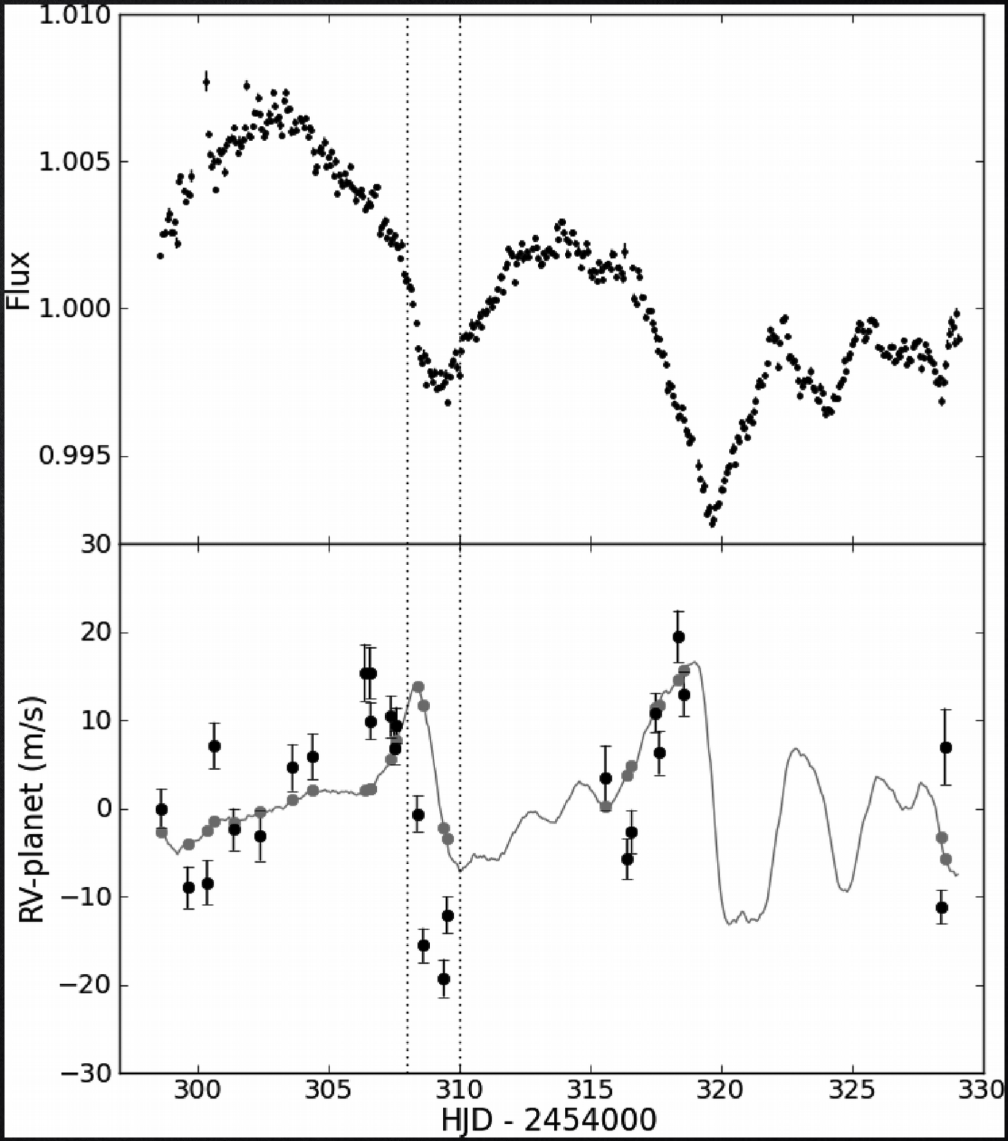

Aigrain+2012

Stellar activity modeling (SOAP 2.0)

SOAP2.0 estimates the photometric and radial velocity (RV) variations induced by active regions. Realistic spot and plage temperature contrast, inhibition of the convective blueshift (CB) inside active regions, as well as the limb brightening effect of plages and a quadratic limb darkening law are considered.

C and Python, available on http://www.astro.up.pt/resources/soap2/

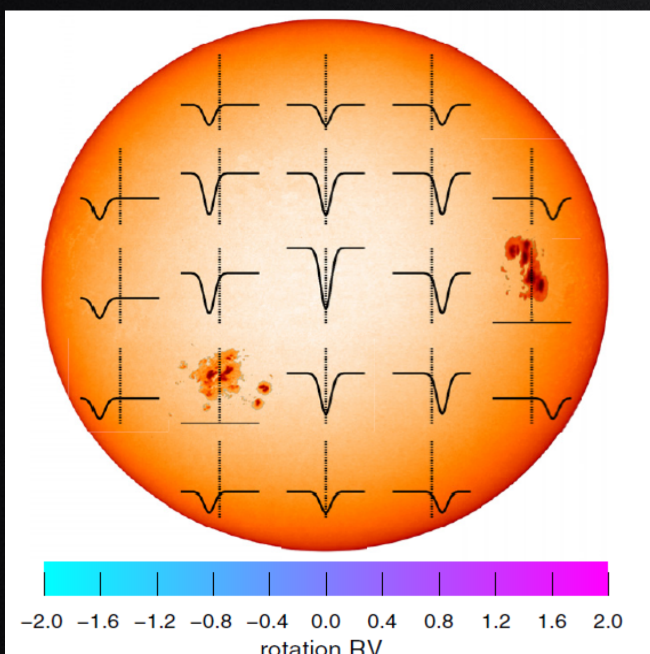

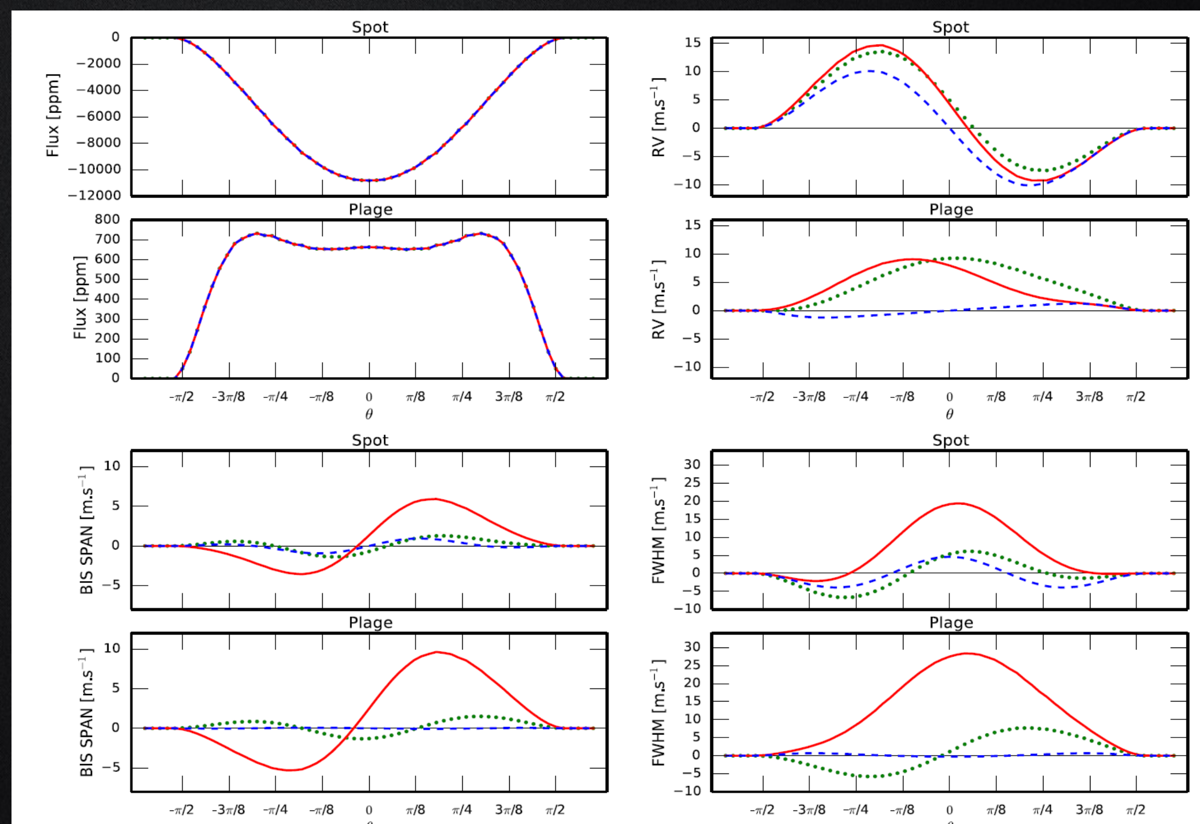

Dumusque+2014

Stellar activity modeling (SOAP 2.0)

SOAP2.0 requires the initial parameters star (**limb darkening coefficients**, **stellar radius**, **stellar rotation period**, **stellar inclination**, **stellar temperature**) and also initial parameters of each active regions (filling factor, longitude, latitude, temperature contrast).

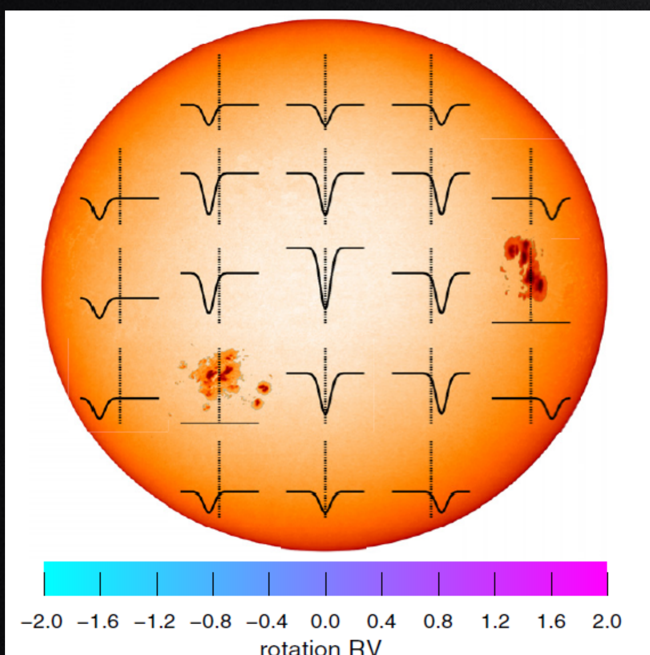

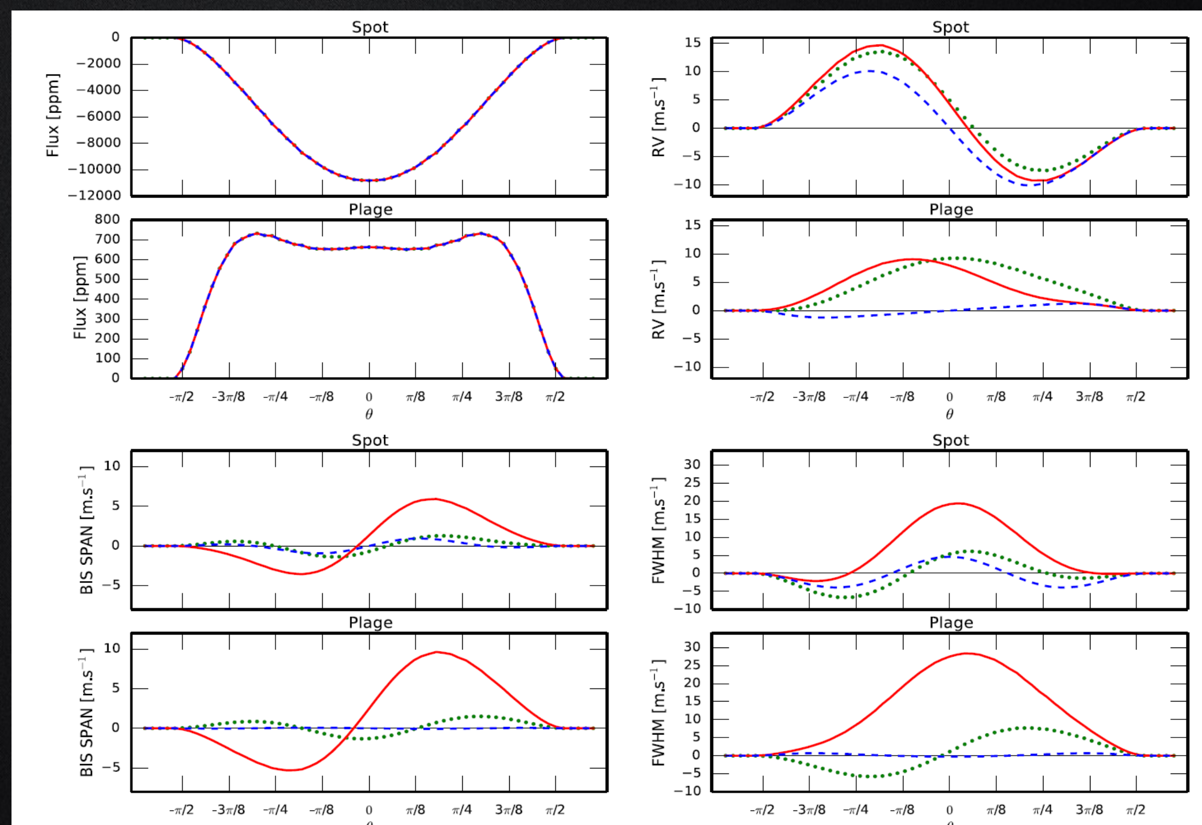

Dumusque+2014

Stellar activity modeling (SOAP 2.0)

HD189733

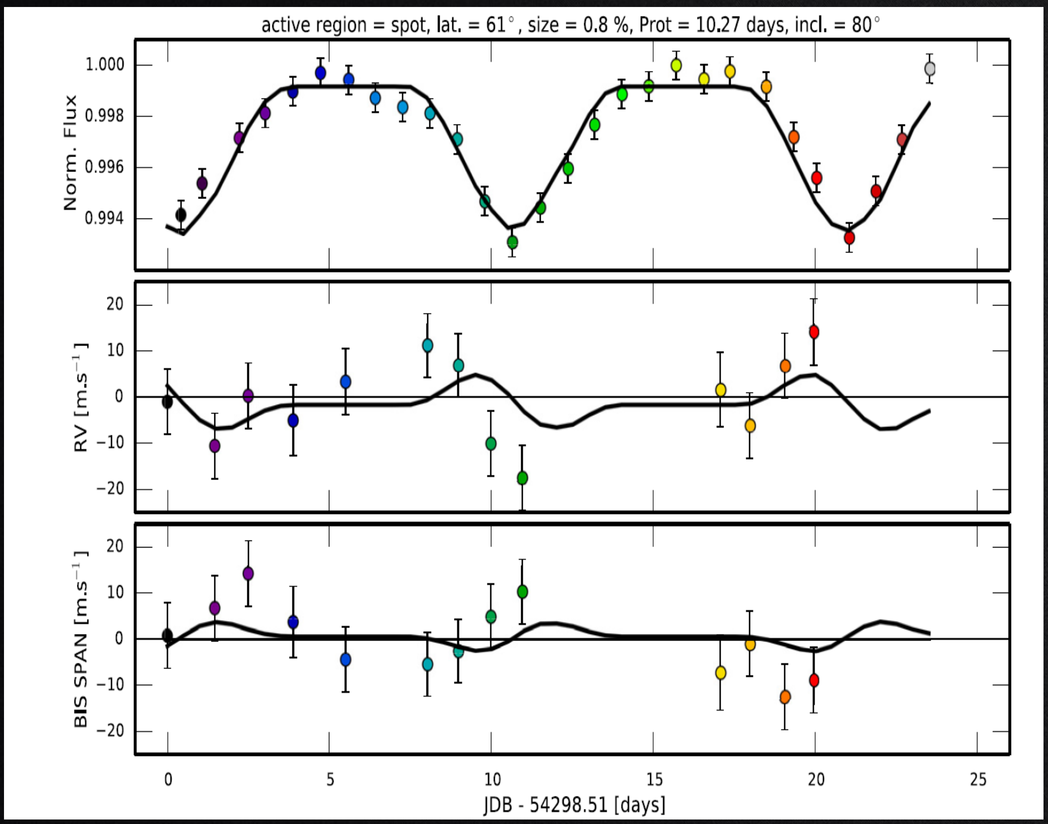

Alpha Cen B

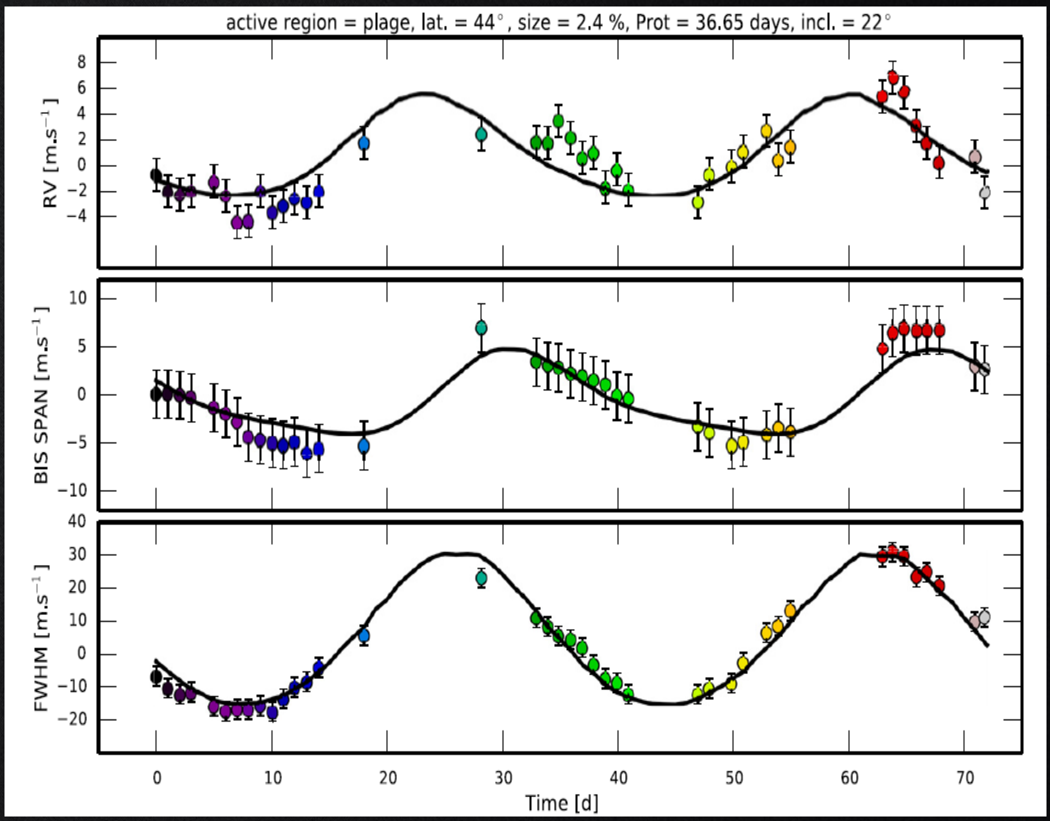

Dumusque+2014

Impact of stellar active region on photometry

Which planet's parameters measurements can be affected?

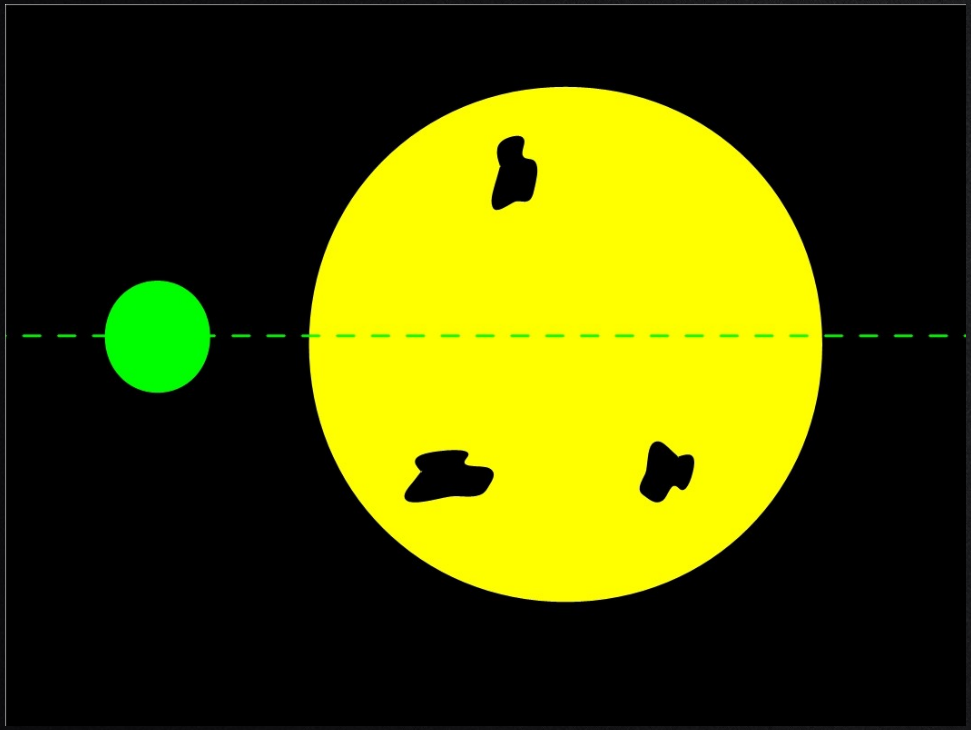

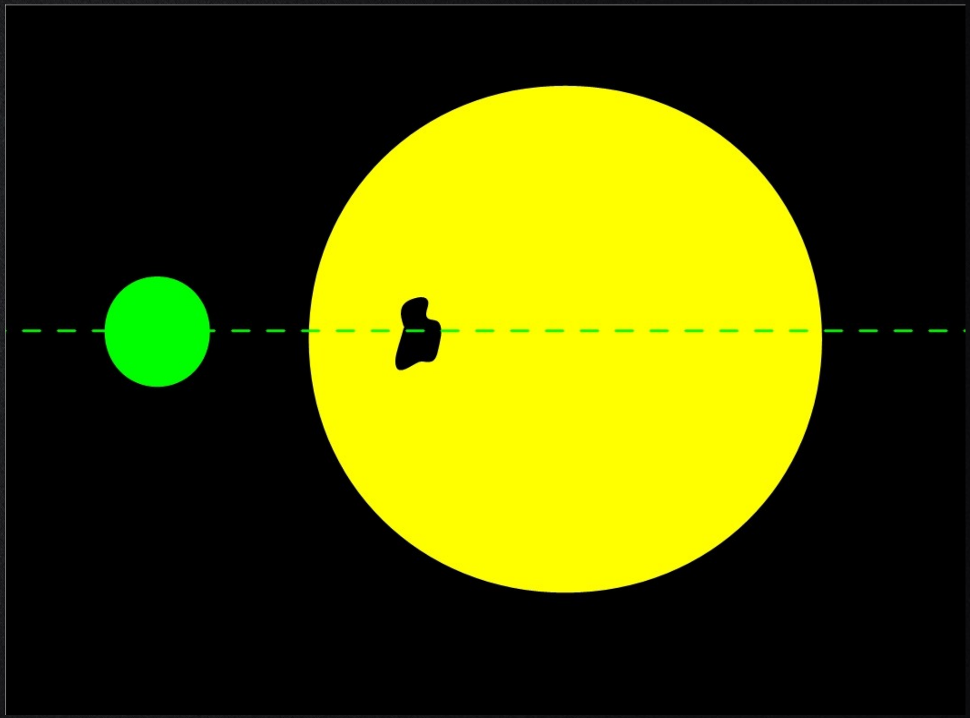

Non-occulted stellar spots

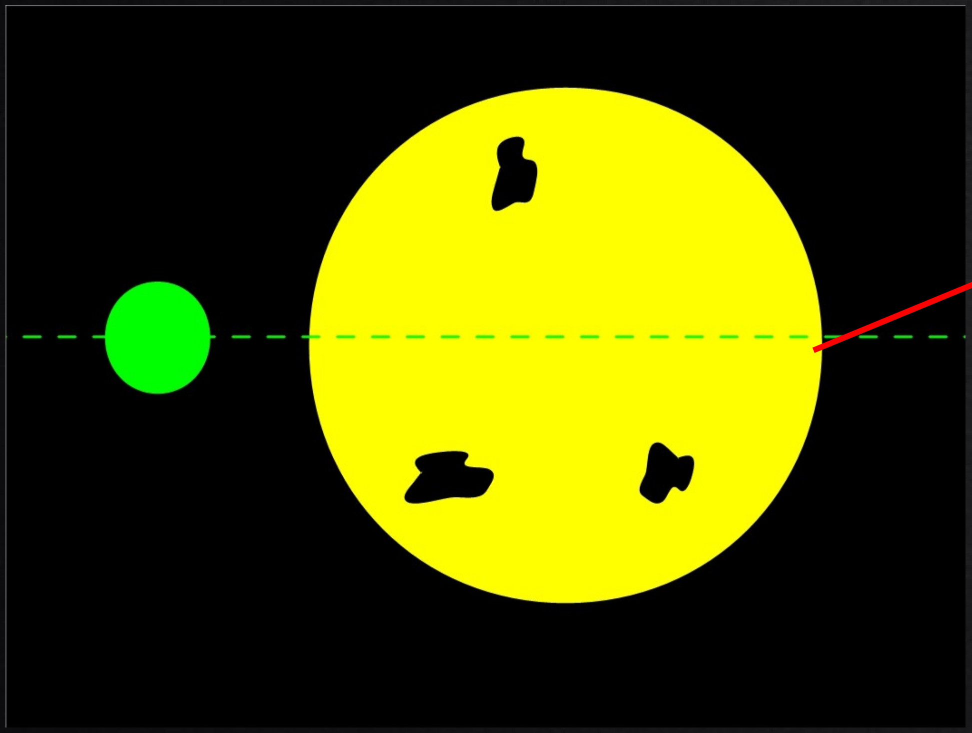

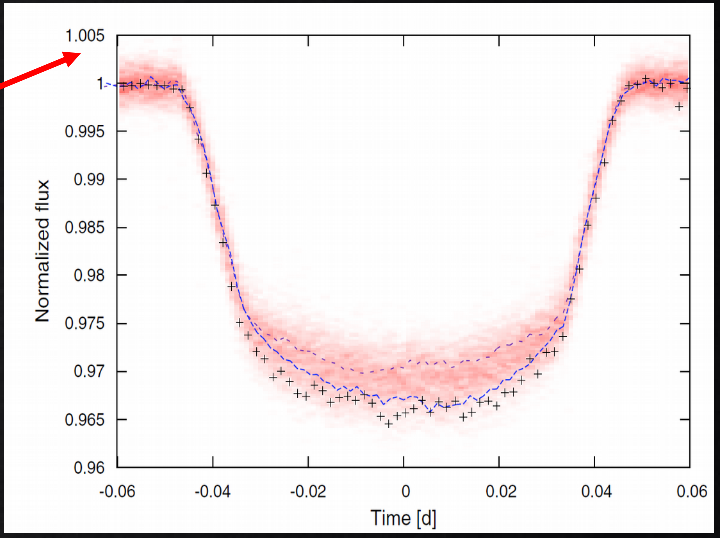

CoRoT-2b (Czesla + 2009)

Overestimation on the planet radius which can reach up to 4%.

Occulted stellar spots

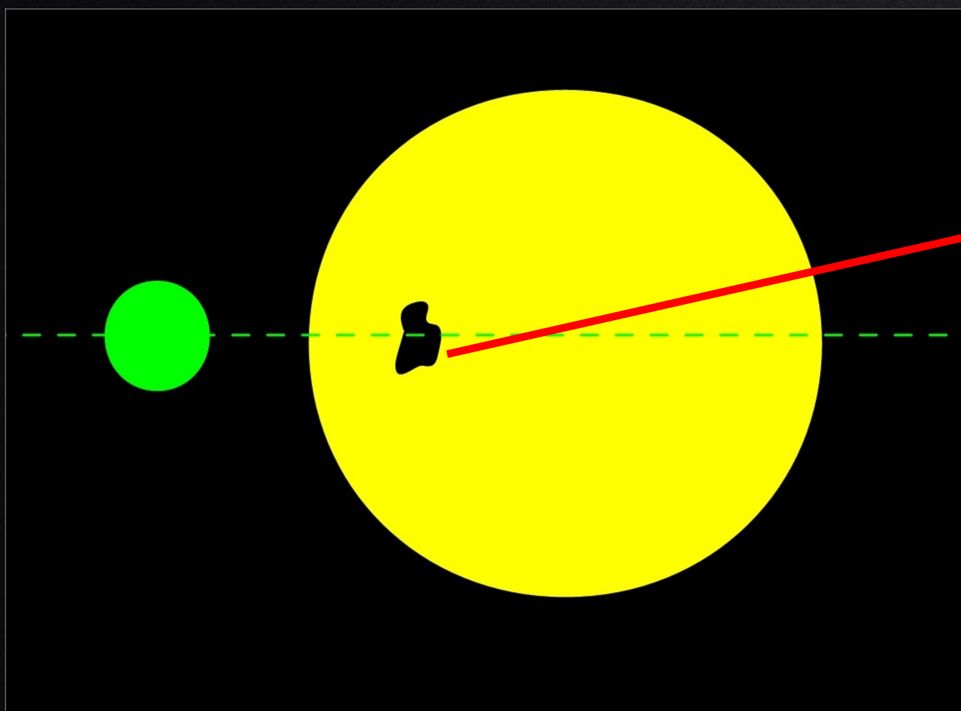

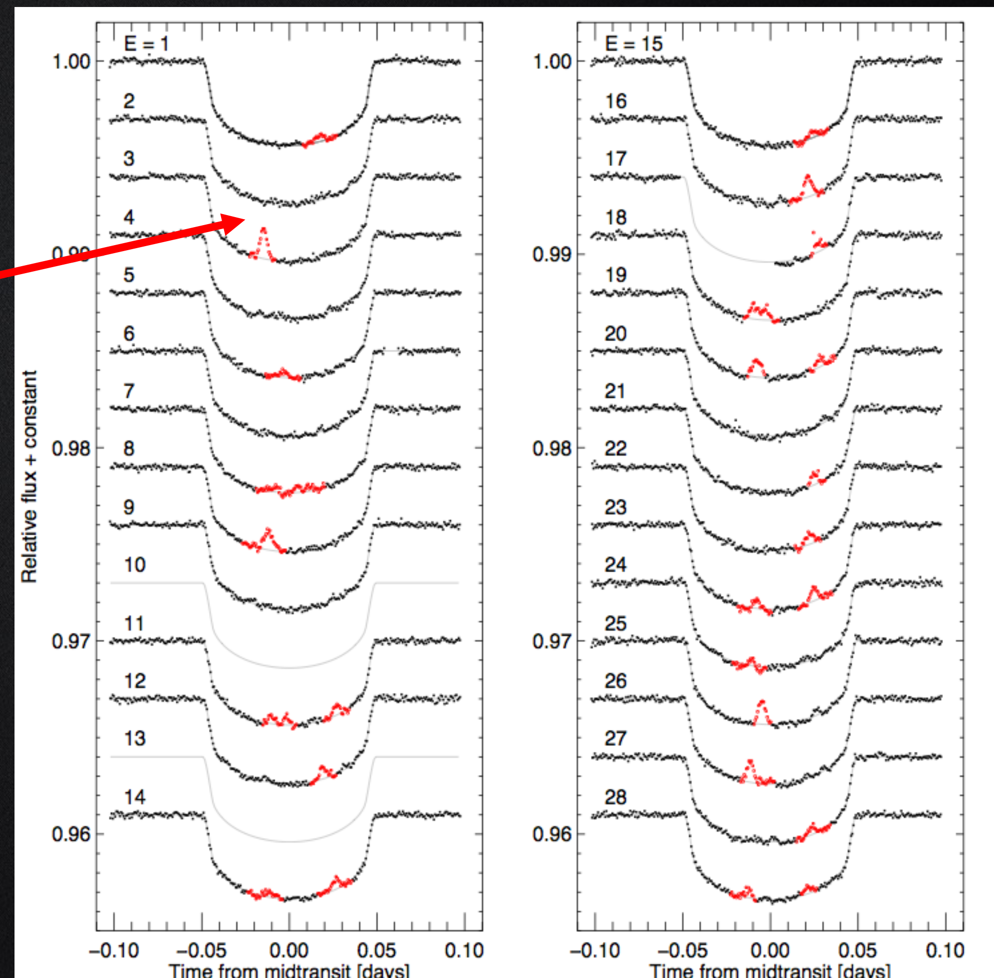

HAT-P-11b observed by Kepler

Occulted stellar spots impact

In the case that the spot occultation anomaly is clearly identifiable, it is well known that it affects our transit timing measurements.

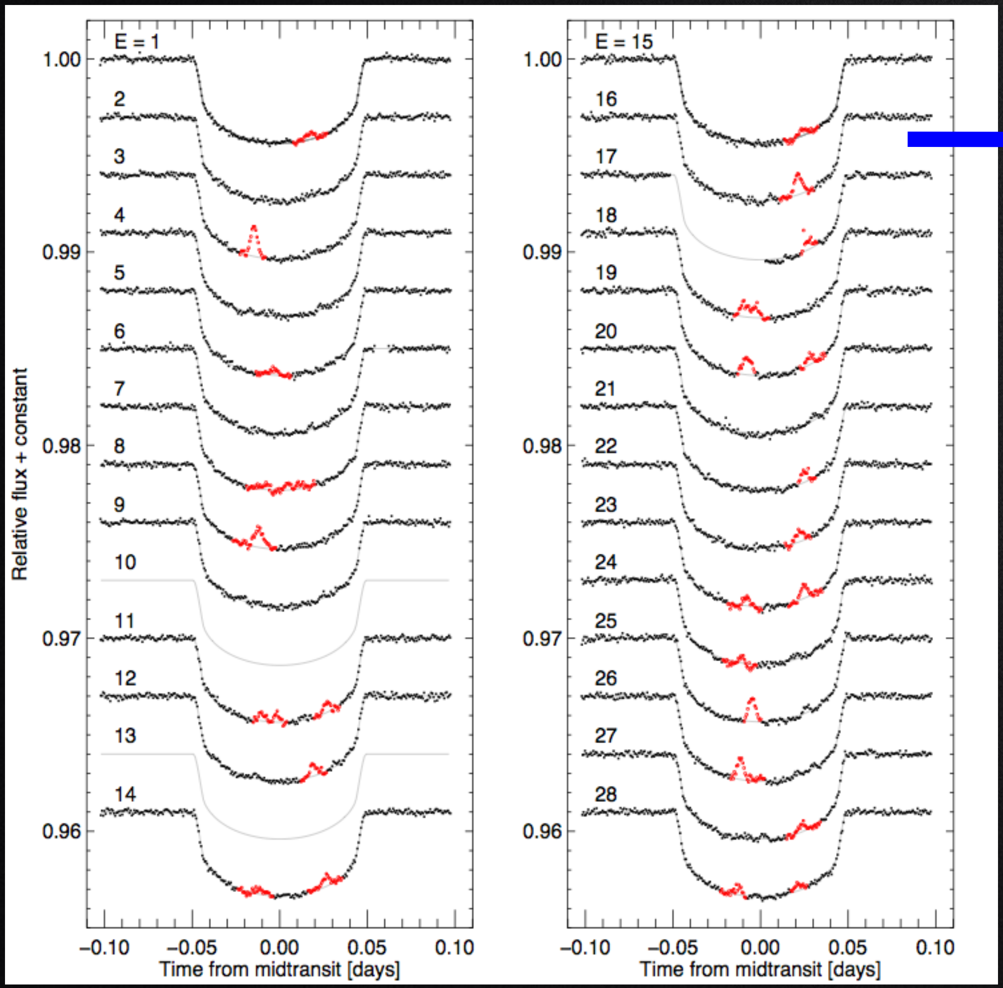

HAT-P-11b observed by Kepler

Some people consider assigning a zero weight to the anomalous points of the light curve (e.g Sanchis-Ojeda & Winn 2011)

May not be the best approach (Oshagh+ 2012, Barros+2013)

Occulted stellar spots impact

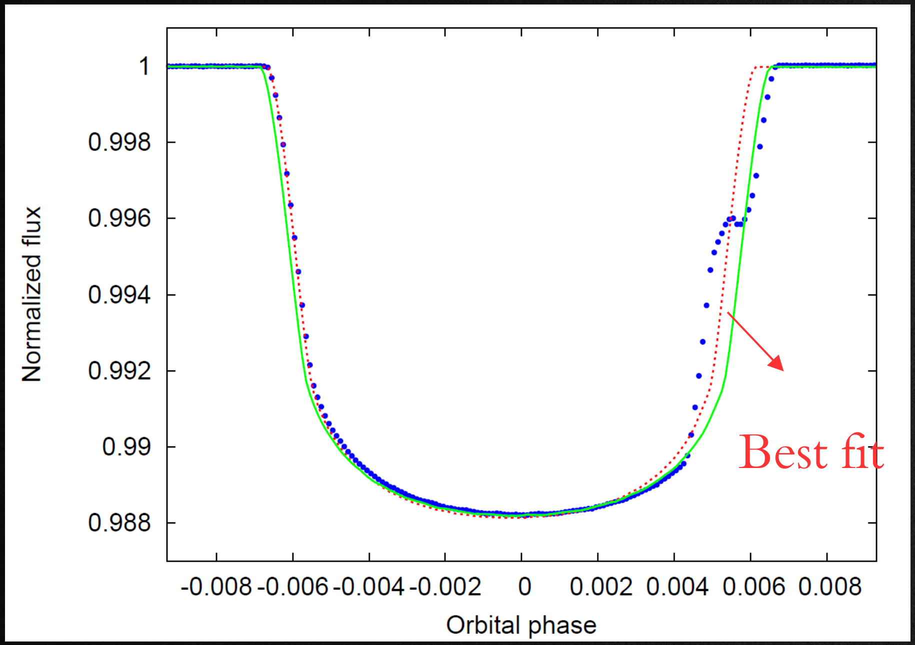

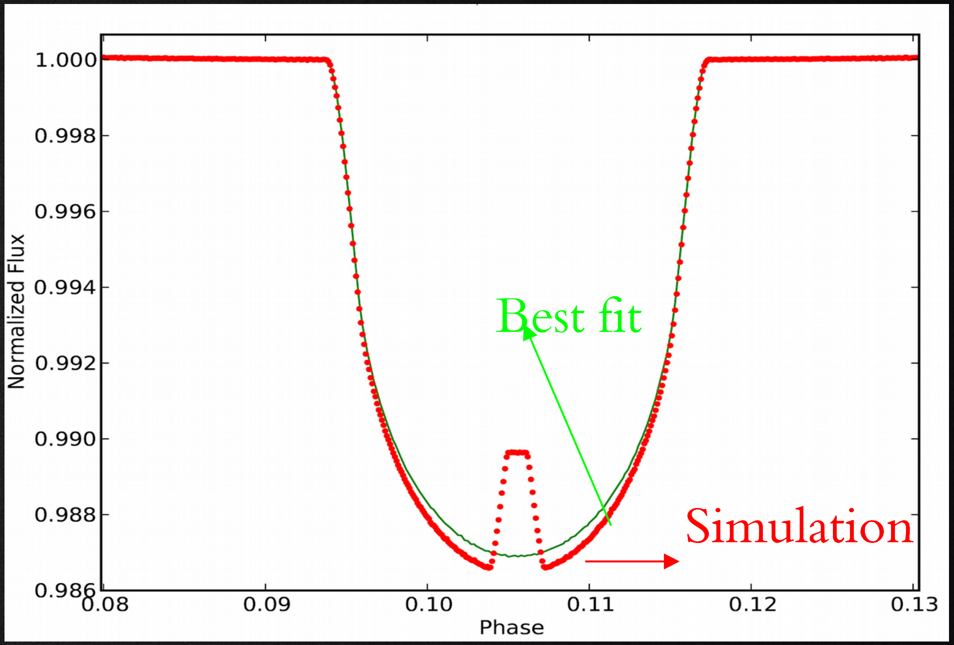

Planet radius estimations

A radius of Neptune size planet transiting a solar-like star and overlapping a spot with filling factor of 1 %, can be underestimated by 4%.

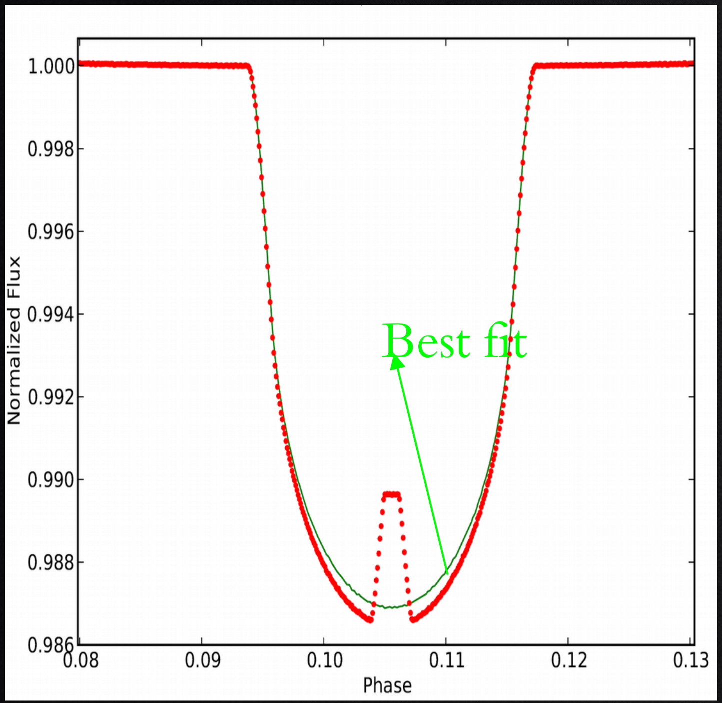

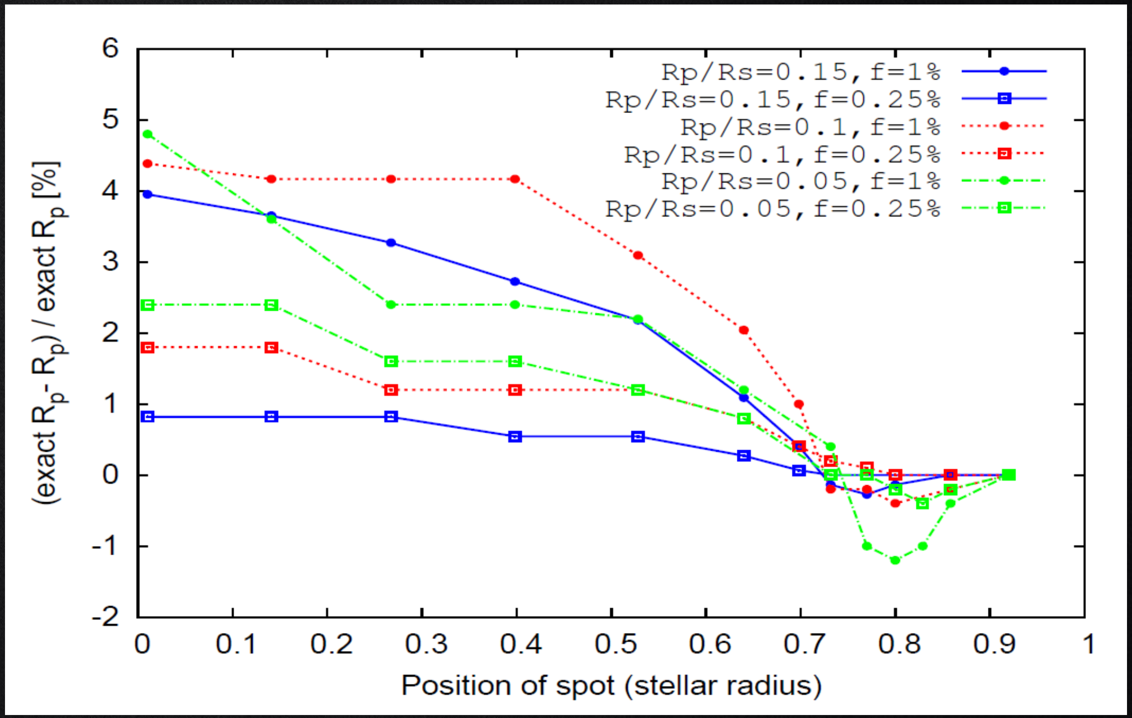

Oshagh+2013b

Transit duration estimation

A Jupiter size planet transiting a solar-like star and overlaps a spot with filling factor of 1% causes transit duration to be 4%, longer or shorter, which affects the planetary inclination measurements.

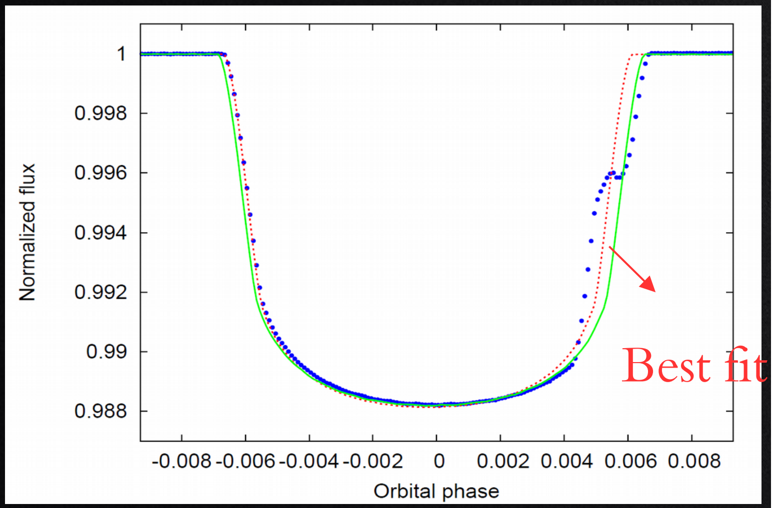

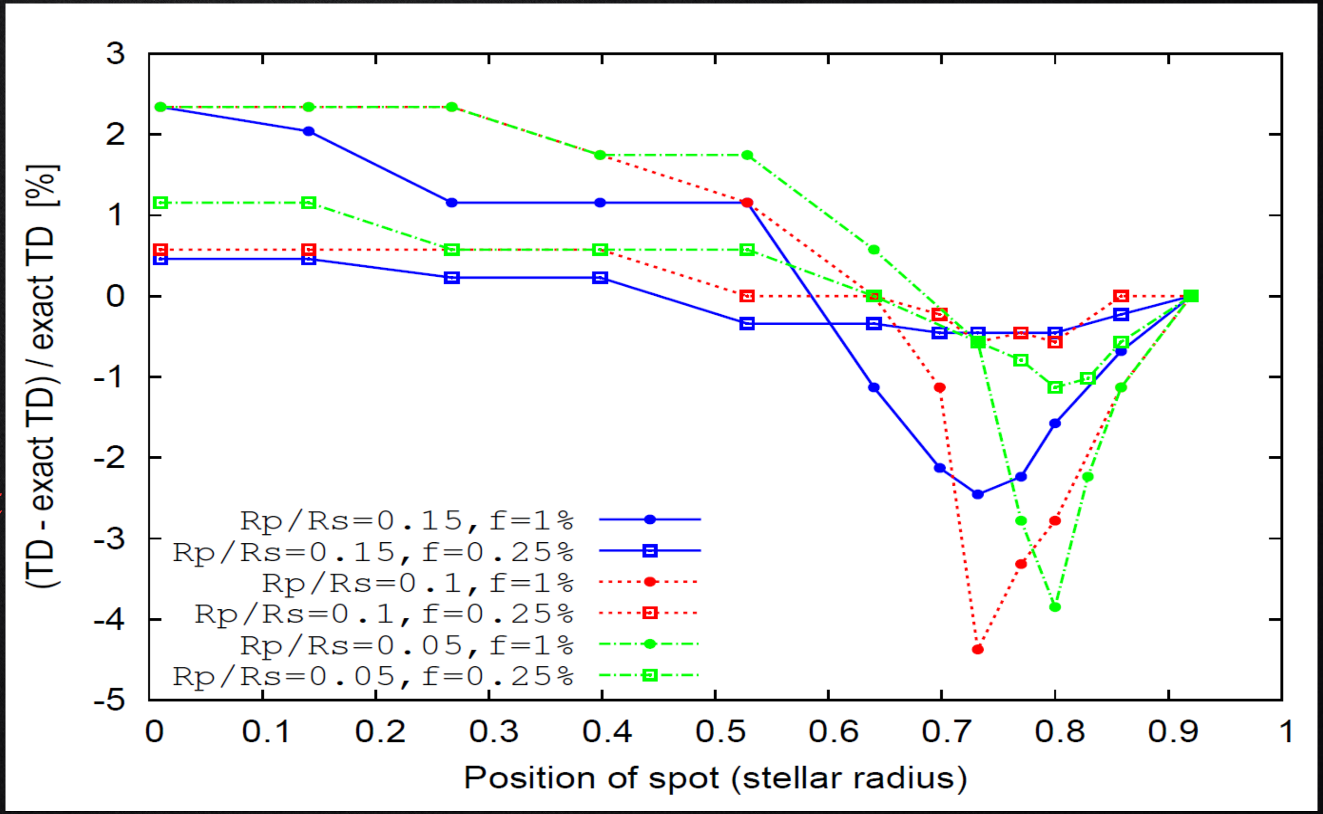

Oshagh+2013b

Transit timing variation (TTV)

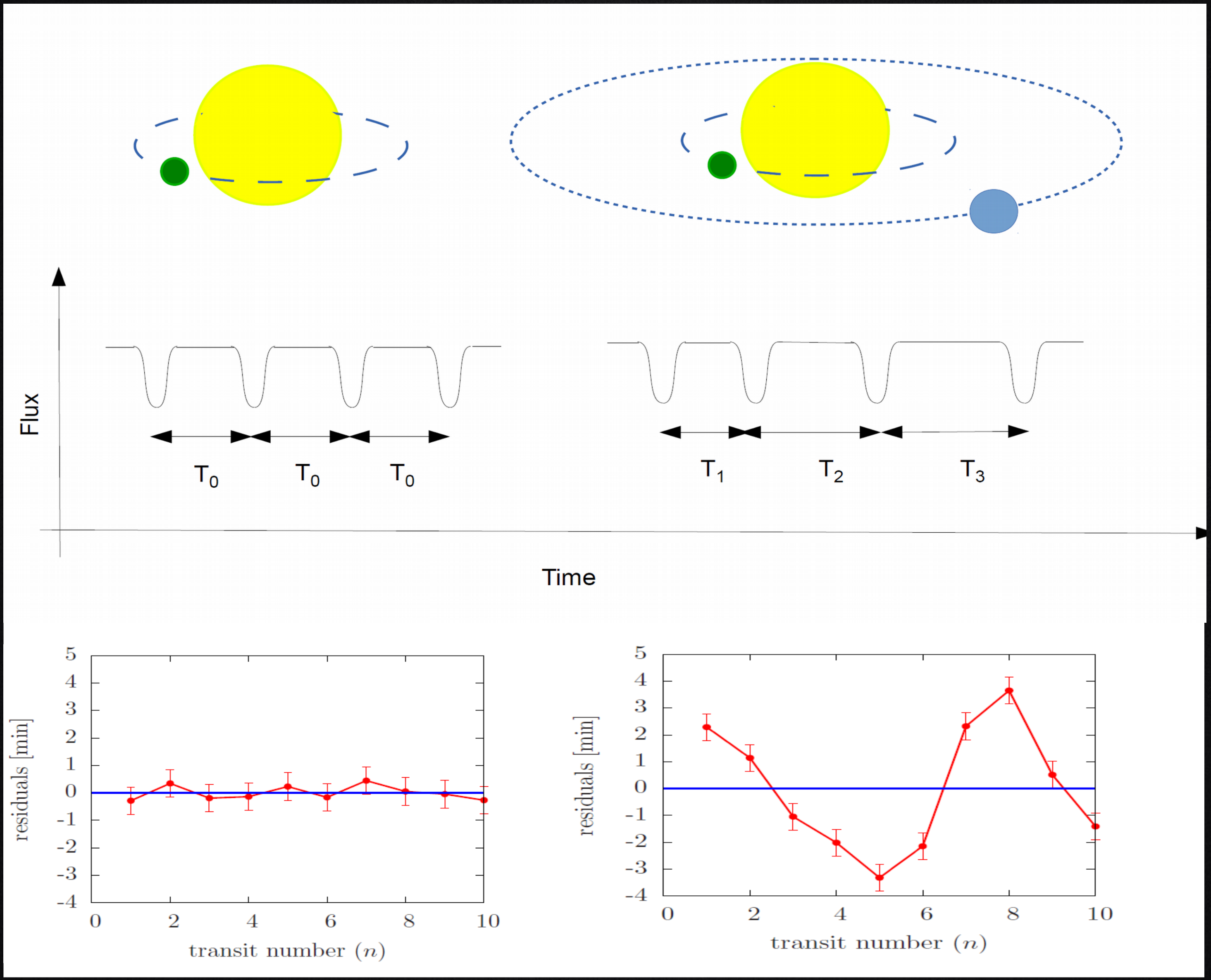

Boue+2012

Transit timing measurements

Jupiter size planet transiting a solar-like star overlaps a spot with a filling factor of 1 %, produces the maximum value of TTV around 300 seconds.

300 seconds amplitude of TTV can be induced by an Earth-mass planet in a mean-motion resonance with a transiting Jupiter-like planet on a 3 day orbit.

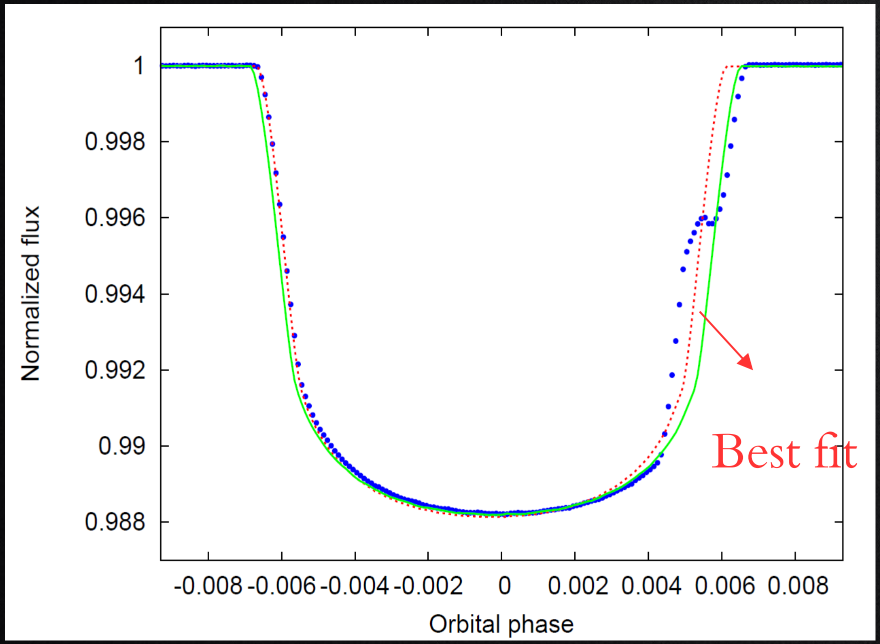

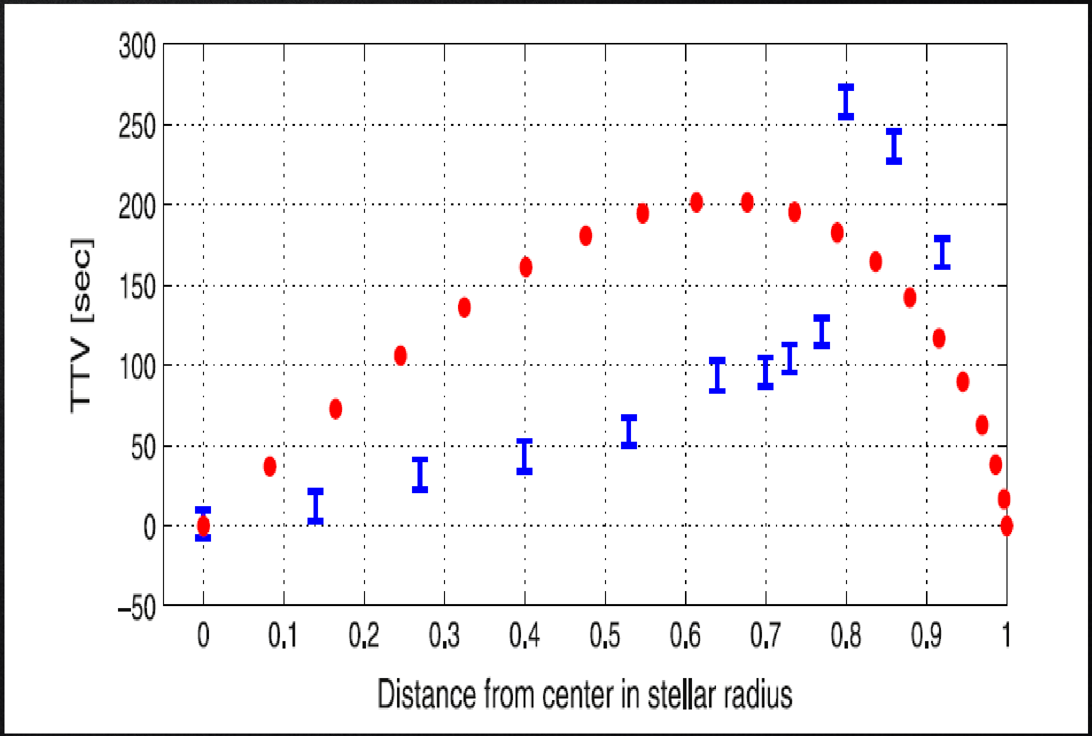

Mazeh+15

Transit timing measurements

Jupiter size planet transiting a solar-like star overlaps a spot with a filling factor of 1 %, produces the maximum value of TTV around 300 seconds.

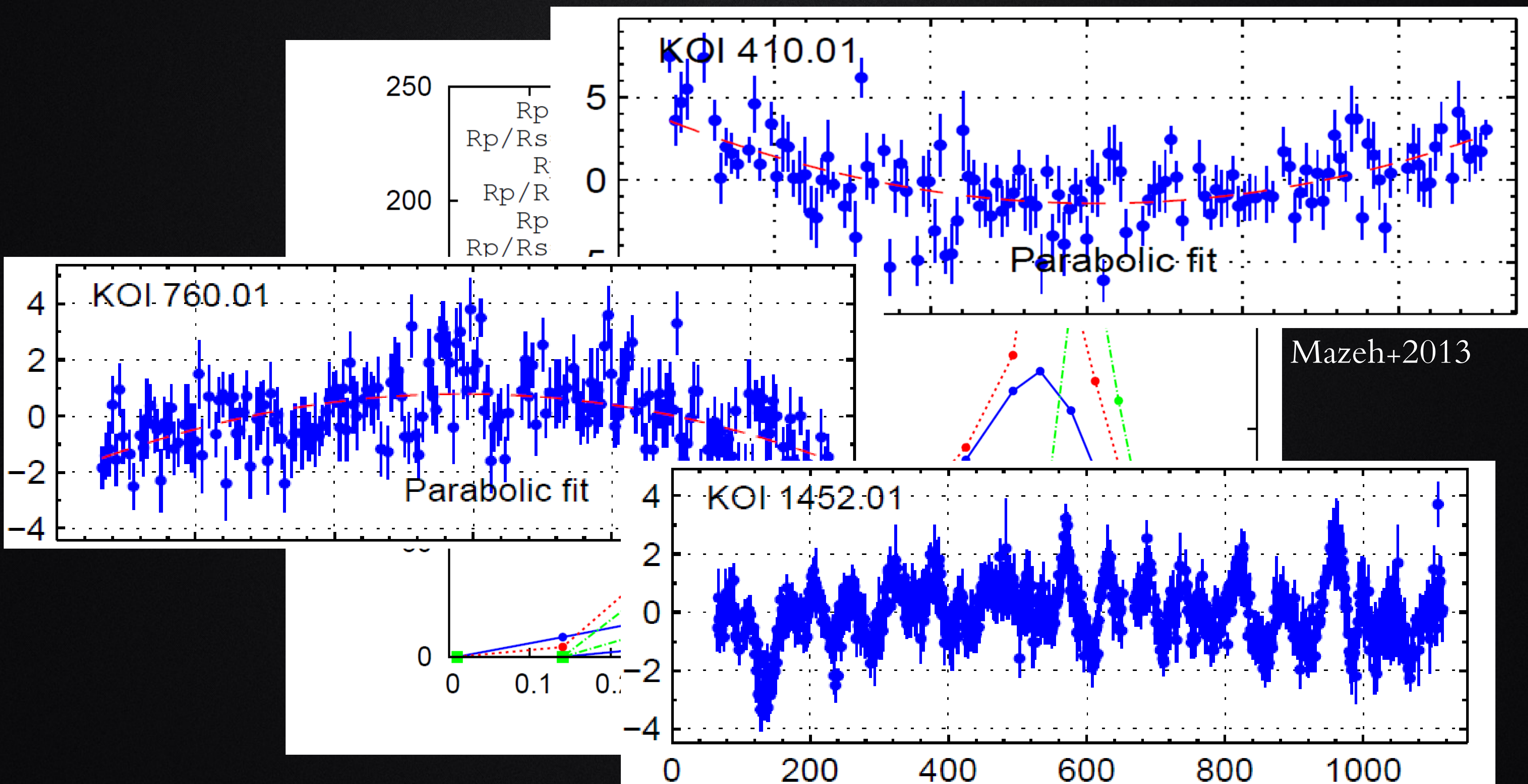

Transmission spectroscopy

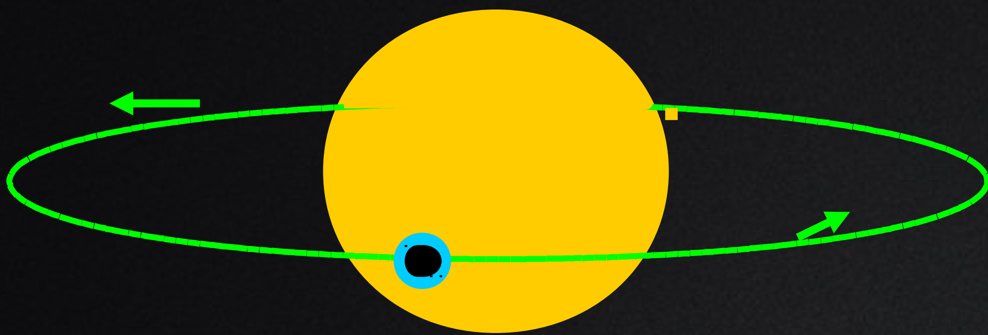

Multi-band photometry

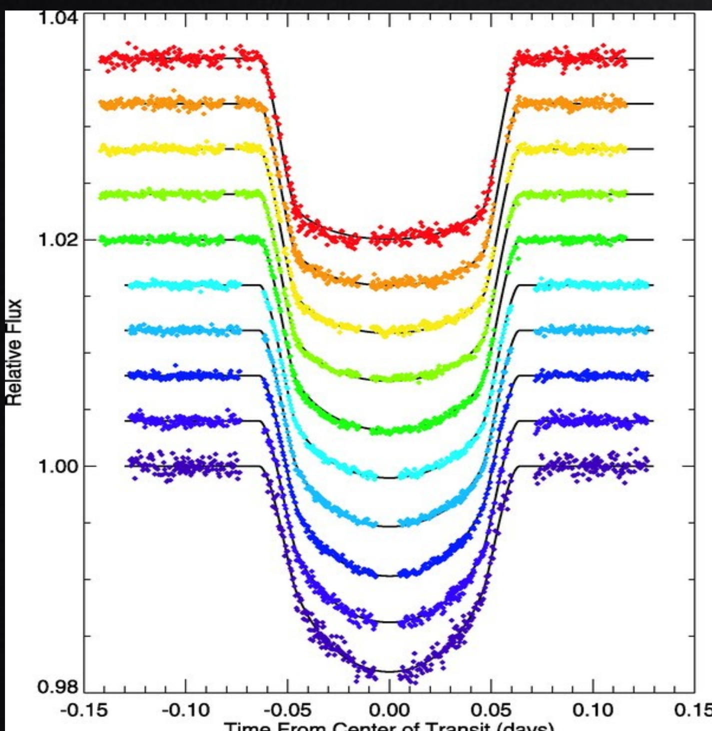

HD 209458b from 290–1030 nm (Knutson +2007)

$$\frac{R_p}{R_*}(\lambda)$$

–Molecular composition
–Thermal structure of the atmosphere

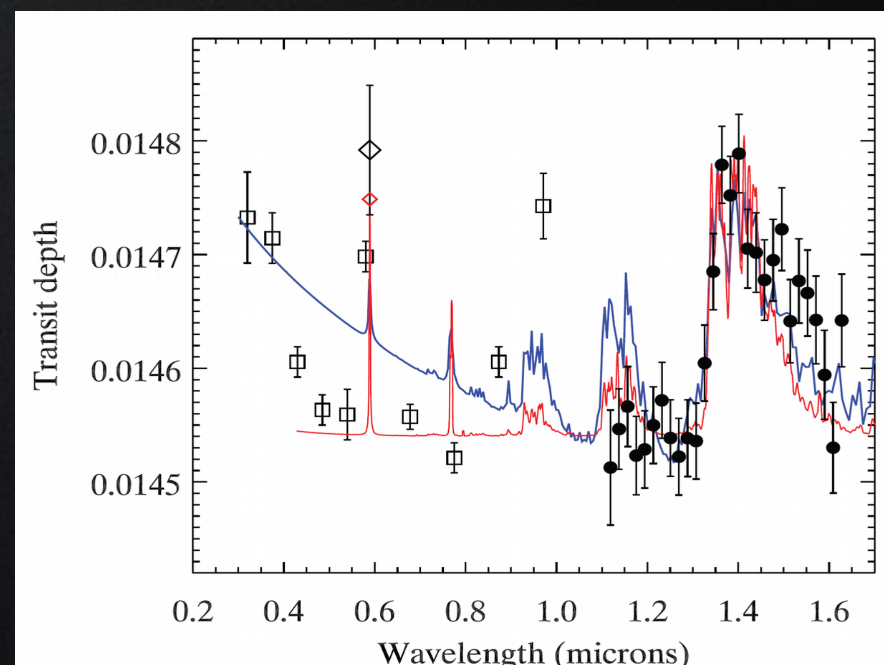

HD 209458b (Deming +2013)

Transmission spectra and activity

The anomalies inside the transit lead to a significant underestimation or overestimation of the planet-to-star radius ratio as a function of wavelength. At short wavelengths, the effect can reach up to a maximum difference of 10% in the planet-to-star radius ratio.

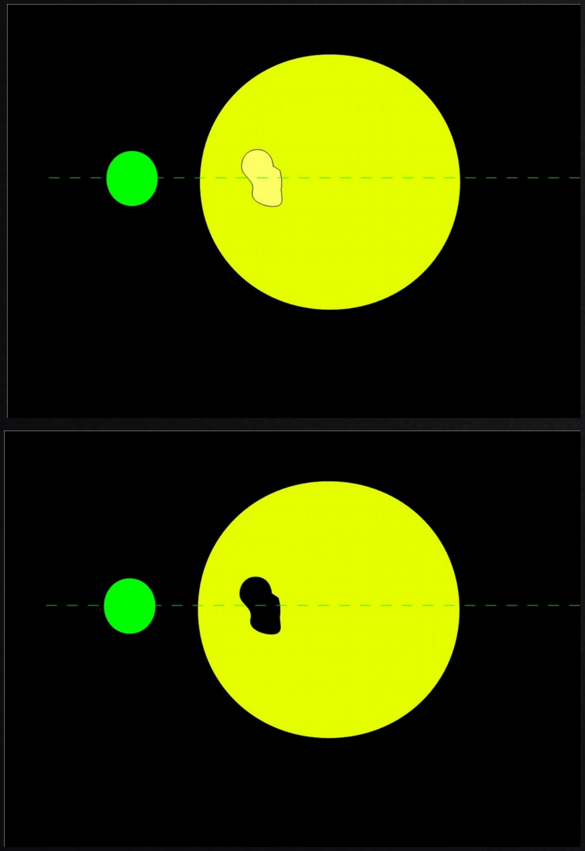

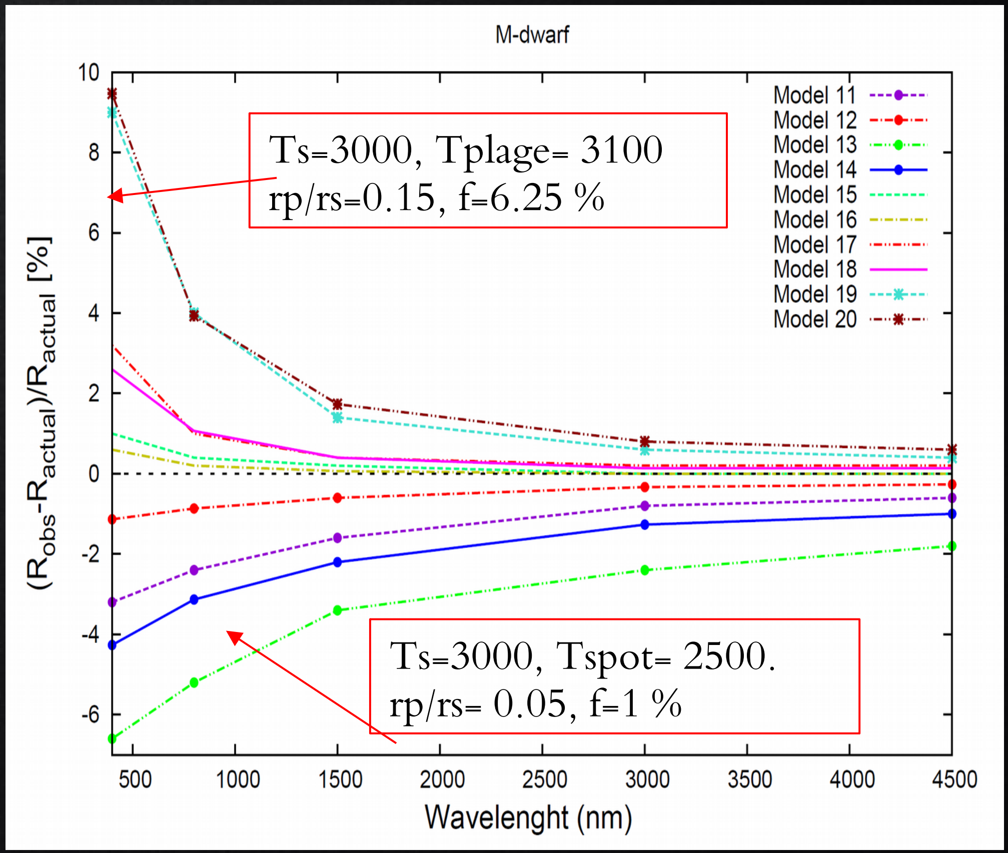

Oshagh+2014

HD 189733 b

Pont+2013 reported excess in the HD 189733b's radius in the short wavelength (300−800nm) and the authors find a good agreement between this observation and the prediction of Rayleigh scattering in the planet atmosphere (blue sky).

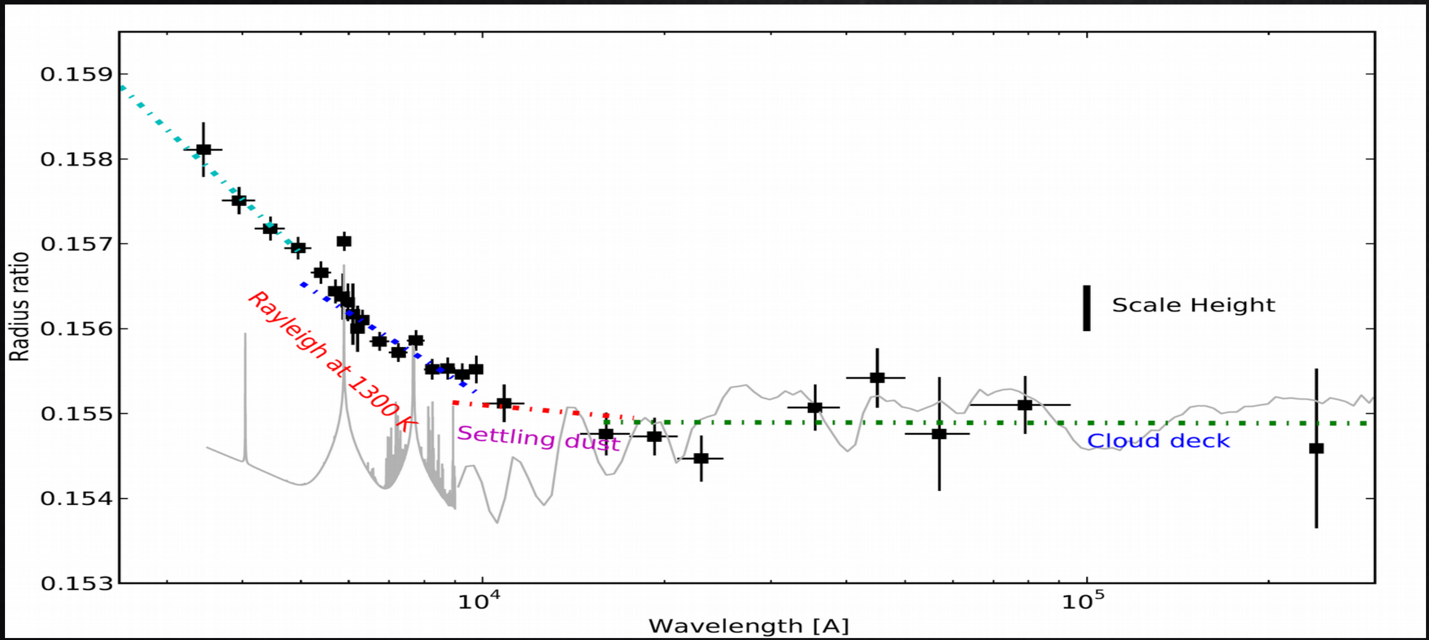

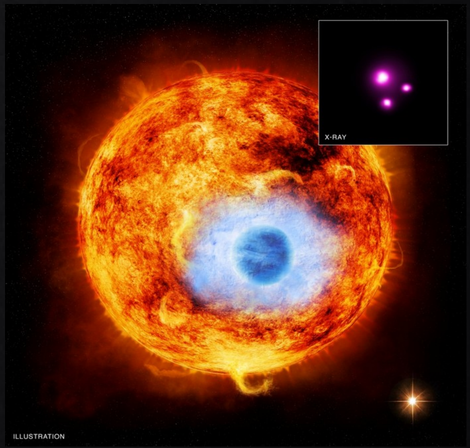

Pont +2013

HD 189733 b

HD 189733 is an active star which shows photometric modulation up to ≃ 2% during its 12 days stellar rotation period (Boisse+2009).

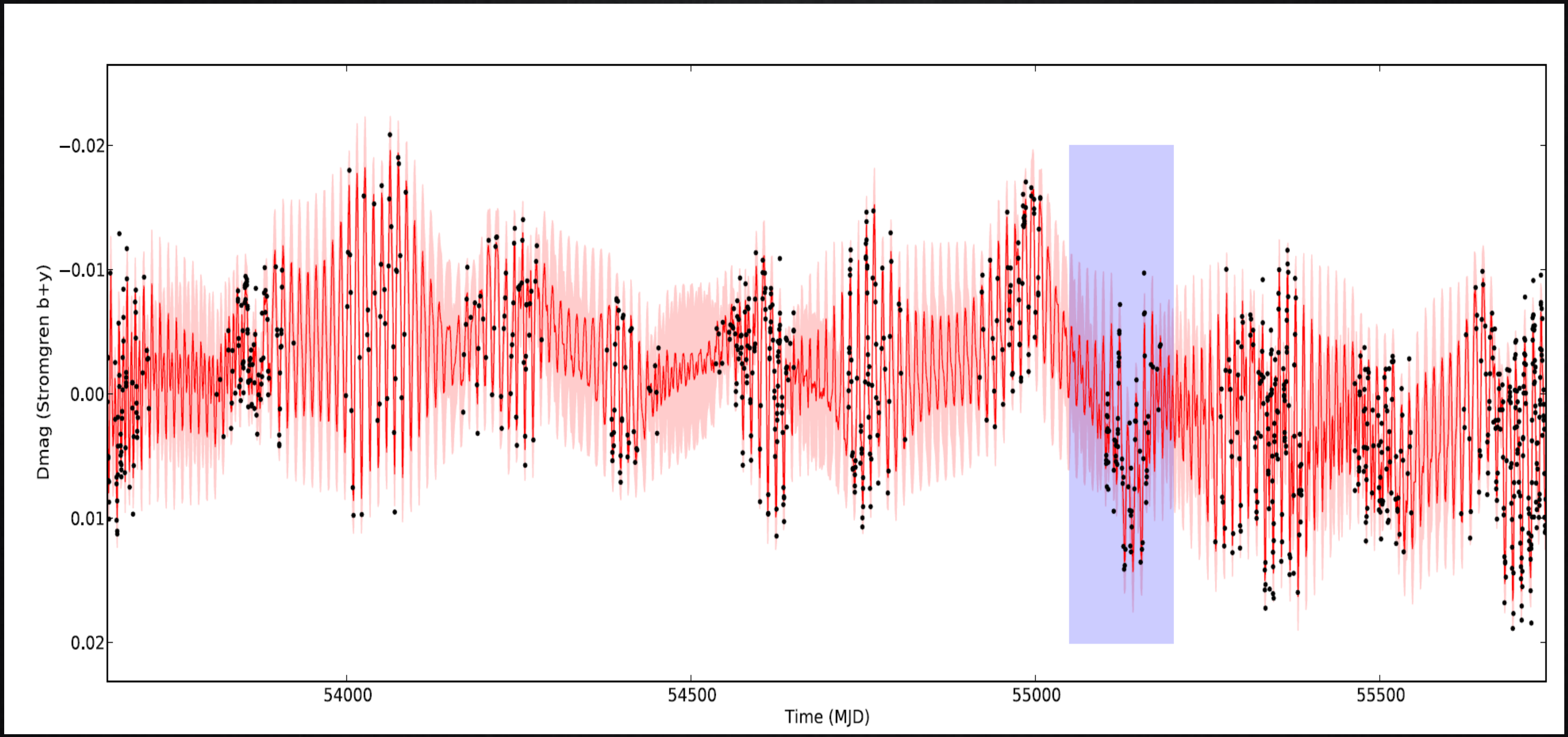

Pont+2013

HD 189733 b

The observed transmission spectrum of HD 189733b can be reproduced simply by considering the overlap of HD 189733b with a stellar plage or by presence of non-occulted stellar spots.

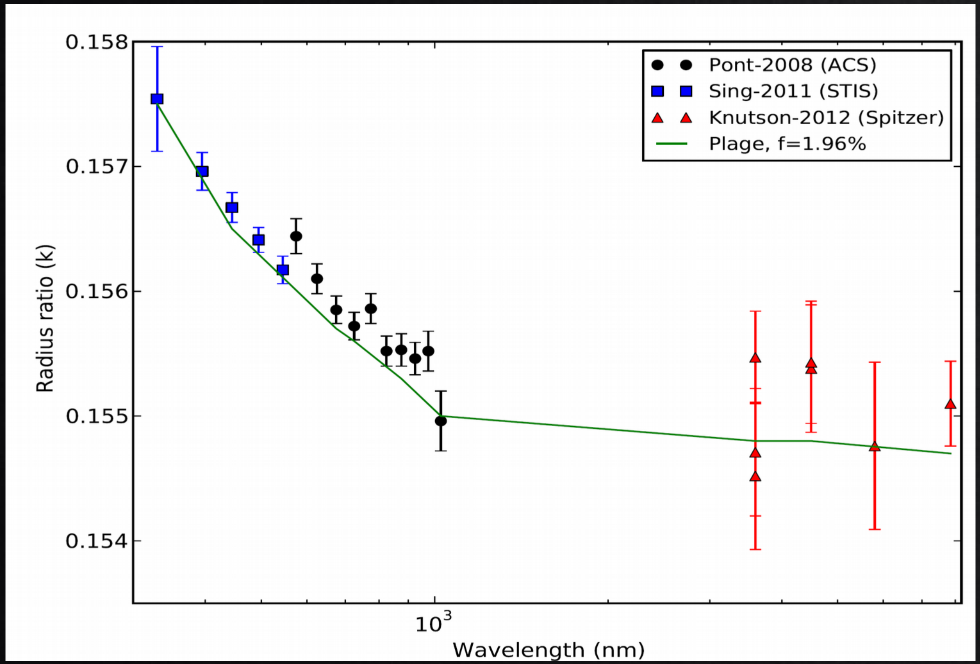

Oshagh+2014

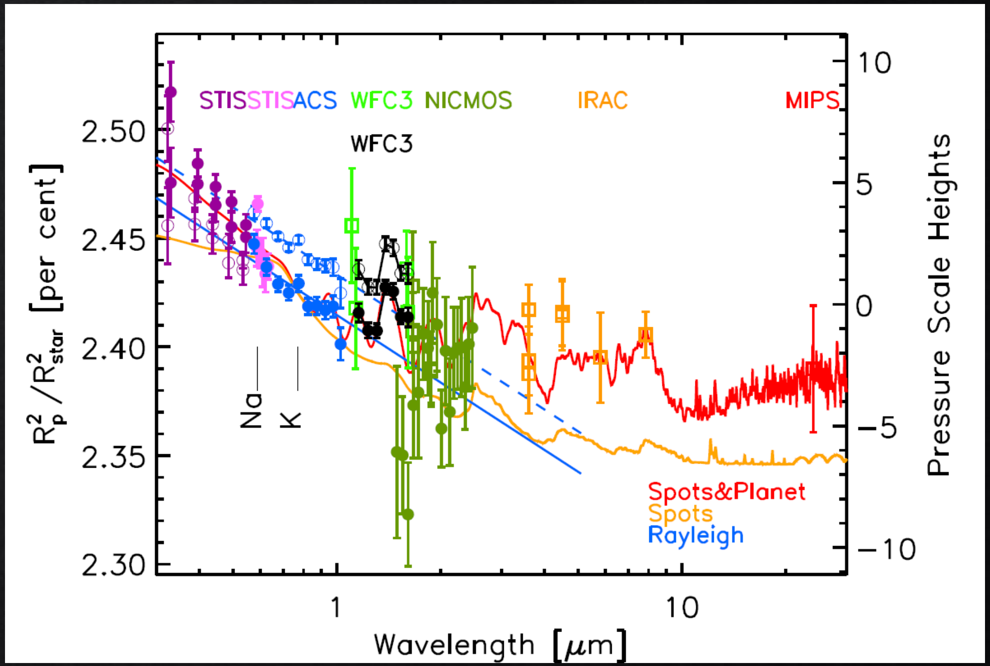

McCullough+2014

Rossiter–McLaughlin effect

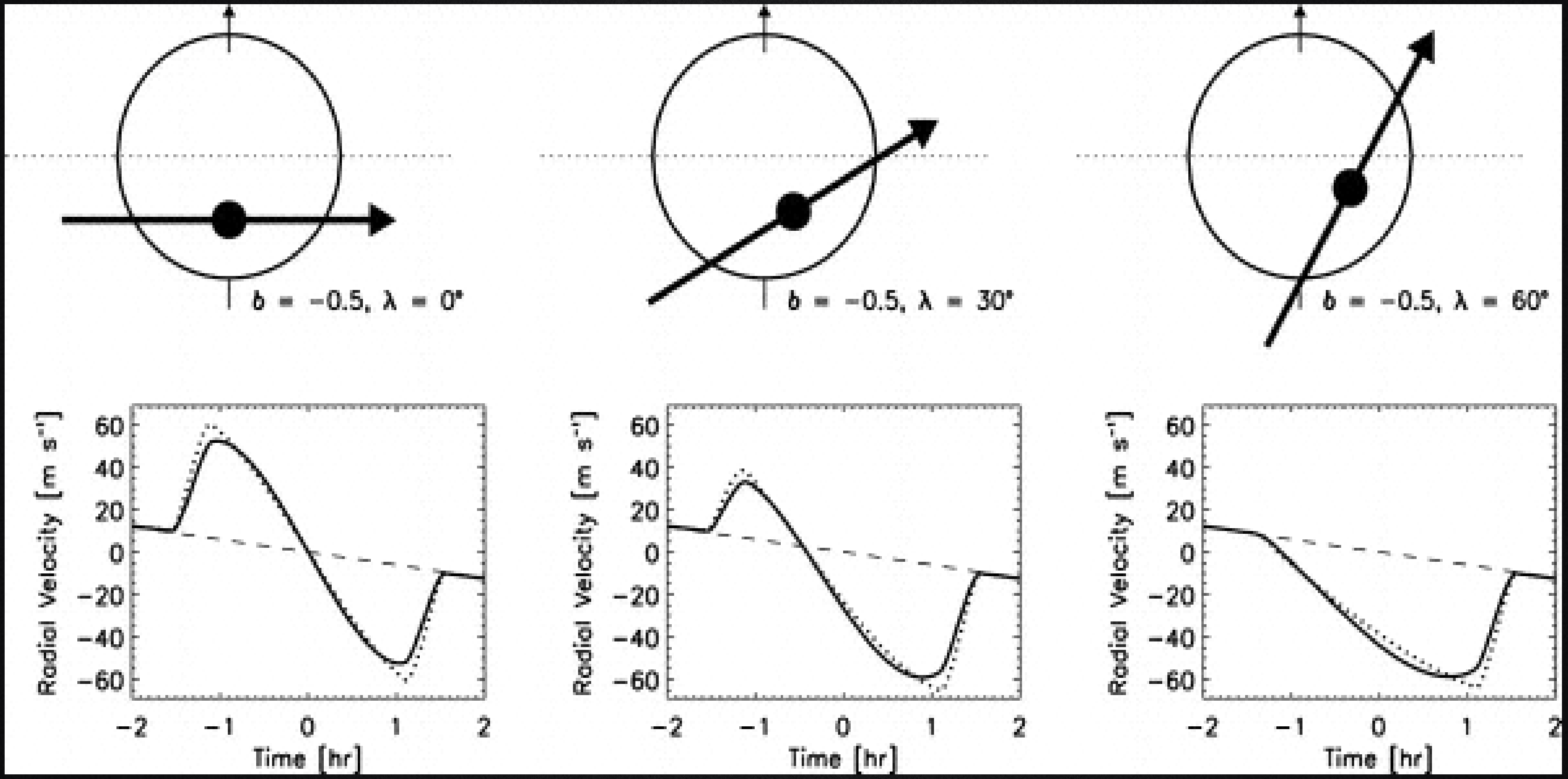

RM and occulted spots

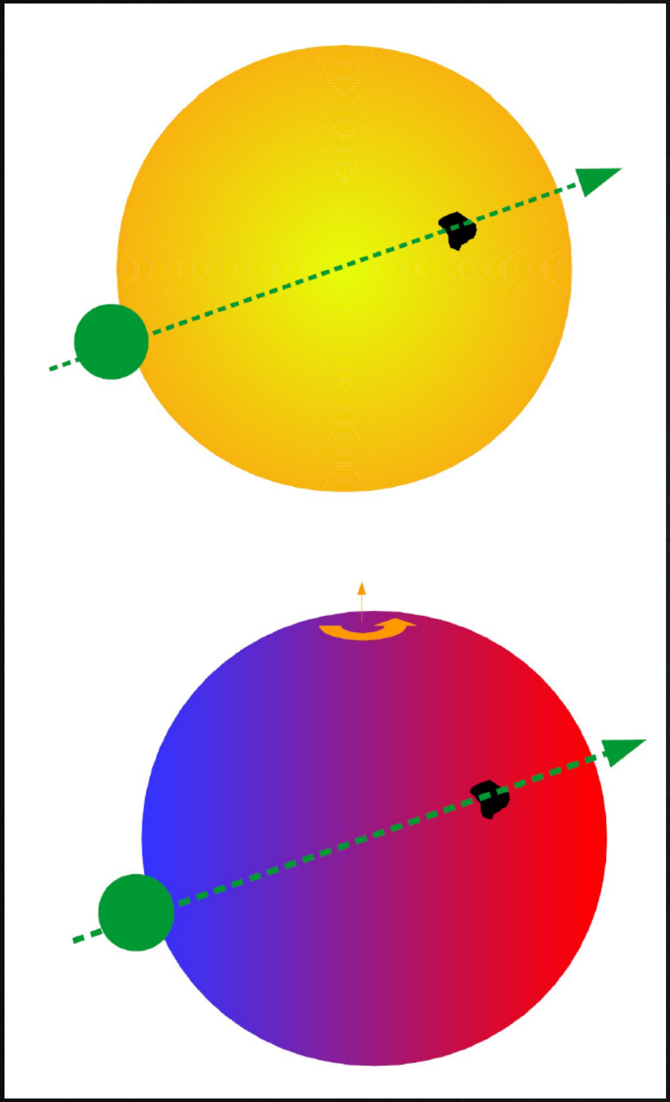

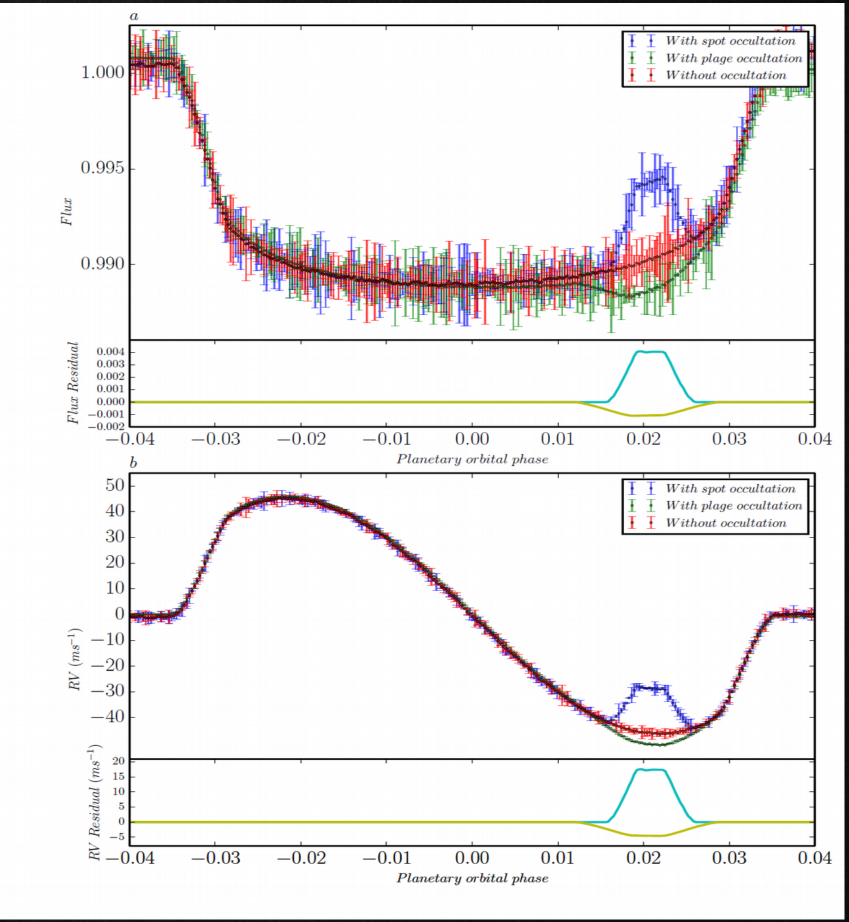

RM and occulted spots

The inaccurate estimation on the spin-orbit angle due to stellar activity can be quite significant (up to 30 degrees), particularly for the edge-on, aligned, and small transiting planets.

Therefore the aligned transiting planets are the ones that can be easily misinterpreted as misaligned owing to the stellar activity.

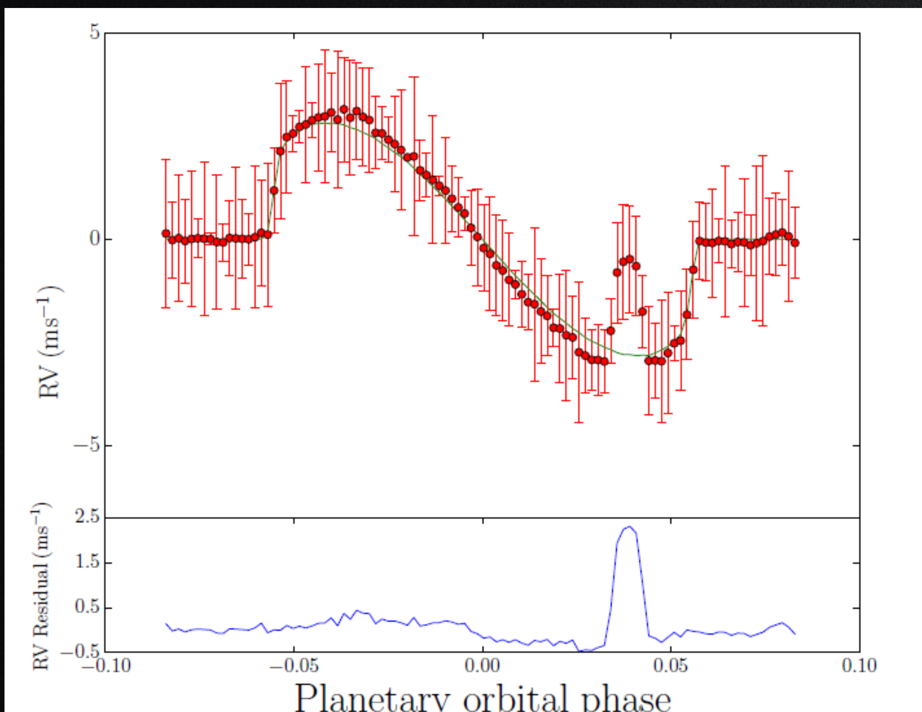

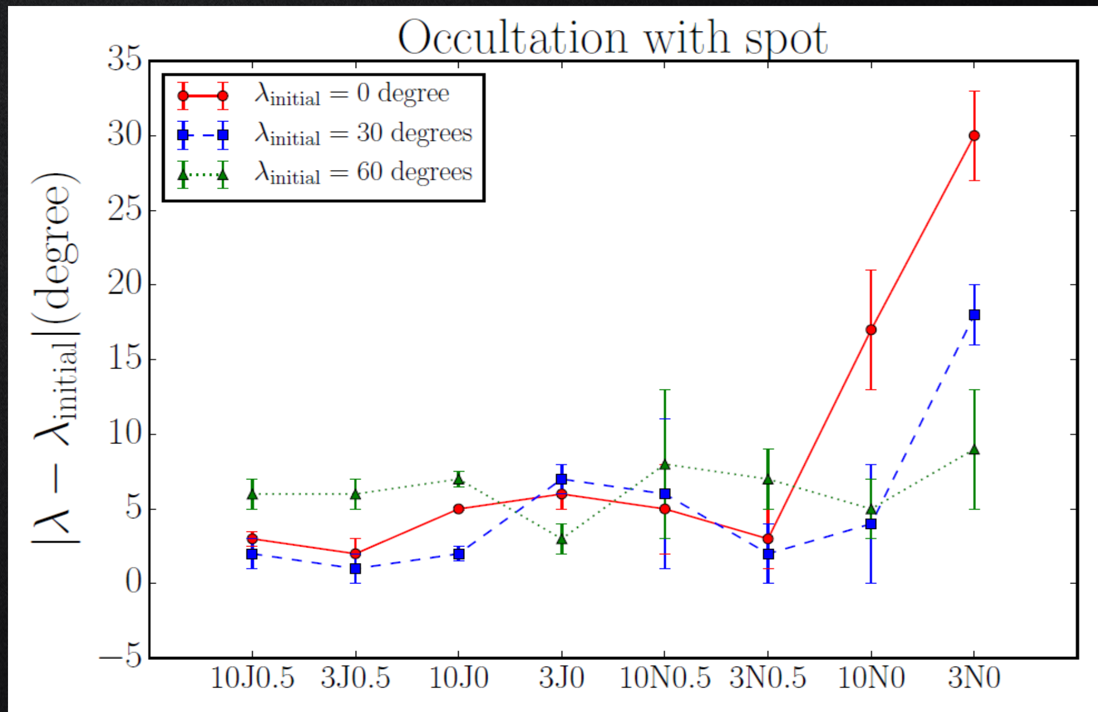

A Neptune-sized aligned planet transits a solar like star with vsini=3 km/s

Oshagh+2016

Modeling activity in photometry

MACULA

MACULA can model rotational modulations in the photometry of spotted stars, numerically. It takes into account differential rotation, non-linear limb darkening, and starspot evolution

Fortran 90 and Python, available on https://www.cfa.harvard.edu/~dkipping/macula.html

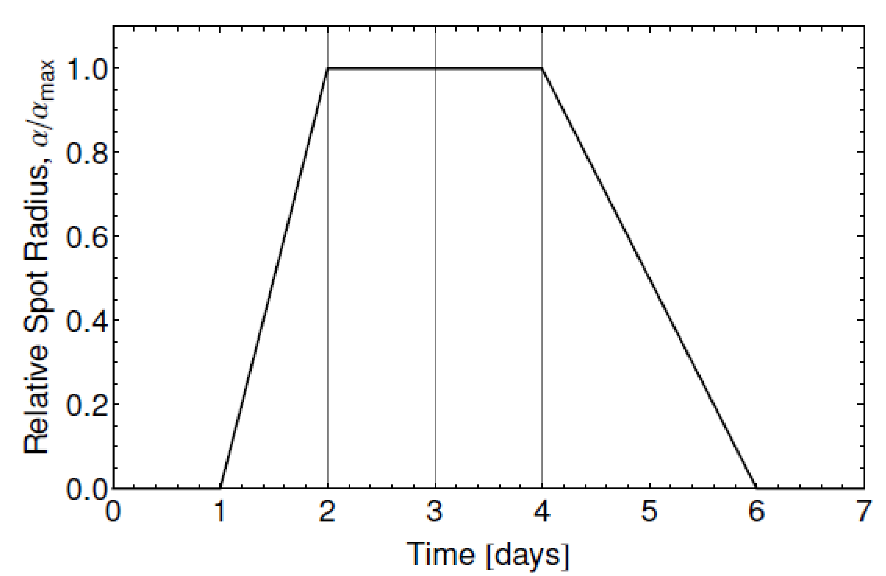

Figure 1. *An example of our linear starspot evolution model. We plot the size of the starspot in units of α_{max} as a function of time. The gridlines (left-to-right) mark the end of ingress, the instant t_{max}, and the start of egress.*

MACULA

MACULA requires as input the stellar parameters (**stellar inclination, stellar rotation period, limb darkening coefficients**) and also active region's parameters (**Longitude, latitude, maximum filling factor, lifetime, grow time, decay time, time of maximum size**)

$$\frac{\alpha_k(t_i)}{\alpha_{\max,k}} = \mathcal{I}_k^{-1}[\Delta t_1 \mathsf{H}(\Delta t_1) - \Delta t_2 \mathsf{H}(\Delta t_2)] - \mathcal{E}_k^{-1}[\Delta t_3 \mathsf{H}(\Delta t_3) - \Delta t_4 \mathsf{H}(\Delta t_4)].$$

and using

$$\Delta t_1 = t_i - t_{\max,k} + \frac{L_k}{2} + \mathcal{I}_k,$$
$$\Delta t_2 = t_i - t_{\max,k} + \frac{L_k}{2},$$
$$\Delta t_3 = t_i - t_{\max,k} - \frac{L_k}{2},$$
$$\Delta t_4 = t_i - t_{\max,k} - \frac{L_k}{2} - \mathcal{E}_k,$$

H(x) is the Heaviside Theta step-function.

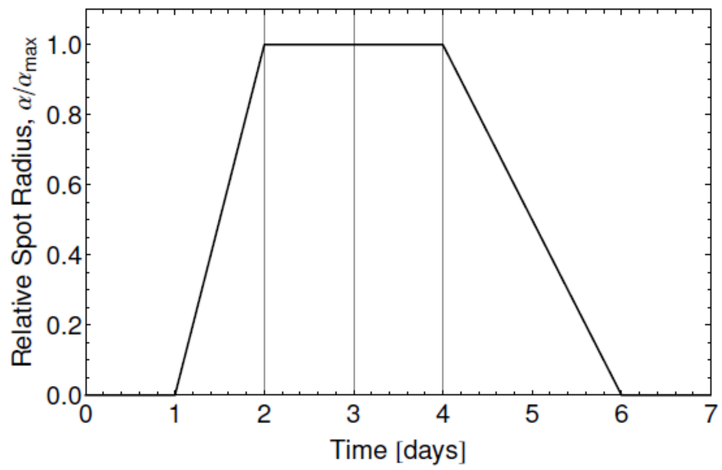

Figure 1. *An example of our linear starspot evolution model. We plot the size of the starspot in units of $\alpha_{\max}$ as a function of time. The gridlines (left-to-right) mark the end of ingress, the instant $t_{\max}$, and the start of egress.*

MACULA

Tau Ceti

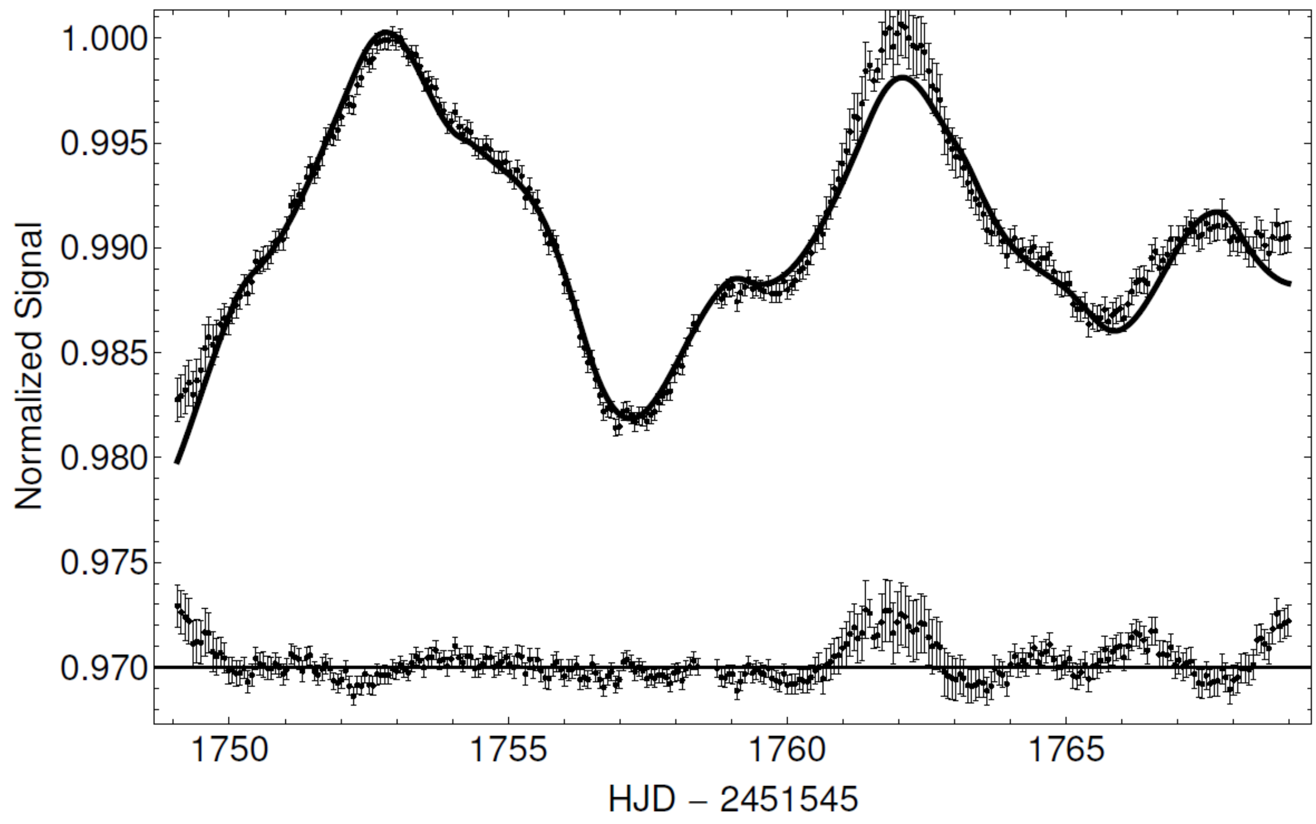

Figure 5. *Maximum a-posteriori two-spot model fit to the 2004 MOST data of κ^1 Ceti using the analytic model presented in this work. Regression performed using* MultiNest *in conjunction with the 2003 & 2005 data. Residuals to the fit are offset by 0.97. Figure may be directly compared to Figure 5 of Walker et al. (2007), where one can see an essentially indistinguishable result.*

Kipping, 2012

SPOTROD

A semi-analytic model for transits of spotted stars limb darkening law and a number of homogeneous, circular spots on their surface.

C and Python, available on https://github.com/bencebeky/spotrod

HAT-P-11

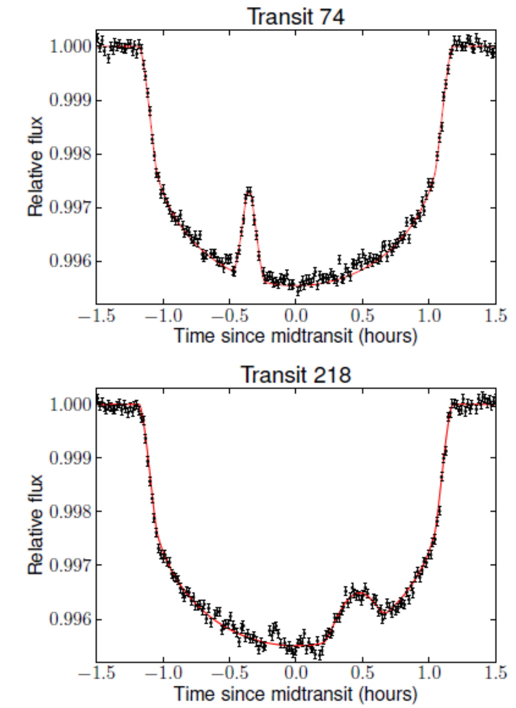

Figure 2. HAT-P-11 transit 74 (top panel) and transit 218 (bottom panel) lightcurves. Dots are *Kepler* short cadence observations, with errorbars given by the `SAP_FLUX_ERR` data column. Red curves are best fit `spotrod` models assuming a single spot on the stellar surface for both transits.

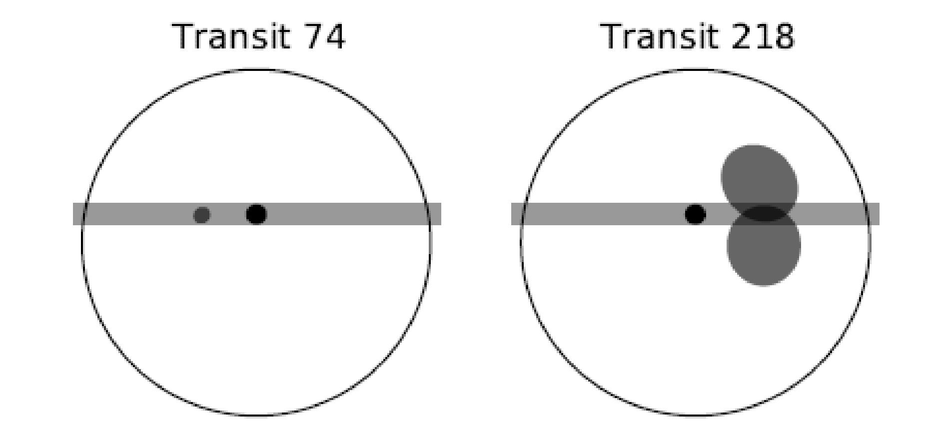

Figure 3. Projected images of HAT-P-11 during transits 74 (left panel) and 218 (right panel). Large circle is the star, solid black small circle is the planet HAT-P-11b at midtransit, gray strip is the transit chord, one or two gray ellipses are best fit solutions for the one or two modes of the spot.

Beky+2014

PRISM

PRISM uses a pixellation approach to represent the star and planet on a two-dimensional array in Cartesian coordinates. This makes it possible to model the transit, LD and starspots on the stellar disc.

IDL, available on ???

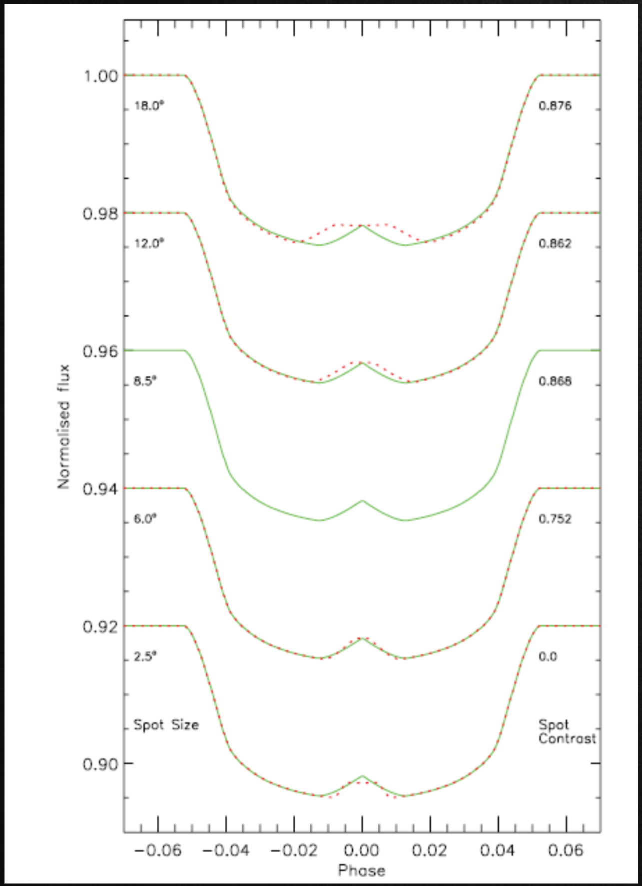

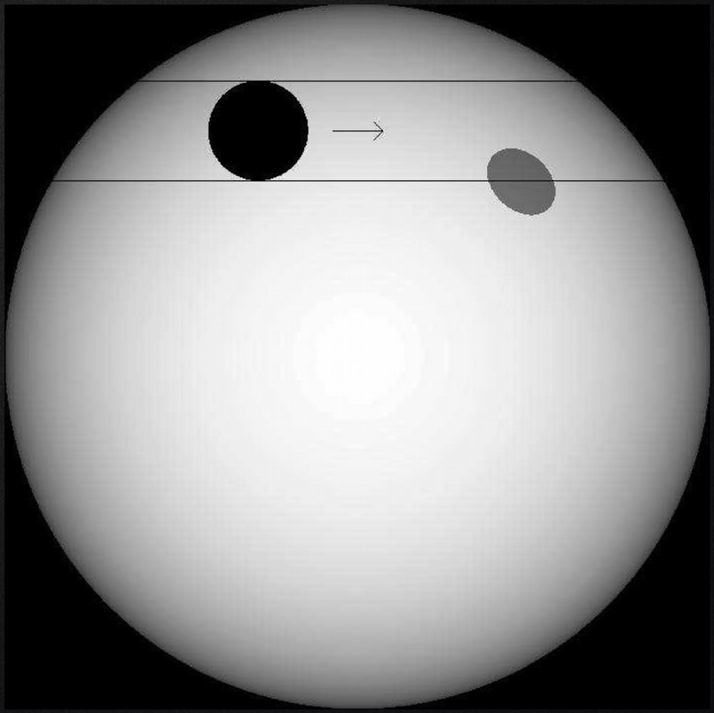

Tregloan-Reed+2013

PRISM

WASP-19b

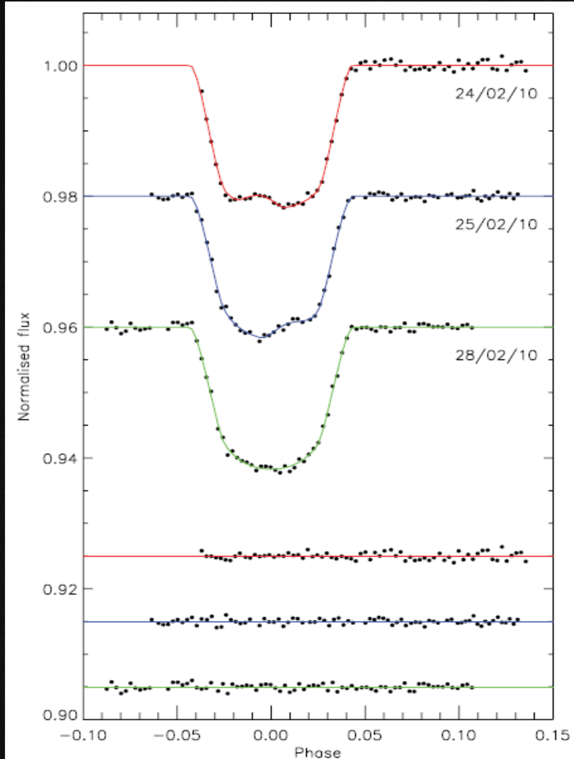

Figure 5. Transit light curves and the best-fitting models. The residuals are displayed at the base of the figure.

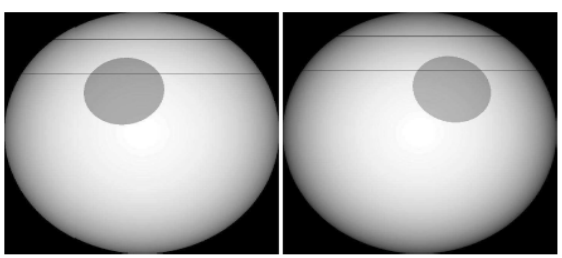

Figure 6. Representation of the stellar disc, starspot and transit chord for the two data sets containing spot anomalies.

Tregloan-Reed+2013

WASP-6b

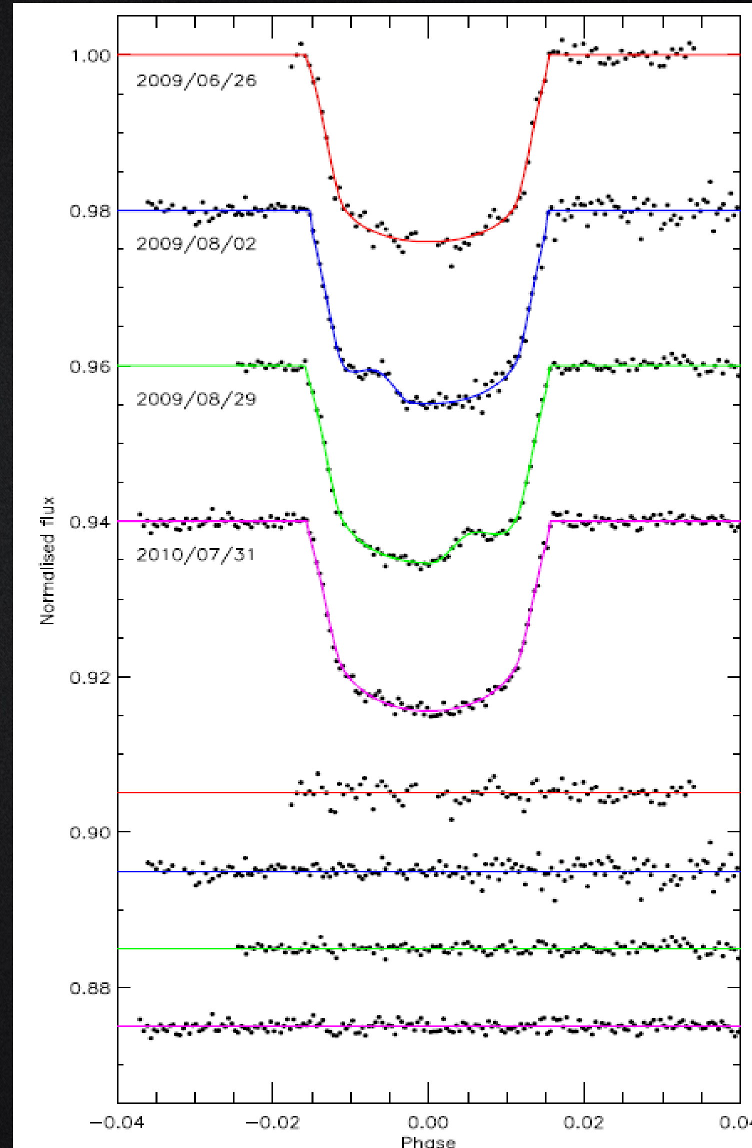

Tregloan-Reed+2015

SOAP-T

SOAP-T produces the expected light curve and the radial velocity signal of a system consisting of a rotating spotted star with a transiting planet. SOAP-T is able to reproduce the "*positive bump*" anomaly in the transit light curve and RV due to a planet-spot overlap (Oshagh + 2013a.).

C and Python, available on http://www.astro.up.pt/resources/soap-t/

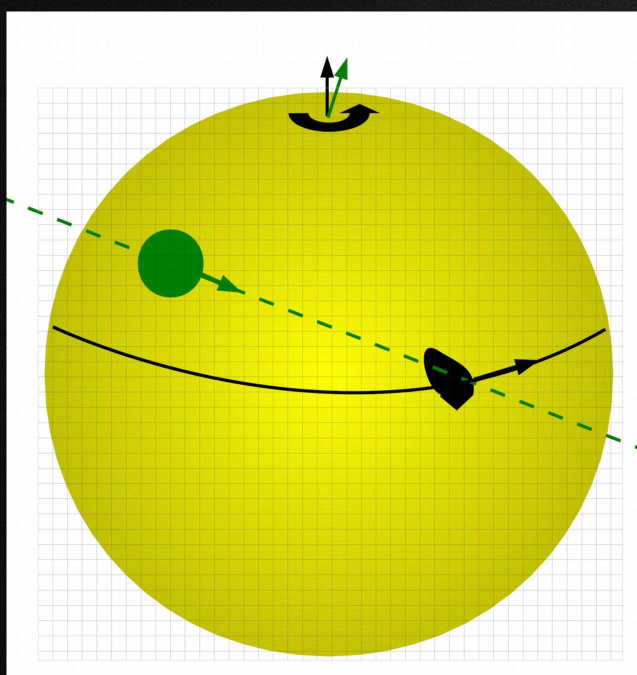

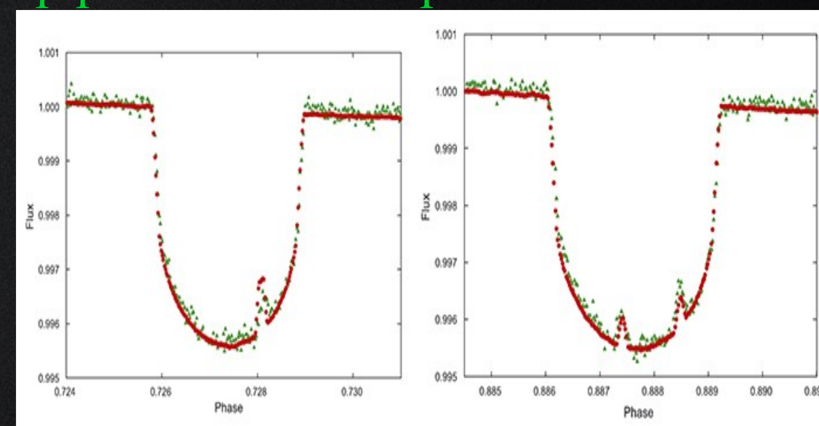

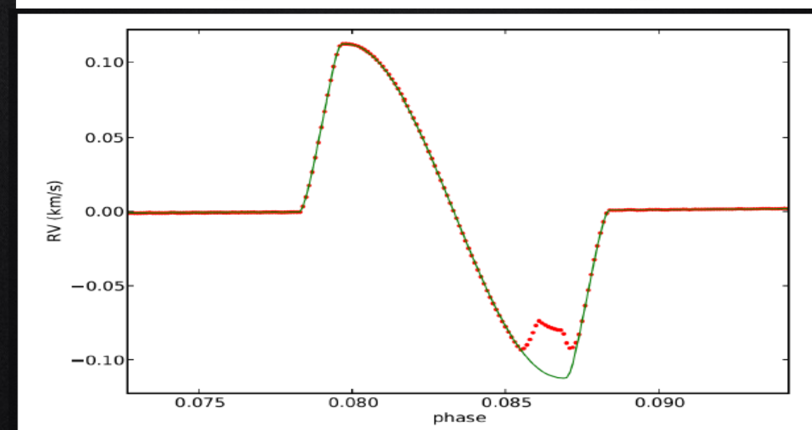

Oshagh et al, A&A, 2013a.

SOAP-T

SOAP-T requires as input the stellar parameters (**stellar inclination, stellar rotation period, limb darkening coefficients, stellar radius, stellar temperature**) and also active region's parameters (**longitude, latitude, filling factor, temperature contrast**) and transiting planet parameters (**planet radius, planet orbital period, eccentricity, argument of periastron, inclination of the orbital plane, projected spin- orbit misalignment**).

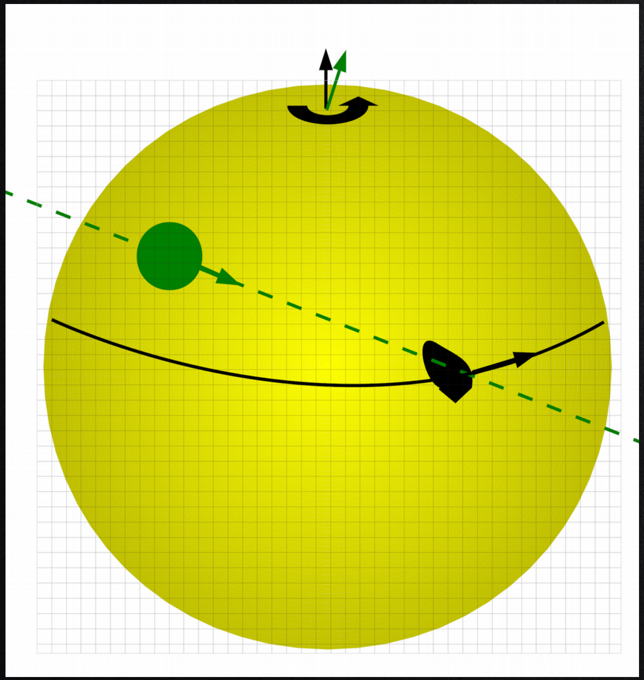

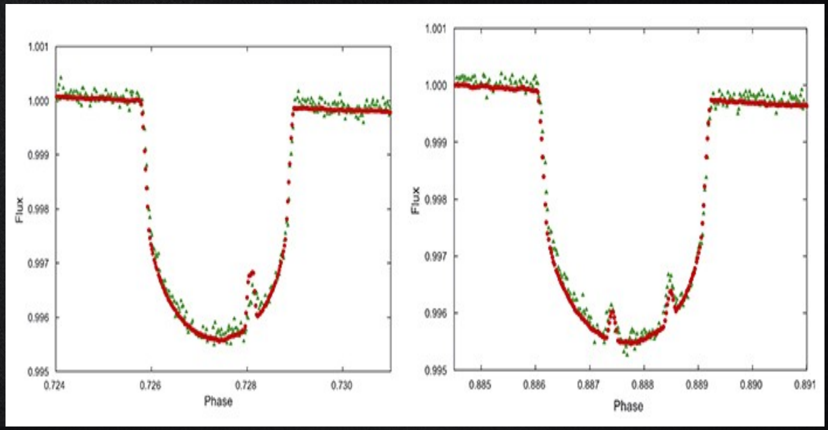

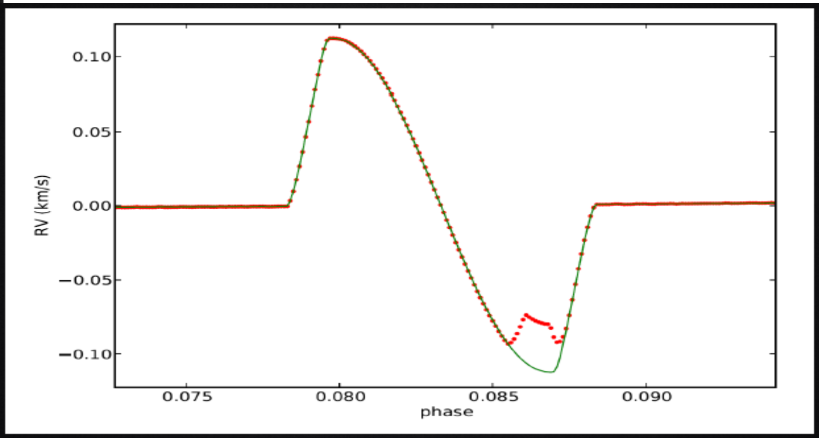

Oshagh+ 2013a.

SOAP-T

HAT-P-11 light curve by Kepler

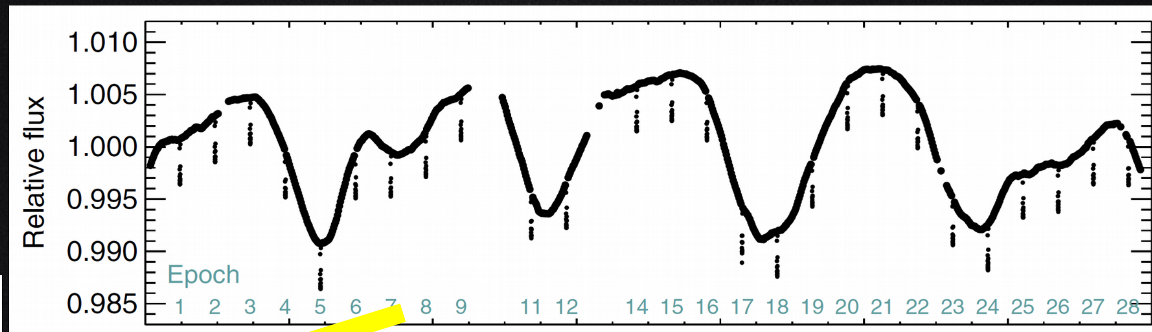

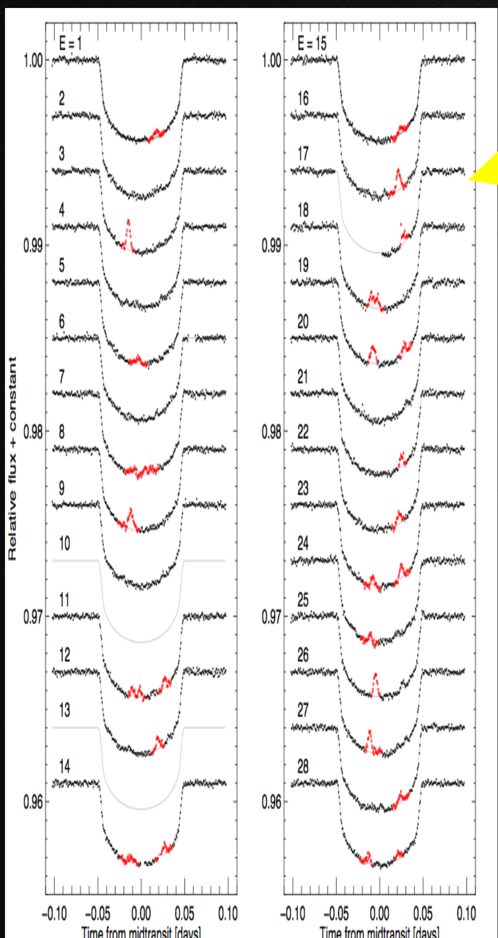

Just inside transits

Folded

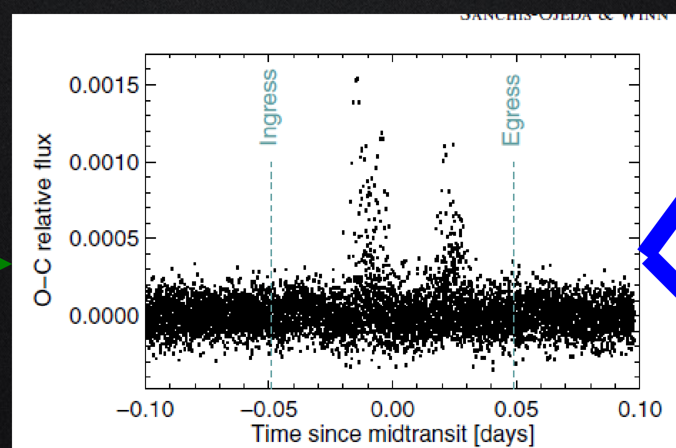

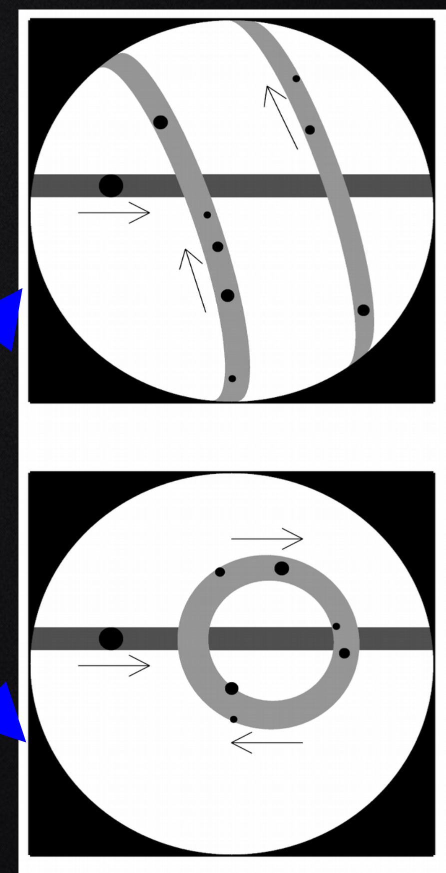

Sanchis-Ojeda & Winn 2011

SOAP-T

HAT-P-11 light curve by Kepler

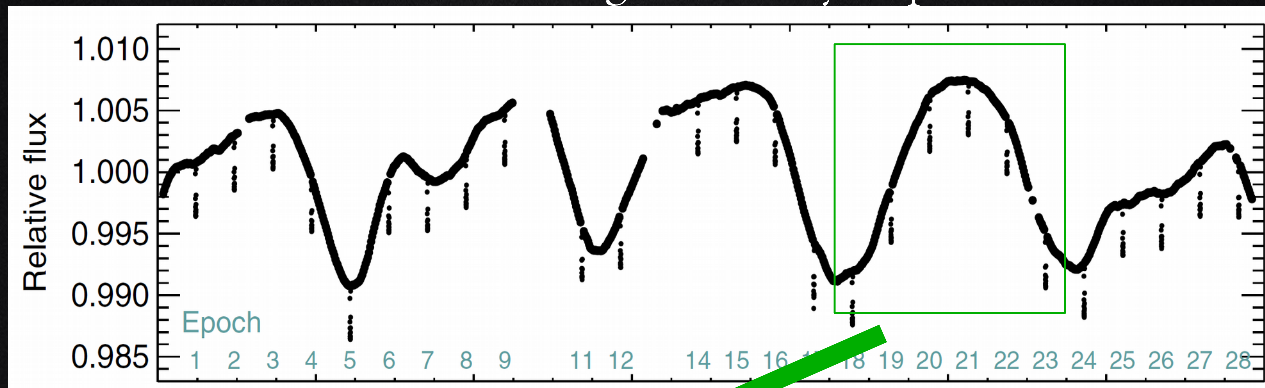

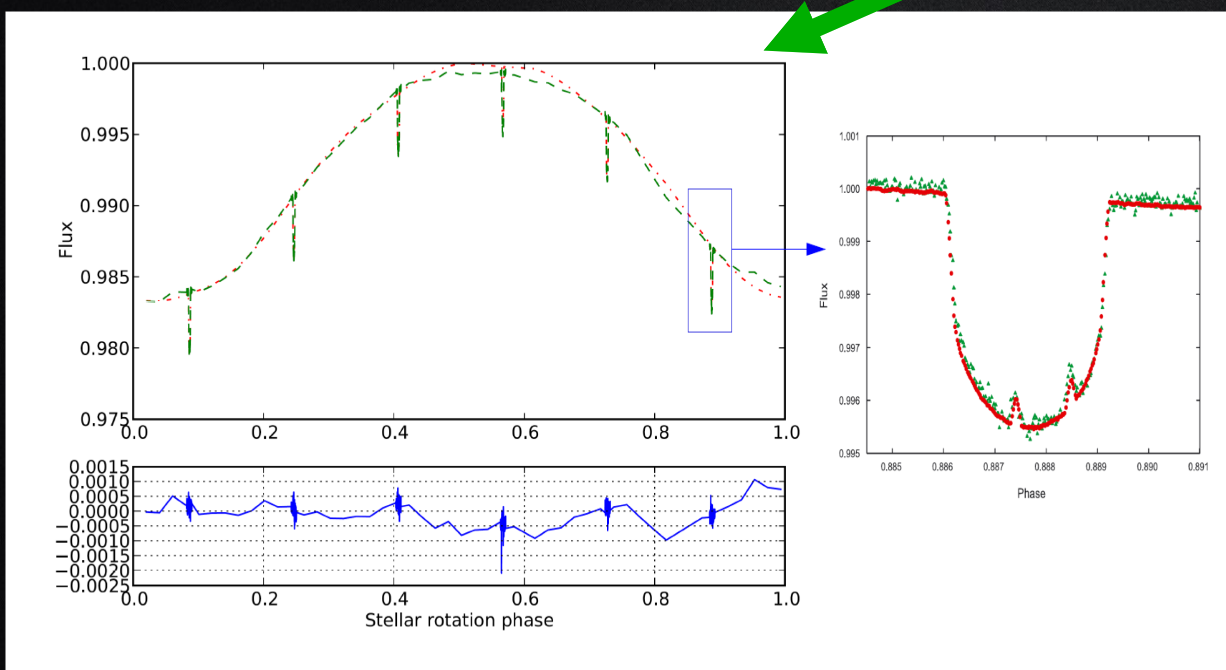

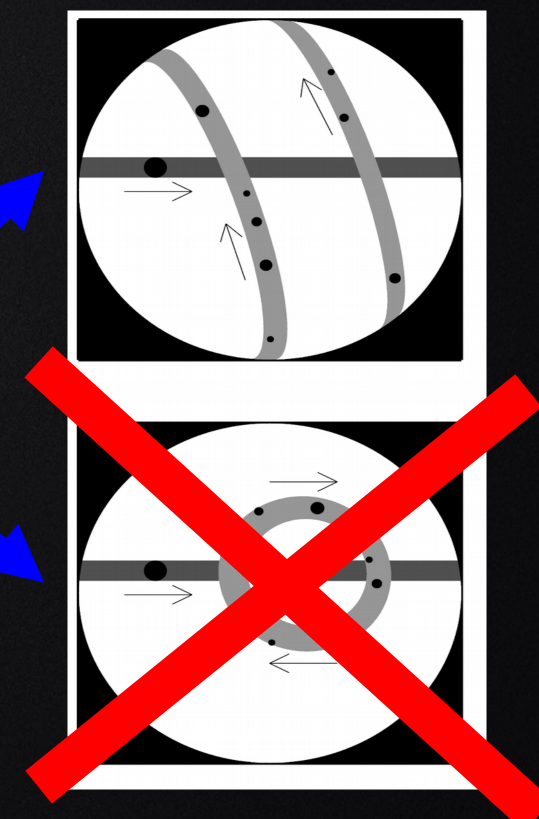

Oshagh et al 2013a

Solar magnetic cycle

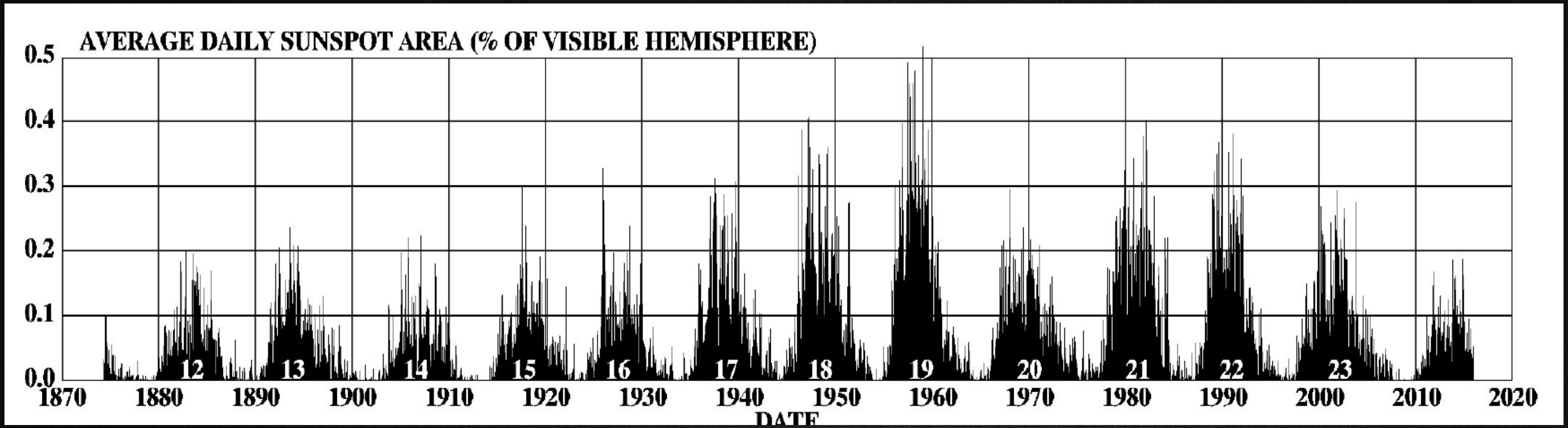

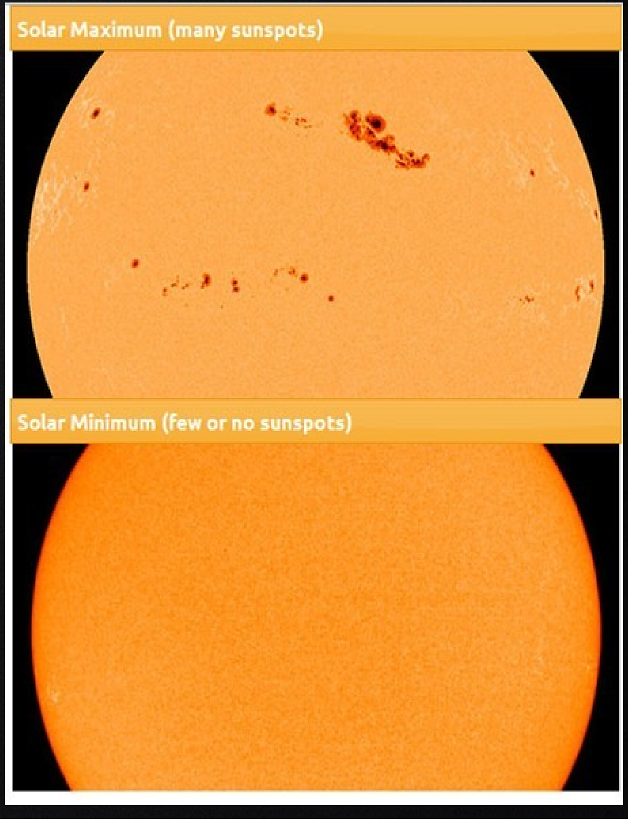

Magnetic cycle

Time scale: months-years
RV amplitude: 1-100 m/s

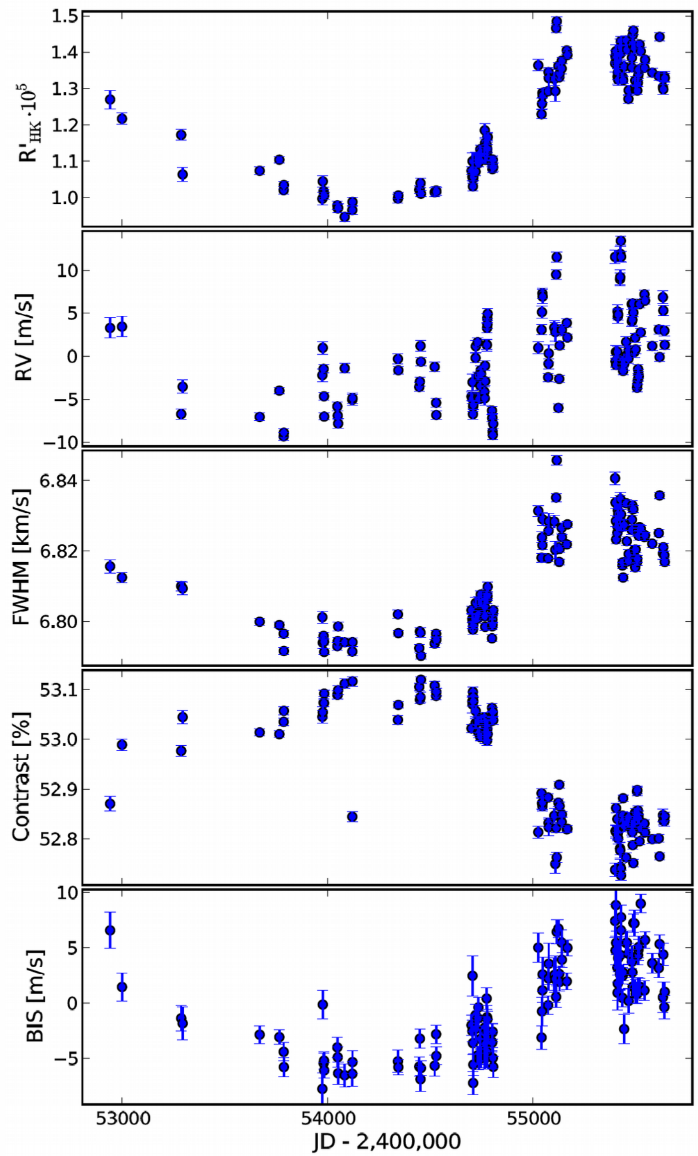

Fig. 16. Time series of R'_{HK}, RV, FWHM, contrast and BIS measurements for the star HD 21693, showing clear correlations between all quantities.

Lovis+ 2011

Magnetic cycle

K dwarfs are less affected by magnetic cycle than G dwarfs

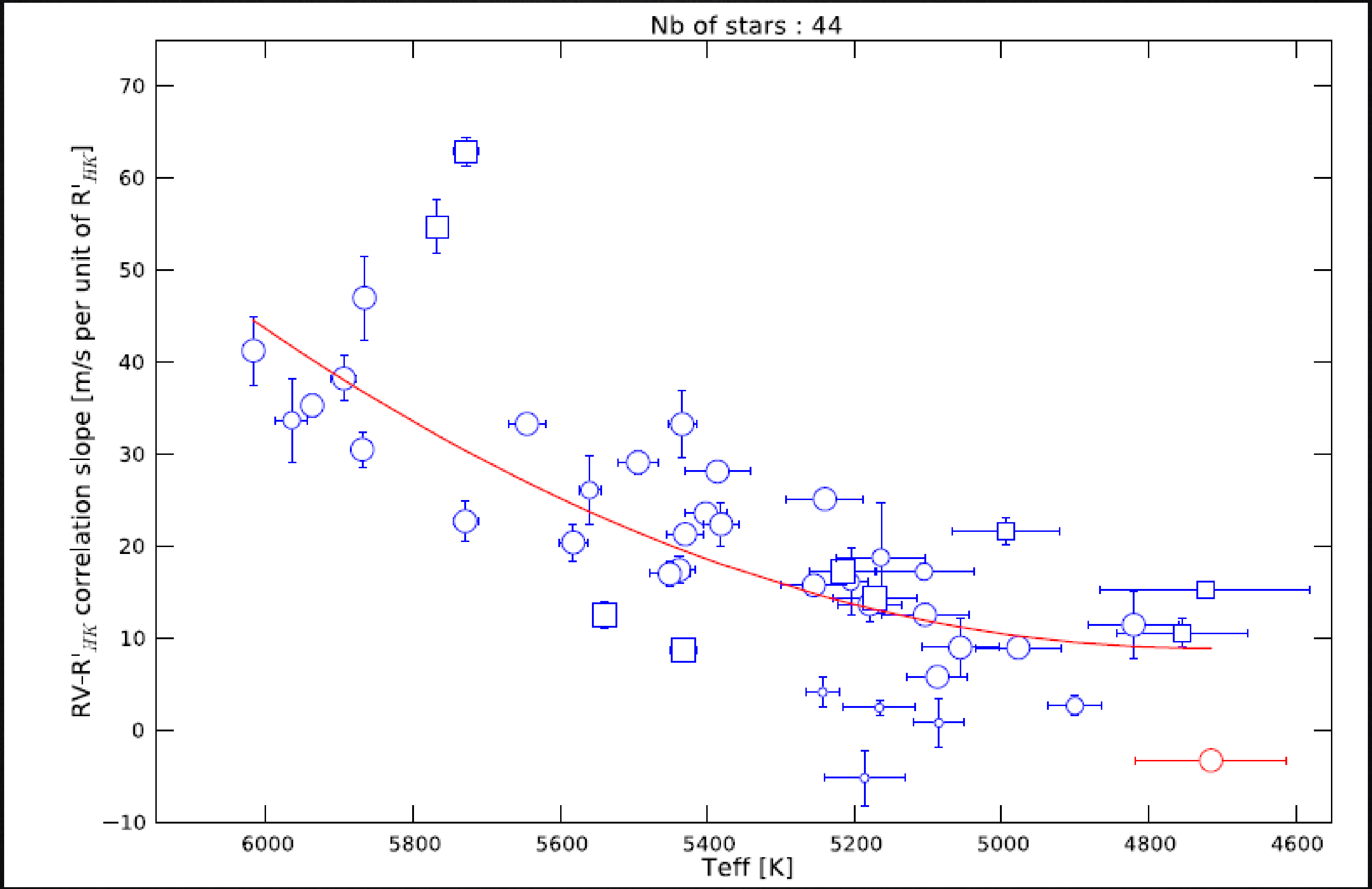

Lovis+ 2011

Magnetic cycle

Same approaches which were described for the stellar activity (activity indicators or modeling it) can be used here, however, one should take into account the active regions evolution.

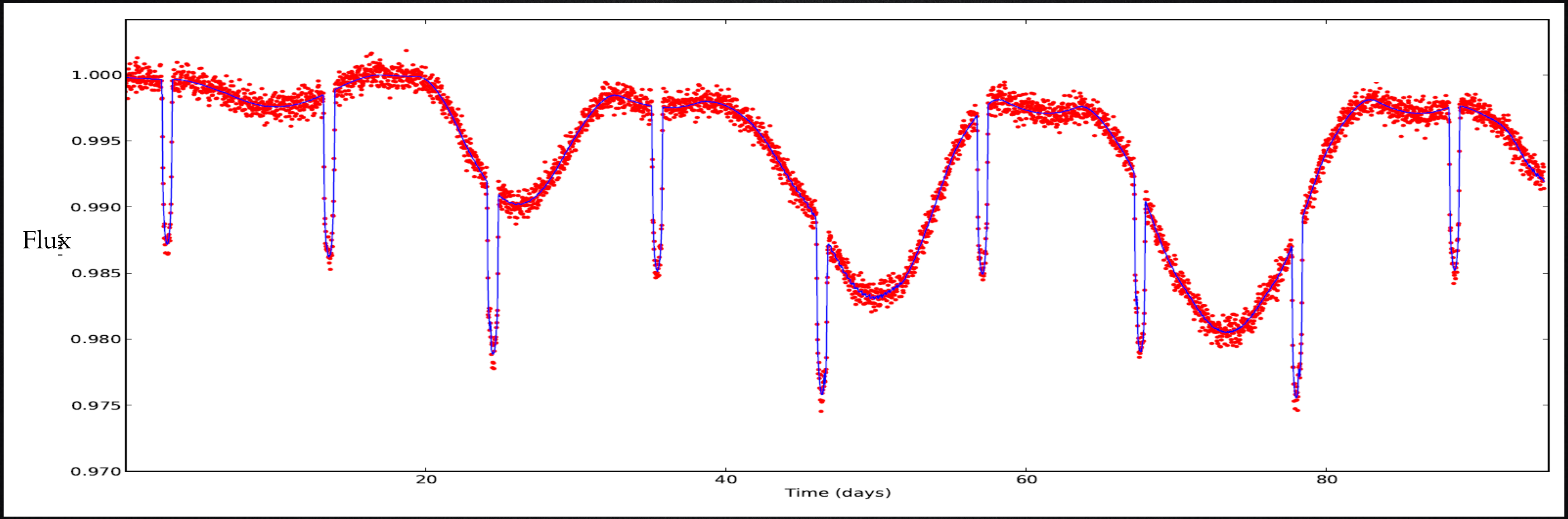

Summary

Photometry		RV
Binning data after observation	Minutes → oscillation	At least 900 seconds integration time
Binning data after observation	Hours → Granulation	Three time observation per night, averaging out
Modeling	Days –> stellar activity	Activity indicators Modeling
Modeling	Years –> magnetic cycle	Activity indicators Modeling

References

1) Boisse, et al. 2011, Disentangling between stellar activity and planetary signals
2) Hall, 2004, Stellar Chromospheric Activity
3) Berdyugina, 2005, Starspots: A Key to the Stellar Dynamo
4) Solanki, 2003, Sunspots: An overview
5) Dumusque, et al. 2014, SOAP2.0
6) Aigrain, et al. 2012, A simple method to estimate radial velocity variations due to stellar activity using photometry
7) Haywood, et al. 2016, The Sun as a planet-host star
8) Queloz, et al, 2001, No planet for HD 166435
9) Oshagh et al. 2013, Effect of stellar spots on high-precision transit light-curve
10) Lovis et al. 2011, Magnetic activity cycles in solar-type stars: statistics and impact on precise radial velocities
11) Reiners, 2012, Observations of Cool-Star Magnetic Fields

Thanks for your attention!

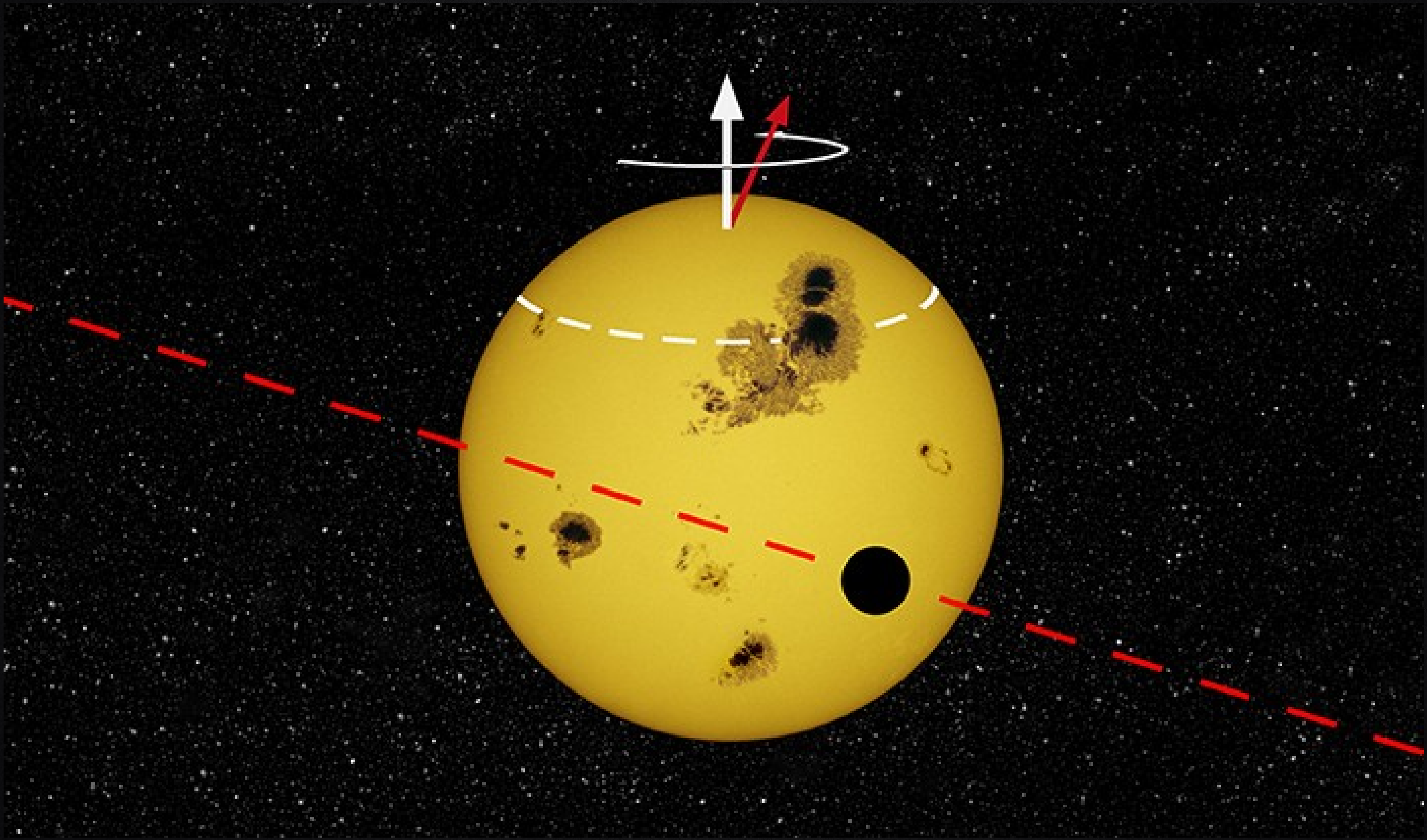

FWHM and simultaneous photometry

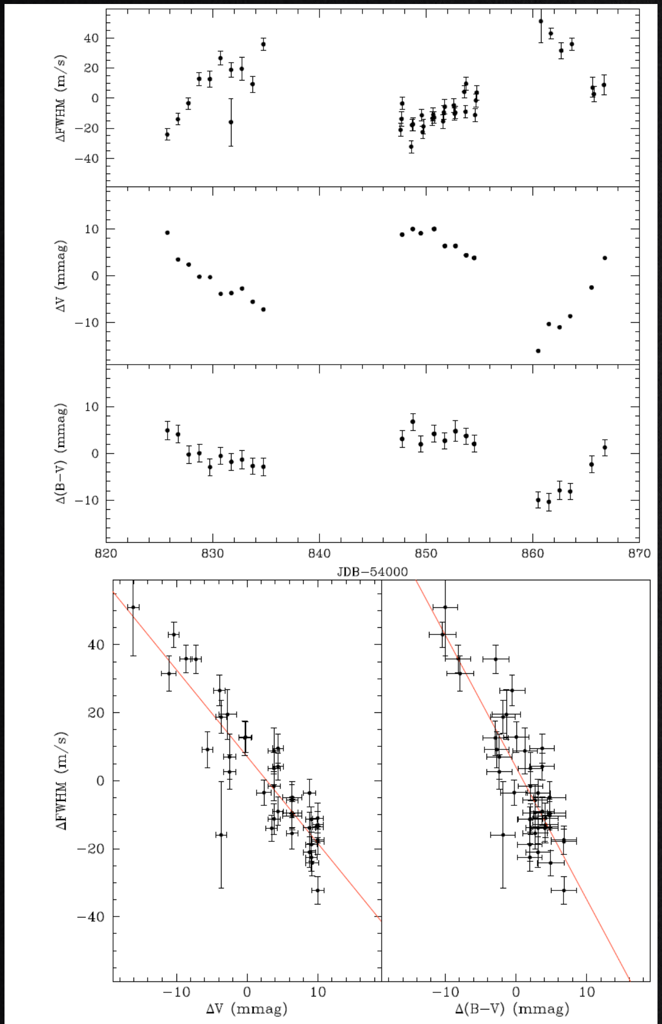

Fig. 2. Swiss Euler telescope photometric measurement obtained simultaneously to the HARPS measurements of the CCF width (*FWHM*). *Top*: time series of the photometric variations for CoRoT-7 computed from an average of short series of exposure totaling 20 min. Also shown are the contemporaneous HARPS *FWHM* measurements. *Bottom*: correlation between the CCF line width and the stellar color and magnitude. The best linear fit to the data is illustrated by a superimposed line.

Queloz+2009

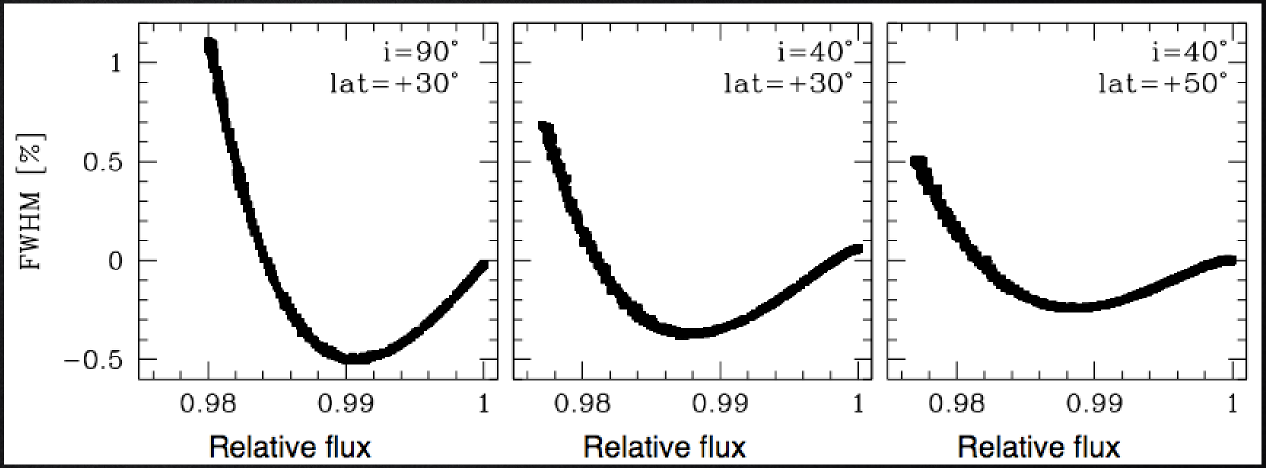

Boisse+2011

Stellar activity modeling (GP using FF')

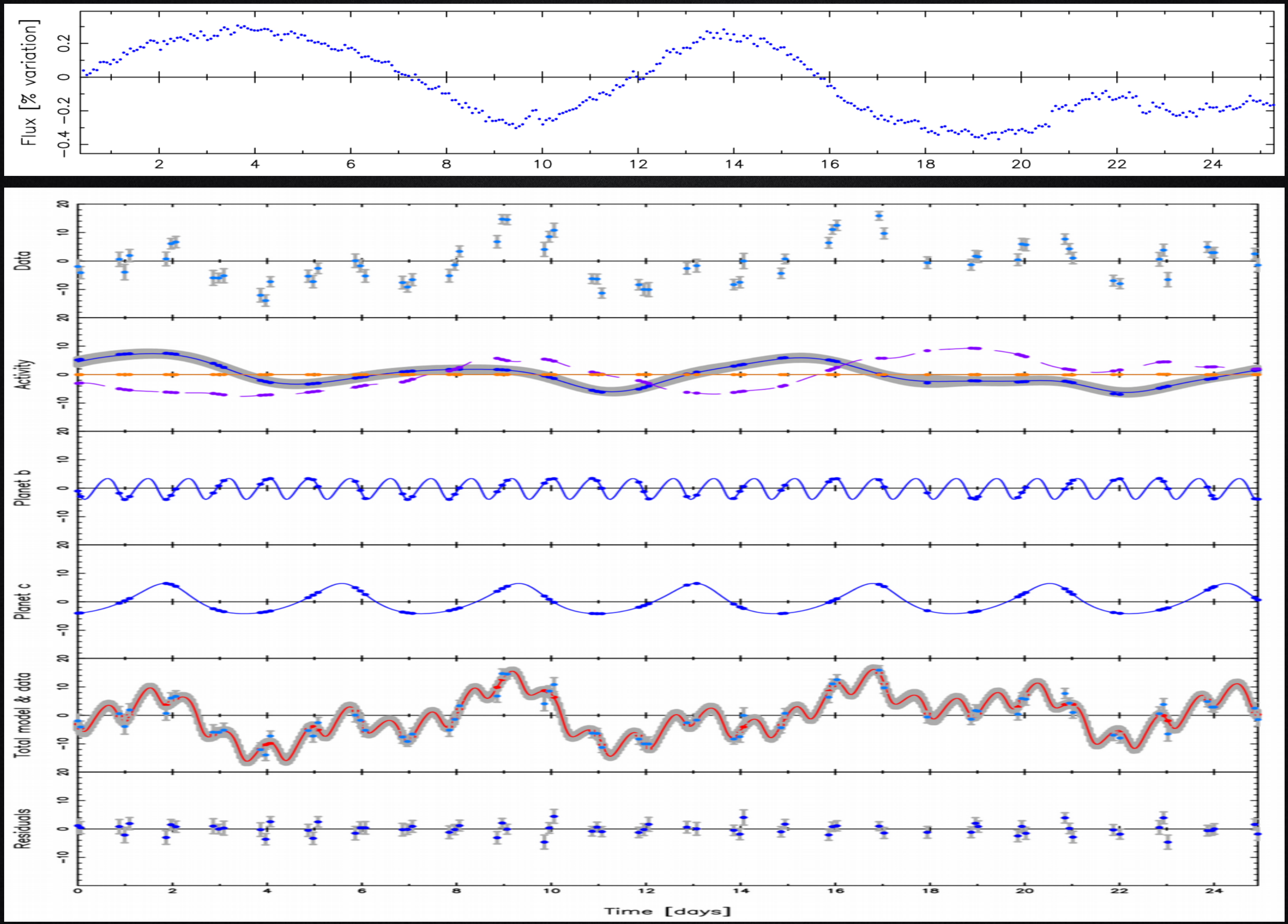

Haywood+2014

Stellar active regions+transit

"Stellar Activity" is a collective name used to describe group phenomena which generate the variability observed in the outer atmospheres of late type-stars mainly due to the presence of highly structured magnetic fields emerging from the convective envelope, namely spots, plage, facula, flares.

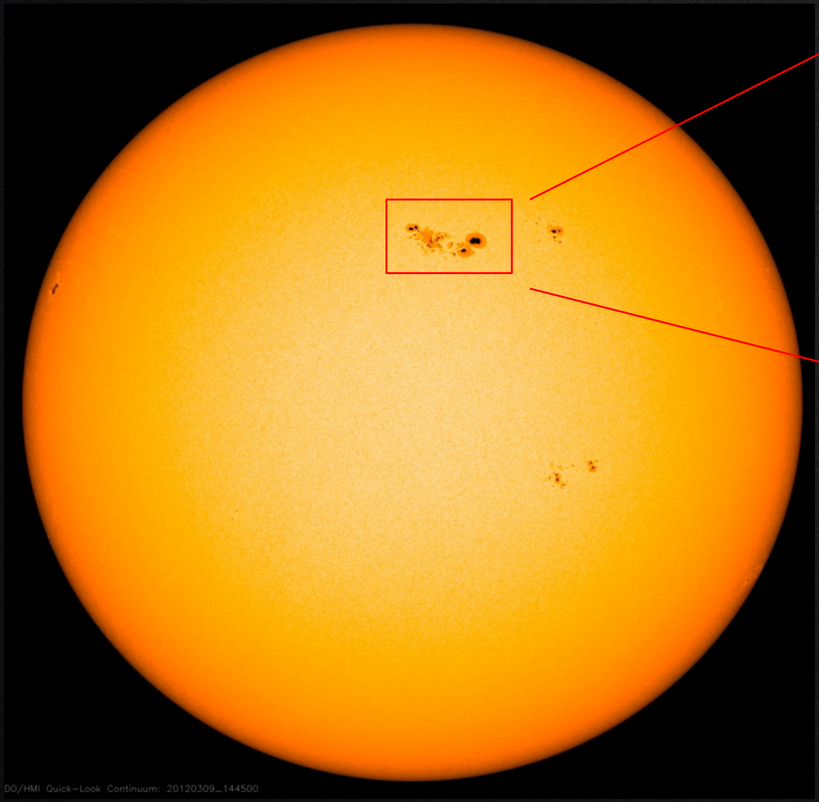

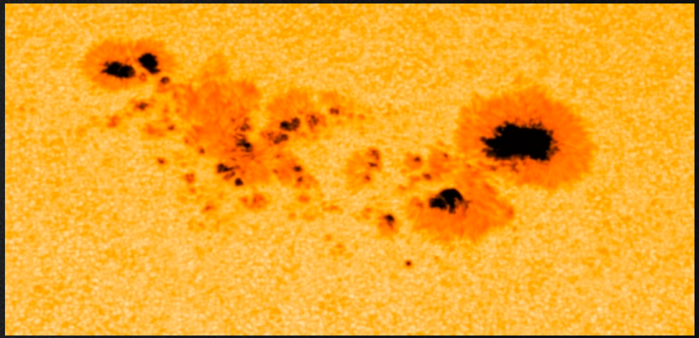

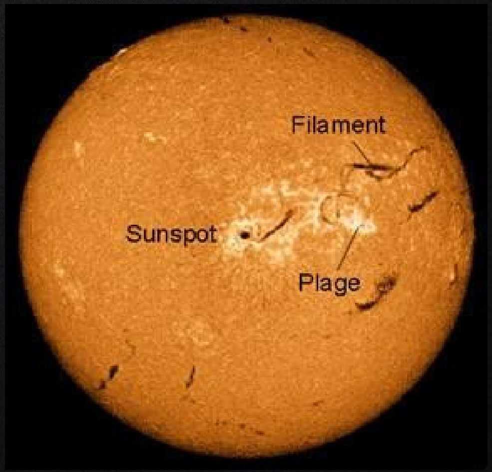

Transit timing measurements

TTV induced by stellar spot occultation may be used to distinguish between prograde and retrograde transiting planets (Mazeh+2014).

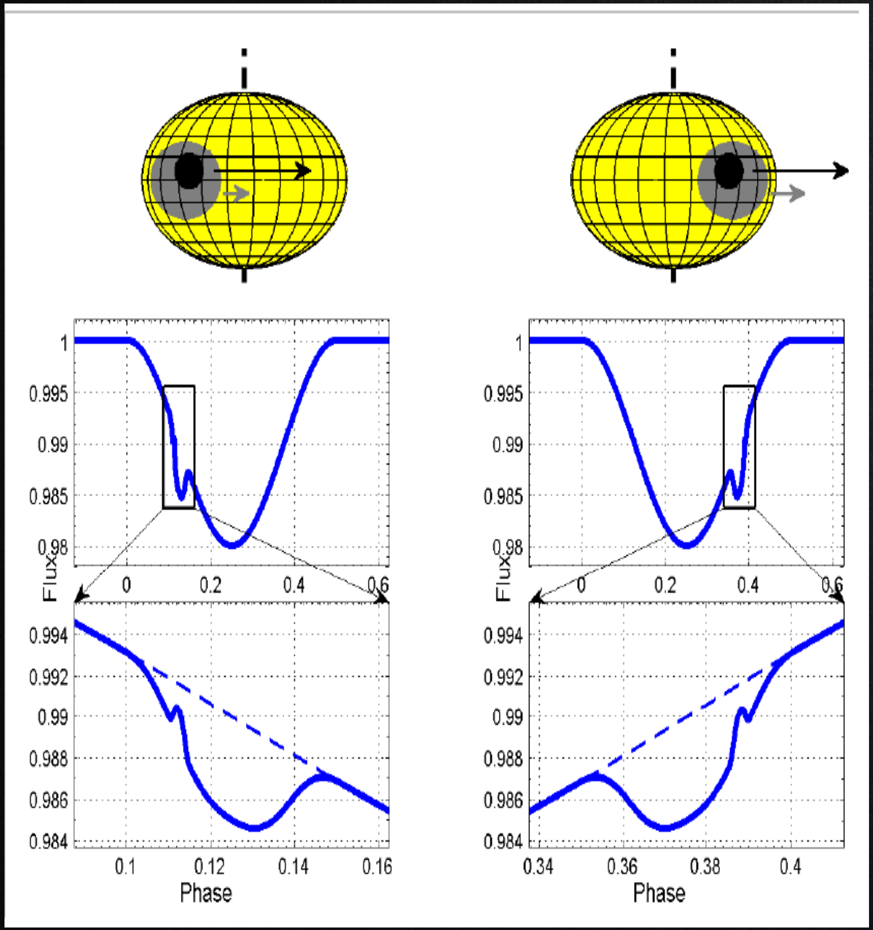

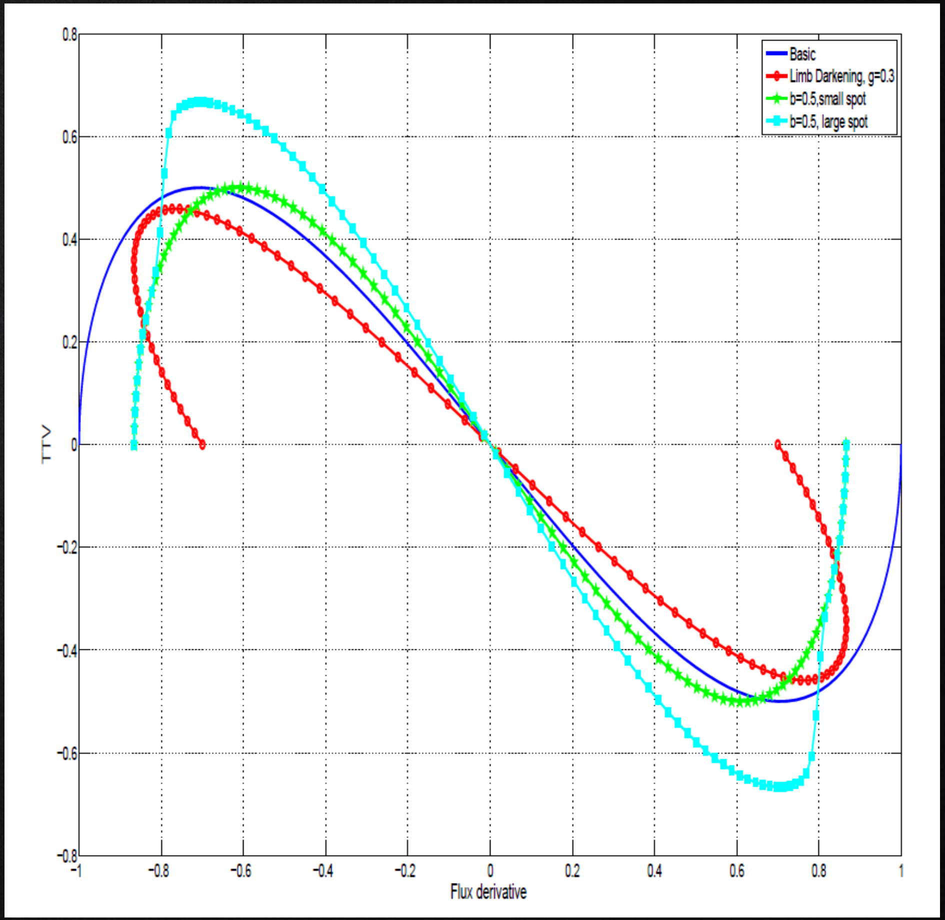

Mazeh+2014

Misalignment of transiting planet

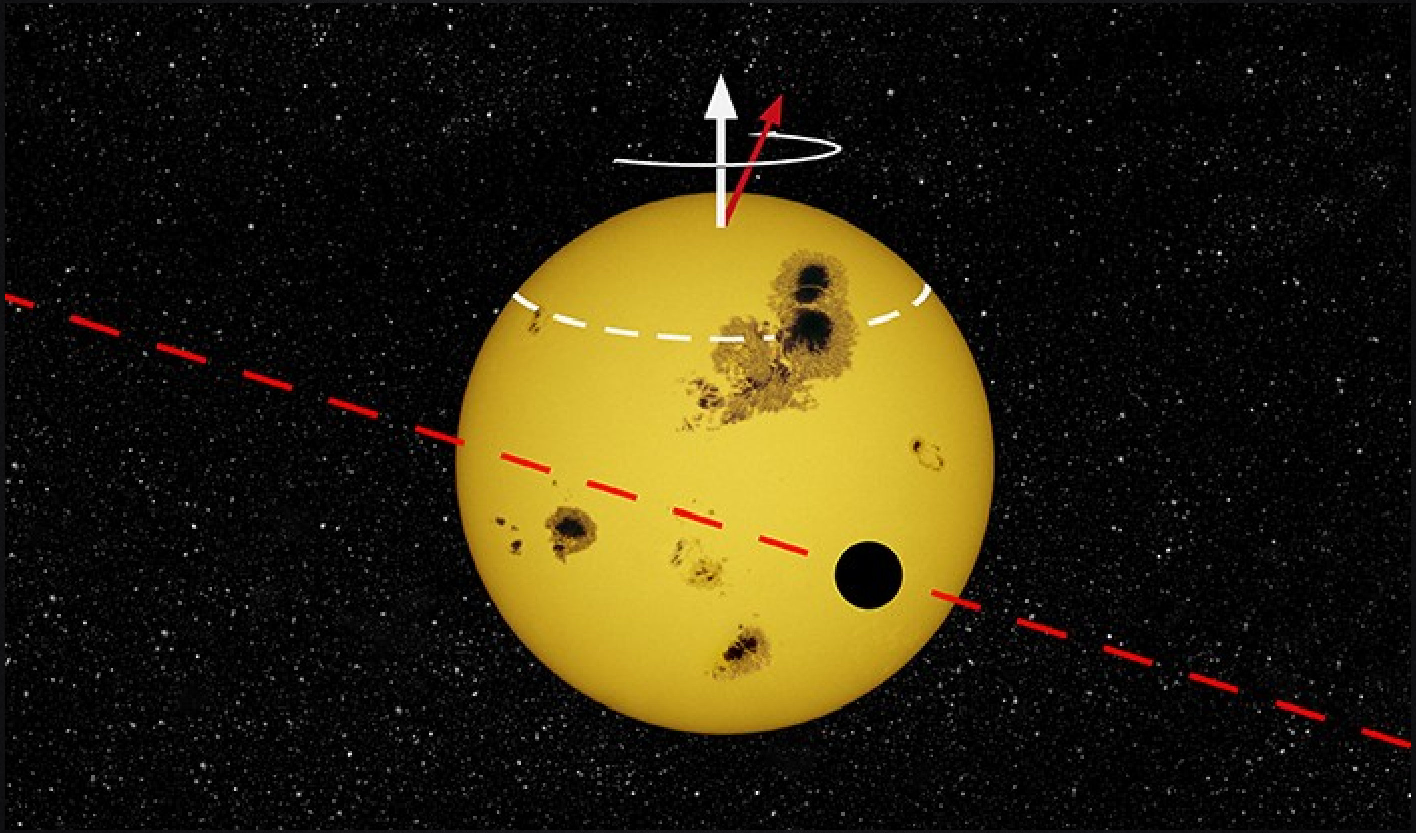

HAT-P-11b

HAT-P-11 light curve by Kepler

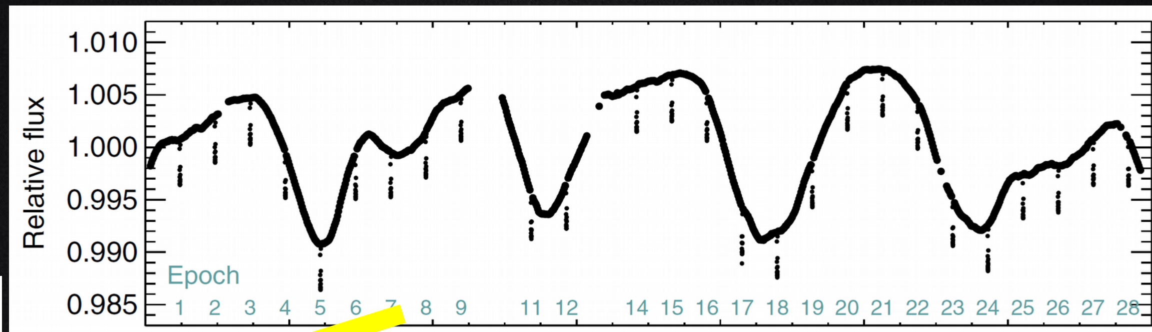

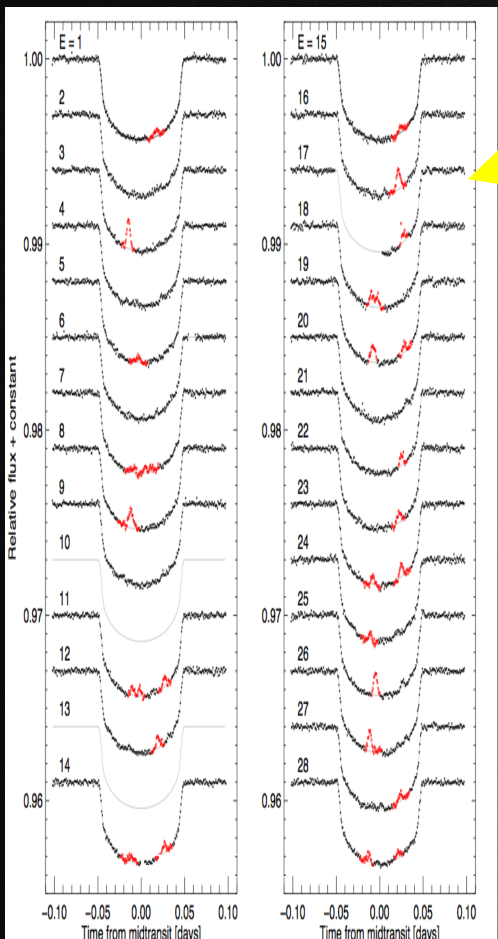

Just inside transits

Folded

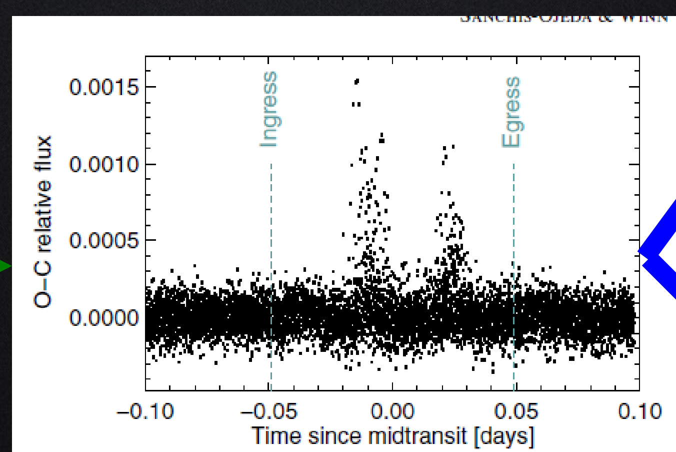

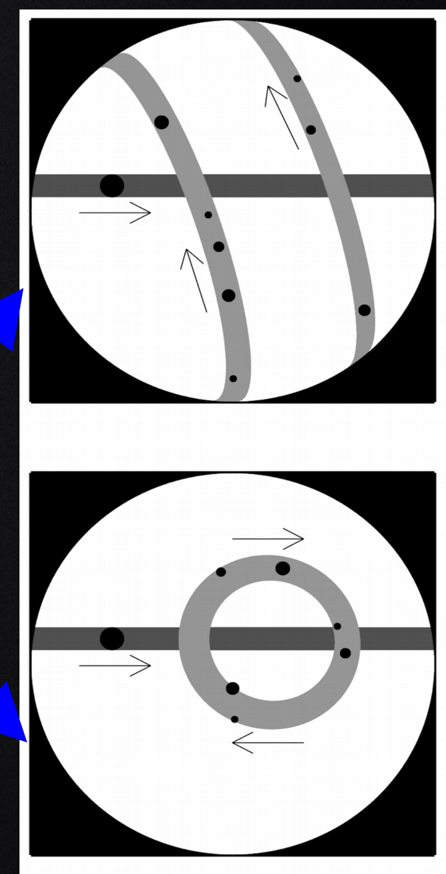

Sanchis-Ojeda & Winn 2011

Kepler-30: multiple transiting planets

Alignment of the stellar spin with the orbits of a three-planet system

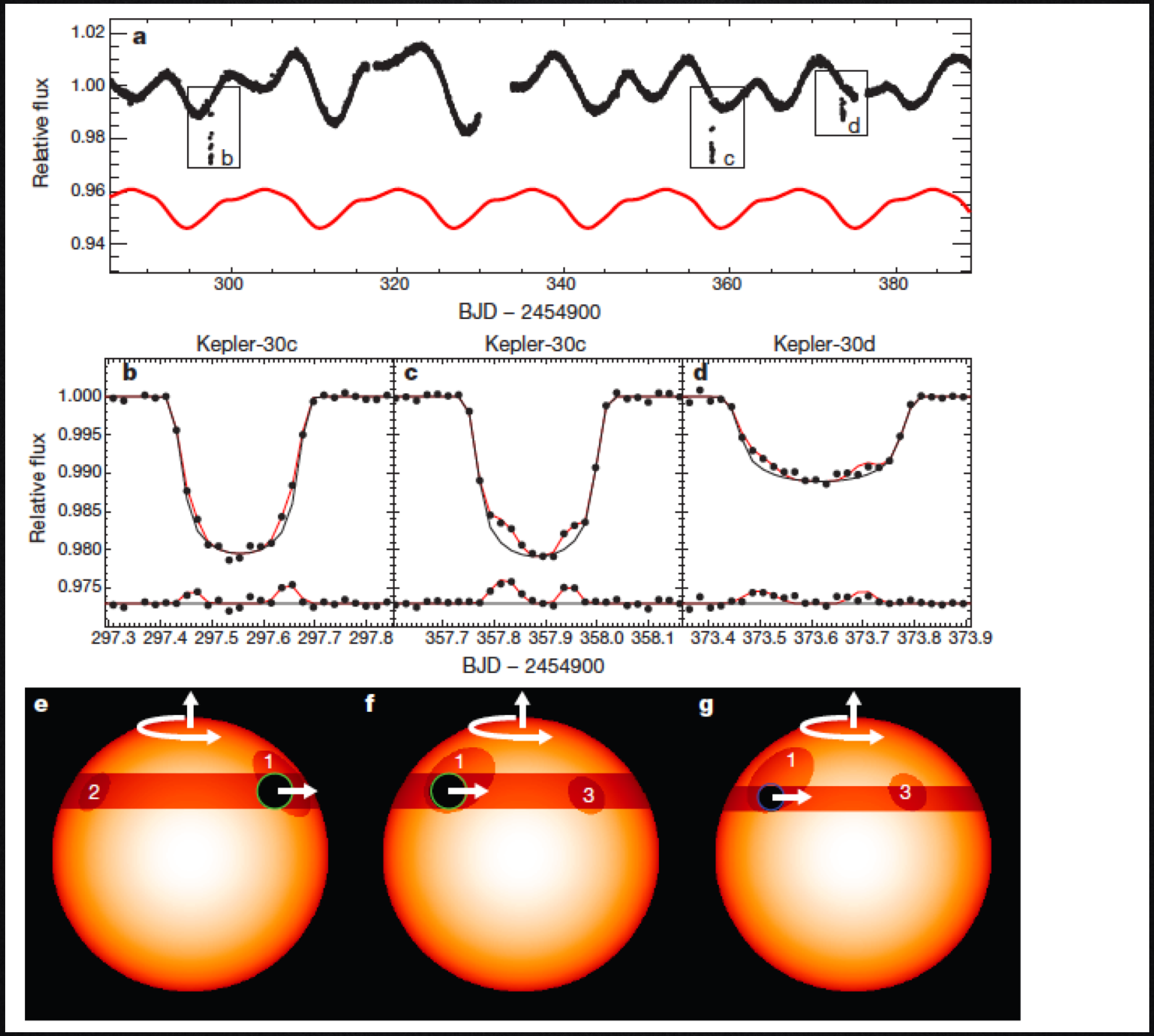

Sanchis-Ojeda+2012

Activity index (Log R'HK)

Log(R'HK) =- 5: the Sun is at minimum activity
Log(R'HK) = -4.75: the Sun is at maximum activity
Log(R'HK) = -4.9: the Sun is at medium activity,

KSINT

Fortran 95, available on http://eduscisoft.com/KSINT/download.php

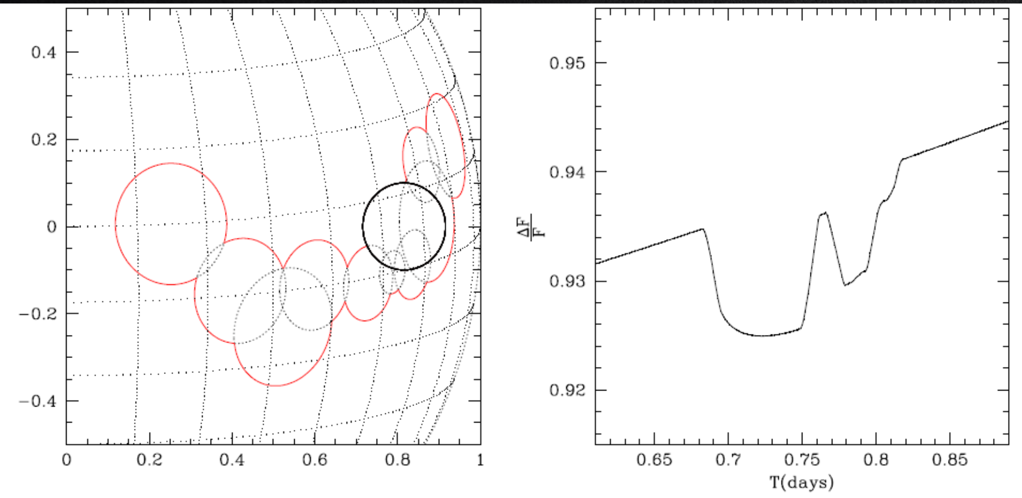

Figure 2. Left: the profile of a Jupiter planet overlapped to a complex spot region composed by ten spots. Black denotes integration on the planet border, red on the spots border. Dotted lines on the objects profiles denote invisible arcs, wherease those on the stellar surface denote stellar meridians and parallels. X and Y axis indicate the positions of the objects on the stellar surface normalized to the stellar radius. Right: the correspondent transit lightcurve during which the overlap of the planets with the spot region on the left side occurs, assuming an orbital period of 3 days for the planet and a rotation period of 9 days for the star.

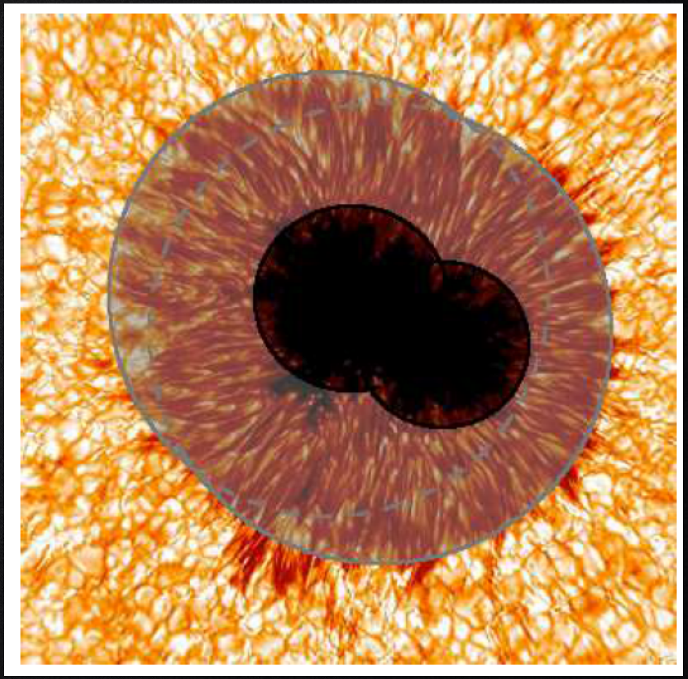

Montalto+2014

KSINT

CoRoT-2

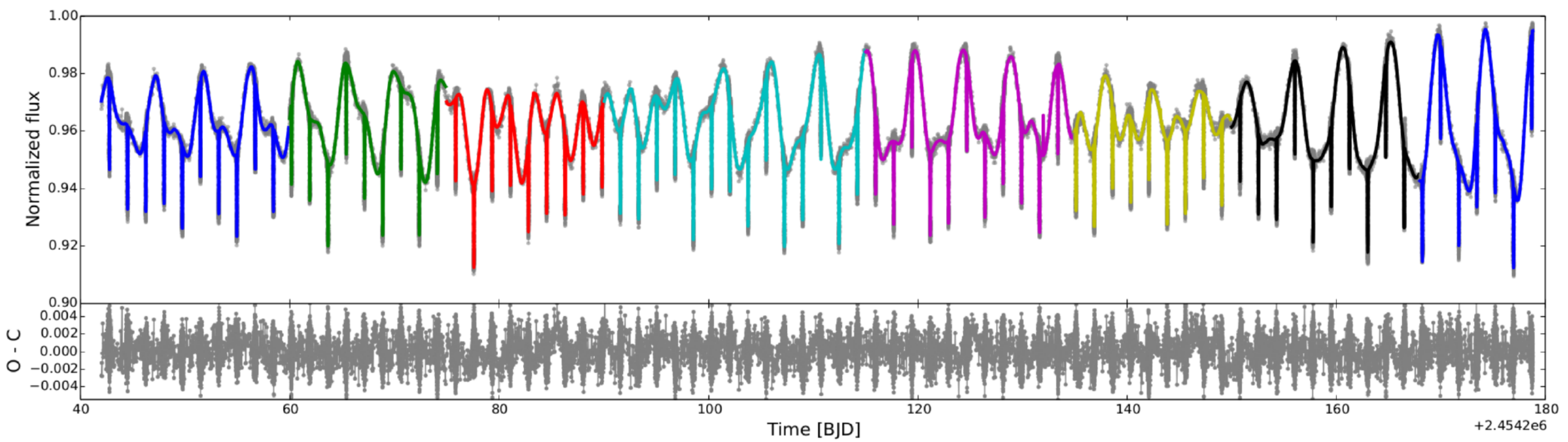

Figure 1: The model light curve from KSint plotted over the data. The eight segments of the fit are divided by color. The residuals are shown in the lower panels, and error bars are not shown for clarity. The larger amplitude of the residuals in correspondence of the transits is due to the full resolution kept for the transits. The out-of-transits binning is of 2016 s, and inside the transits 32 s.

Montalto+2014

SOAP-T

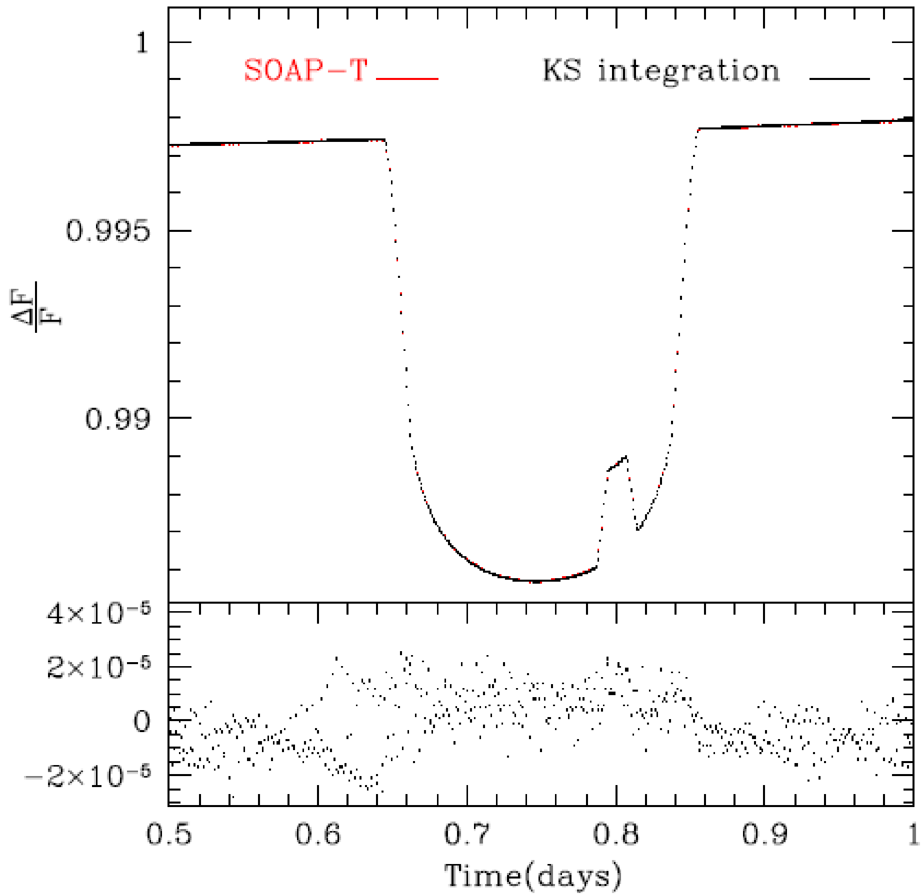

Figure 4. Top: A comparison between KS integration (Kelvin-Stokes integration) and SOAP-T (Oshagh et al. 2013) for the case of a single circular spot crossed by a transiting planet. Bottom: the difference between the SOAP-T and the KS lightcurve.

Montalto+2014